N 70 12223

NASA CR 107046
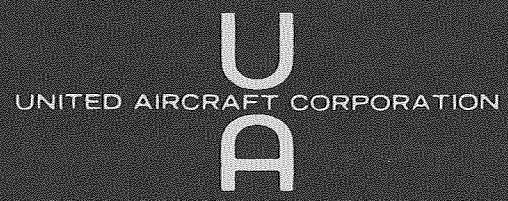
EAST HARTFORD, CONNECTICUT

H-910375-4
Studies of Nuclear Light Bulb
Start-Up Conditions and
Engine Dynamics

NASA Contract No. NASw-847

CASE FILE
COPY

UNITED AIRCRAFT CORPORATION

U
A

United Aircraft Research Laboratories

EAST HARTFORD, CONNECTICUT

United Aircraft Research Laboratories

U
A
UNITED AIRCRAFT CORPORATION

EAST HARTFORD, CONNECTICUT

H-910375-4

Studies of Nuclear Light Bulb
Start-Up Conditions and
Engine Dynamics

NASA Contract No. NASw-847

REPORTED BY _Thomas S. Latham_

Thomas S. Latham

Harold E. Bauer

Harold E. Bauer

Richard J. Rodgers

Richard J. Rodgers

APPROVED BY _James W. Clark_

James W. Clark, Chief
Fluid and Systems Dynamics

DATE September 1969

NO. OF PAGES 108

COPY NO. 66

FOREWORD

An exploratory experimental and theoretical investigation of gaseous nuclear rocket technology is being conducted by the United Aircraft Research Laboratories under Contract NASw-847 with the joint AEC-NASA Space Nuclear Propulsion Office. The Technical Supervisor of the Contract for NASA is Captain C. E. Franklin (USAF). Results of portions of the investigation conducted during the period between September 15, 1968 and September 15, 1969 are described in the following five reports (including the present report) which comprise the required ninth Interim Summary Technical Report under the Contract:

1. Roman, W. C., J. F. Klein, and P. G. Vogt: Experimental Investigations to Simulate the Thermal Environment, Transparent Walls and Propellant Heating in a Nuclear Light Bulb Engine. United Aircraft Research Laboratories Report H-910091-19, September 1969.

2. Mensing, A. E. and J. F. Jaminet: Experimental Investigations of Heavy-Gas Containment in R-F Heated and Unheated Two-Component Vortexes. United Aircraft Research Laboratories Report H-910091-20, September 1969.

3. Krascella, N. L.: Theoretical Investigation of the Radiant Emission Spectrum from the Fuel Region of a Nuclear Light Bulb Engine. United Aircraft Research Laboratories Report H-910092-12, September 1969.

4. Latham, T. S., H. E. Bauer, and R. J. Rodgers: Studies of Nuclear Light Bulb Start-up Conditions and Engine Dynamics. United Aircraft Research Laboratories Report H-910375-4, September 1969. (present report)

5. Johnson, B. V.: Exploratory Experimental Study of the Effects of Inlet Conditions on the Flow and Containment Characteristics of Coaxial Flows. United Aircraft Research Laboratories Report H-910091-21, September 1969.

Studies of Nuclear Light Bulb Start-Up

Conditions and Engine Dynamics

TABLE OF CONTENTS

TABLE OF CONTENTS (Continued)

Studies of Nuclear Light Bulb Start-Up

Conditions and Engine Dynamics

SUMMARY

Analytical studies were conducted to determine the operating conditions of a nuclear light bulb engine during start-up and the transient response of the engine to various perturbations at the nominal full-power operating level. The basic nuclear light bulb engine design was refined, where necessary, to include modifications which resulted from recent criticality studies and test program results.

The start-up study was performed using a simplified analytical model of the basic engine. Three linear power ramps were used and the general engine response, auxiliary power requirements and thermal stress levels were investigated. The calculated responses in temperature and pressure were similar for all of the power ramps. It appears that there will be no major problems with engine control or with excessive thermal stress levels during start-up. Some type of auxiliary power will be required for the turbopump unit during start-up.

Finite-difference approximations to the time-dependent thermal, fluid dynamics and neutron kinetics equations were used to describe the operating characteristics of the engine. These equations were programmed on a UNIVAC 1108 digital computer to construct a dynamic simulation for predicting the response of the engine to selected perturbations occurring at the nominal full-power operating condition. A preliminary transient analysis was performed using the model, which simulates an uncontrolled engine, to determine the basic stability characteristics and to identify the parameters which would provide the most effective control mechanisms. Responses to perturbations in the uncontrolled system can be characterized by either steady-state or damped oscillations with a characteristic frequency of about 1 cycle/sec. It was concluded that control of the engine could be achieved primarily by control of fuel injection rate.

RESULTS AND CONCLUSIONS

1. The sequence of events during a linear start-up power ramp is basically independent of the length of the start-up ramp. There is a rapid rise in average fuel temperature which occurs during the first 1 to 3 percent of the total start-up time. Shortly after the fuel temperature rise, there is a similar rapid rise in propellant temperature. Due to the large heat capacity of the solid moderator (5124 Btu/(deg R) for the BeO, 6440 Btu/(deg R) for the graphite), temperatures in these regions lag the fuel and propellant temperatures considerably. As a result, the bulk moderator materials do not reach nominal full-power operating temperatures until 200 to 300 sec after initiation of start-up, regardless of the length of the start-up ramp.

2. The critical mass of U-233 varies during start-up from 18.6 lb at zero power conditions to 30.9 lb at full power. For a start-up ramp which is long relative to the time required to heat the moderator, the critical mass increases continuously until full power is reached. When the start-up ramp is short relative to the moderator heating time, the critical mass also increases continuously, but does not reach the steady-state critical mass until the moderator temperatures have reached the steady-state, full-power values. For example, for a 60 sec start-up, a critical mass of 28.2 lb is required when full power is reached; the critical mass approaches 30.9 lb asymptotically after about 300 sec.

3. Auxiliary power will be required for start-up. Due to the rapid pressure rise associated with the rapid fuel and propellant temperature rises, more pumping power is needed than the turbine is able to deliver during the early stages of start-up.

4. Temperature differences and rates of temperature rise in components throughout the engine were calculated. No serious thermal stress problems occurred during the start-up transients studied.

5. Typical responses of the uncontrolled engine to various perturbations in reactivity, fuel injection rate, chamber pressure, turbopump wheel speed, and fuel region radius are in the form of oscillations in power which are usually damped, but in some instances are sustained at a constant amplitude. The frequency of the oscillations is about 1 cycle/sec. Two factors tend to drive the oscillatory response: (1) a positive reactivity coefficient associated with moderator temperature, and (2) the tendency for the fuel injection rate to exceed the steady-state rate whenever chamber pressure drops below 500 atm.

6. It was concluded that control of the engine (in particular, further damping of oscillatory responses) could be achieved by controlling fuel injection rate.

INTRODUCTION

Investigations of various phases of gaseous nuclear rocket technology are being conducted at the United Aircraft Research Laboratories under Contract NASw-847 with the joint AEC-NASA Space Nuclear Propulsion Office. Since 1967, the principal effort has been directed toward the vortex-stabilized nuclear light bulb engine. The basic design of this engine is described in Ref. 1, and subsequent investigations which were performed to supplement and investigate the basic design in greater detail are reported in Refs. 2 through 6. Generalized studies of gaseous nuclear rocket engine design feasibility are reported in Ref. 7. The typical vortex-stabilized nuclear light bulb rocket engine design which has resulted from these studies has the following characteristics:

1. Cavity configuration -- seven separate cavities having a total overall volume of 170 ft^3, each having a length of 6 ft.

2. Cavity pressure -- 500 atm.

3. Specific impulse -- 1870 sec.

4. Total propellant flow (including seed and nozzle transpiration coolant flow) -- 49.3 lb/sec.

5. Thrust -- 92,000 lb.

6. Engine power -- 4600 megw.

7. Engine weight -- 70,000 lb.

8. Ratio of average density in fuel-containment region to neon density at edge of fuel -- 0.7.

9. Equivalent axial-flow Reynolds number in neon vortex -- 5500.

The majority of the work under Contract NASw-847 up to 1969 has been concerned with the design and operating characteristics of a nuclear light bulb engine operating at full power in a steady state. Preliminary investigations of start-up characteristics of a nuclear light bulb engine are discussed in Ref. 1, but these investigations were performed primarily for the purpose of determining the requirements for a variable-area nozzle during start-up and do not include a detailed analysis of engine conditions during the transient. Since there have been no major changes to the basic engine design of Ref. 1 as a result of the continuing studies of engine operating characteristics, this design was used as a basis for a transient analysis of the engine.

The objectives of the work described herein were (1) to determine the transient operating conditions during reactor start-up with particular emphasis on flow, temperature, and critical mass characteristics during the start-up ramp, (2) to develop a computer simulation program for studying the dynamic response of the nuclear light bulb engine to perturbations which occur at nominal full-power operating conditions, and (3) to perform initial exploratory calculations with this dynamic simulation program to investigate stability and to identify parameters with which control of the engine might be achieved.

NUCLEAR LIGHT BULB ENGINE DESIGN

The principle of operation of the nuclear light bulb engine is discussed in detail in Ref. 1, and sketches illustrating the principle of operation of the engine are shown in Fig. 1. Energy is transferred by thermal radiation from gaseous nuclear fuel suspended in a neon vortex to seeded hydrogen propellant. The vortex and pro- pellant regions are separated by an internally-cooled transparent wall. A seven- cavity configuration is employed, rather than a single cavity, to increase the total surface radiating area at the edge of the fuel for a given total cavity volume.

Neon is injected from the transparent wall to drive the vortex, passes axially toward the end walls, and is removed through a port at the center of one or both end walls (Fig. 1b). The neon discharging from the cavity, along with any entrained fuel and fission products, is cooled by being mixed with low-temperature neon, thus causing condensation of the nuclear fuel to liquid or solid form. The condensed fuel is centrifugally separated from the neon and pumped back to the vortex region. The neon is further cooled by rejecting heat to the primary hydrogen propellant, and is then pumped back to drive the vortex.

The seven cavities are surrounded by a beryllium oxide moderator region which fills the interstitial regions. The beryllium oxide region is surrounded by an annular graphite moderator region (see Fig. 1). These two axial moderator regions are separated by an internally-cooled beryllium flow divider which separates the flow in the two regions. The moderator is supported by 24 beryllium tie rods which pass through the moderator regions. In addition to the axial moderator regions there are upper and lower moderator regions which form the ends of the cavity. These end moderator regions consist of a beryllium oxide region, which is adjacent to the cavity end walls, and a graphite region. The heat deposited in the moderator by neutron and gamma ray heating and the heat transferred to the moderator and structure by conduction, convection, and radiation is also transferred to the primary hydrogen propellant before it enters the cavity region. A schematic diagram of the nuclear light bulb engine flow circuits is shown in Fig. 2.

The reference engine design used in the engine dynamics studies is basically similar to that described in Ref. 1, with appropriate modifications based on more recent calculations of moderator requirements, heat deposition rates, and conduction and convection heating. Since the basic design does not differ appreciably from that of Ref. 1, only the modifications to the design and the resulting nominal full-power operating characteristics will be discussed.

Modifications to Basic Engine Design

There have been two types of modification to the basic engine design: a revision of heat deposition rates, and a revision of the coolant flow circuits which remove heat from the moderator and structure. The revision of heat deposition rates resulted from a detailed criticality study (Ref. 2) which indicated a requirement for additional moderator material in the upper (accessory region) and lower (nozzle region) ends of the engine to minimize neutron losses. The Ref. 2 study also resulted in more accurate estimates of neutron and gamma ray heating than were available for the studies in Ref. 1. The changes in the coolant flow circuits were made necessary by the redistribution of heat deposited in the moderator and structural components.

Revised Heat Deposition Rates

The heat deposition rates used in the engine dynamics study are shown in Table I. The percentage of the total energy which is deposited in the moderator and structure is 12.15 percent. The principal cause for the reduction in this value from the 15 percent reported in Ref. 1 is the decrease in neutron and gamma ray heating predicted in Ref. 2. Additional changes are due to a revision of the amount of heat transferred to the transparent structure, cavity liner, and end walls by conduction and convection, and due to a change in the fission product decay heating in the fuel cycle circuit.

The variation in fission product decay heat with time was estimated by assuming that all of the fission products formed in the cavity would remain in the fuel cycle circuit. Since the majority of the fission products which contribute to the decay heat are gases at low temperature, such as xenon or krypton, they probably cannot be separated from the neon. Even if separation were possible, there would still be a heat source which would have to be cooled unless the fission products were expelled from the engine. If all of the fission products remain in the fuel cycle circuit, their contribution to the total heating in the circuit will increase with operating time. The estimated contribution of the fission products to the fuel cycle heat load was estimated from data in Ref. 8 and is shown in Fig. 3.

Revision of Coolant Flow Circuits

The coolant flow schematic used in the final reference design and in the engine dynamics studies is shown in Fig. 2. The fuel cycle circuit is cooled directly by the primary hydrogen propellant. The fuel cycle heat exchanger was located in the primary hydrogen propellant circuit to provide a lower sink temperature for the neon; this minimizes the amount of bypass flow required to lower the mixed-mean temperature of the neon-fuel mixture to a level which would condense the fuel. The cavity liner, tie rods, and flow divider (see Fig. 1) are cooled in three parallel circuits

6

to reduce the pressure loss in the tie rods and flow divider. The quantity of heat generated in the tie rods and flow divider is relatively small, and the entire mass flow rate in the secondary circuit is not required to maintain the desired temperature levels in these components.

Nominal Full-Power Operating Characteristics

The engine dynamics model is based on a variation from steady-state operation. Therefore, the nominal full-power operating conditions (such as heat deposition rates, convection and conduction heat loads, and component specifications) are input values for the model.

The temperature, enthalpy and pressure levels in the primary hydrogen propellant circuit, the secondary hydrogen circuit and the fuel cycle circuit are given in Tables II, III, and IV, respectively. Pressure losses in the fuel cycle circuit were not calculated since detailed design studies of certain components, such as the separator, have not been made.

The specifications and operating conditions in the flow divider, tie rods, and cavity liner are given in Tables V, VI, and VII, respectively. Since these components are cooled by parallel circuits, the sum of their flow rates is equal to 42.3 lb/sec and the mixed-mean outlet temperature is approximately equal to that of the cavity liner. The pressure loss in the flow divider and tie rods is negligible with respect to that in the cavity liner; an orifice or other flow restriction must be used in the tie rod and flow divider flow paths to match the pressure loss in the three components at the desired flow rates.

The specifications and operating conditions for the transparent structure are given in Table VIII. The combined heat load to the transparent structure from both the fuel and the propellant was calculated based on the analysis of Ref. 6.

The specifications and operating conditions in the solid moderator regions are shown in Table IX. The solid moderator is divided into six regions for the engine dynamics analysis since the variation in heat deposition in the six regions is sufficient to require a different coolant hole configuration in each region.

The specifications and operating conditions for the hydrogen-neon and hydrogen-hydrogen heat exchangers are shown in Table X. It is assumed that all heat exchangers were single-pass, counterflow, shell-and-tube configurations with the primary hydrogen propellant flowing in the tubes since its pressure level is approximately 200 atm above the other coolant pressure. The fuel cycle circuit requires only one heat exchanger. The secondary hydrogen circuit requires seven units due to the larger quantity of heat transferred.

ENGINE START-UP STUDY

Preliminary analyses of engine start-up were undertaken to determine (1) the forms of nuclear fuel desirable for start-up and transition to full power, (2) the temperature and flow condition profiles during start-up, (3) the critical mass requirements during start-up, (4) the temperature differentials which may cause thermal stress in sensitive components, and (5) the concepts for control of a start-up sequence.

Sequence of Events

The start-up steps are as follows: (1) close nozzle (it was shown in Ref. 1 that a variable-throat-area nozzle would be necessary to limit the flow rate of propellant during start-up); (2) fill both the hydrogen ducts and the neon system from storage until the neon density is equal to the neon density at the edge of the fuel cloud at nominal full-power operation (0.926 lb/ft^3, or a pressure of 20 atm at 600 R); (3) turn on neon recirculation pump; (4) inject fuel until critical mass is reached; (5) increase power level and adjust flow rates and pressure to maintain criticality and pressure balance throughout the system and to limit component temperatures to desirable levels; (6) inject propellant seeds at about 10 percent of full power (this occurs at an equivalent black-body radiating temperature of 8500 R); and (7) raise power to desired level.

To make the studies tractable, it has been assumed that start-up can be controlled such that power will increase on a linear ramp from zero power to full power (4,600 megw). Three start-up rates were considered; these were linear power ramps rising to 4,600 megw in 1, 5, and 10 min. It was assumed that the fission energy was deposited uniformly in the fuel cloud. Equations were derived which describe the energy balance in a unit cell during the start-up process. At low powers, the loss rate of energy from the fuel region is governed by conduction and convection, with convection being the principal energy loss mechanism, while at high powers, radiation becomes the dominant energy loss mechanism.

Candidate Nuclear Fuel Forms

Three forms of fuel were considered; uranium particles, UF$_6$, and molten uranium. UF$_6$ and particles show merit as start-up fuels, while either particles or liquid uranium appear suitable for full-power operation. All of the fuel forms have physical and chemical properties which must be considered over the ranges of operating conditions in the nuclear light bulb engine. Some of the physical properties were investigated in this study; the influence of chemical properties should be the subject of further investigations.

UF$_6$ vapor pressure data were taken from Ref. 9 and are shown in Fig. 4. In using UF$_6$, one requirement should be that the nuclear fuel feed be heated such that the temperature of the UF$_6$ is always above the boiling point. It will be shown later that the fuel region pressure rises very rapidly during the intial stages of a start-up ramp and, therefore, to insure that the UF$_6$ remains vaporized, it should be heated to 900 R or above. Another factor to be considered in the use of UF$_6$ is its dissociation in the fuel region and the resulting partial pressure of fluorine which adds significantly to the total operating pressure of the engine. Calculations performed at UARL have indicated that, at fuel partial pressures of the order of 200 atm (full-power conditions), UF$_6$ will be totally dissociated at temperatures of about 13,000 R. It is shown later that average fuel temperatures of 13,000 R are reached a few seconds after start-up for even the longest linear power ramp considered. Thus, UF$_6$ should probably be considered only as a low-power start-up fuel form, if at all.

An alternative method for injecting and circulating fuel would be to employ a uranium dust or molten uranium aerosol transported by a carrier gas. If the carrier gas were neon (the gas employed for buffer and bypass flow) an aerosol or dust-to-carrier-gas mass flow ratio greater than two would result in the introduction of fewer non-fuel atoms per atom of nuclear fuel than when UF$_6$ is employed. Fuel-mass-to-carrier-gas flow ratios of six or greater would be most desirable, and the feasibility of achieving these flow rate ratios with nuclear fuels should be investigated further. The melting point for uranium is about 2500 R; therefore, the temperatures in the thru-flow ports exiting from each unit cell must remain above this temperature if molten uranium is to be the fuel form. However, molten uranium is more apt to plate on the recirculation system duct walls than would a cooler, condensed uranium. It is felt that the buffer gas bypass flow which serves to cool the spent fuel and vortex buffer gas as it enters the thru-flow port should be regulated to rapidly cool the uranium to temperatures well below its melting point.

There are little data available on the vapor pressure of uranium at elevated fuel partial pressures and temperatures. However, extrapolations of expressions for uranium vapor pressure near one atm from Ref. 10 indicate that the boiling point of uranium might be about 12,000 R for fuel partial pressures of 200 atm (the average fuel partial pressure in the nuclear light bulb engine is estimated to be 175 to 200 atm in Ref. 2). This means that, in quenching the spent nuclear fuel upon entry into the thru-flow ports, there is a temperature range from about 12,000 R to 2500 R during which the uranium is condensed in a liquid form. To prevent the liquid uranium from plating on the thru-flow duct walls during this period, cold neon bypass flow must be introduced continuously to maintain a steep temperature gradient and to essentially blow the fuel droplets and/or crystals away from the walls.

Start-Up Simulation Model

The model used for simulation of the start-up characteristics of the nuclear light bulb engine differs from that of the engine dynamics model since wide variations in temperatures and flow rates occur during start-up. Furthermore, less detailed information on component operating conditions is required for the preliminary investigation of start-up characteristics. The analysis is divided into three steps; (1) calculation of the variation of average fuel temperature with time; (2) calculation of the operating conditions in the fuel cycle circuit and secondary hydrogen coolant circuit as a function of time; and (3) calculation of the operating conditions in the primary hydrogen propellant circuit as a function of time.

The variation with time of fuel temperature during start-up is the most important factor in the analysis, since the heat transfer mechanism changes during start-up as the fuel temperature changes. During the early phase of start-up, when the average fuel temperature is low (< 10,000 R), the heat is removed from the fuel by conduction and convection to the neon buffer flow and the secondary hydrogen coolant. As the average fuel temperature increases, the fuel radiating temperature increases (fuel radiating temperature is assumed to be one-third of the average fuel temperature) and the amount of heat transferred by radiation increases. When the average fuel temperature reaches 15,000 R (fuel radiating temperature = 5000 R), the radiation heat transfer becomes dominant and the percentage of the total heat transferred by radiation approaches that during full-power operation.

The assumptions used in the start-up studies are: (1) the entire engine is initially at 600 R; (2) all of the heat removed in the fuel cycle circuit and the secondary hydrogen circuit is transferred to the primary hydrogen propellant circuit; (3) only the heat storage capacity of the neon and fuel in the cavity and the heat storage capacity of the solid moderator are considered in calculating temperature levels; and (4) the residence times in the various components are small relative to the length of the start-up ramp, and may be neglected. The sequence of events during start-up are listed in Table XI.

Calculation of Fuel Temperature During Start-Up

The variation of fuel temperature during start-up is based on a heat balance in the cavity region. It is assumed that the fuel injection rate would be controlled to produce a linear power ramp. The heat generated in the cavity is equal to the total power less the neutron and gamma ray heating (0.89 x total power). The heat generated in the cavity must be balanced by the sum of six heat storage and heat loss terms: (1) the heat stored in the fuel; (2) the heat stored in the neon; (3) the conduction and convection heat loss from the fuel; (4) the conduction and convection heat loss from the neon; (5) the conduction and convection heat loss to the transparent structure; and (6) the radiation heat loss. The resulting differential equation is of the form:

$$\frac{dT_F}{dt} = At - BT_F - CT_F^4 \qquad (1)$$

where:

T_F = average fuel temperature, deg R

t = total elapsed time since initiation of start-up, sec

In this equation, the first term in the expression for dT_F/dt is related to the heat generation, the second term is related to the conduction and convection heat losses, and the third term is related to the radiation heat loss. The value of the constant A varies with the slope of the power ramp. The constant B is on the order of 10^{-1} and the constant C is on the order of 10^{-13}. For a particular power ramp, the third term may be neglected if T_F is small (< 2000 R). Initial values of T_F and dT_F/dt may be found by direct integration of Eq. (1) with the third term eliminated. After determining T_O and dT_F/dt during the initial start-up phase, the complete equation may be solved over the entire start-up period by forward difference methods.

The variation of average fuel temperature during start-up is shown in Fig. 5 for three selected start-up times. The fuel temperature rises rapidly during the first 2 to 5 percent of the start-up time. During this period the radiation heat transfer is small. When the radiation heat transfer becomes dominant, the rate of increase in fuel temperature becomes proportional to the fourth root of time (or the fourth root of the power level, since power level is directly proportional to time) and the engine behaves in a manner similar to that of a ramp perturbation at full power.

The variation of the fuel temperature with time is approximated by two equations of the form

$$T_F = Dt^m \qquad (2)$$

where m is approximately 1.0 during the initial phases of start-up and 0.25 during the later phases. These expressions for fuel temperature are used to calculate the heating and temperature levels in the full cycle circuit and in the secondary hydrogen circuit.

Fuel Cycle Circuit Conditions

The heat deposited in the fuel cycle is due to conduction and convection heating of the fuel and neon in the cavity and fission product decay heating. It is assumed that all of the heat in the fuel cycle would be deposited in the primary hydrogen propellant in the hydrogen-neon heat exchanger (the product of the flow rate and specific heat in the primary hydrogen propellant is always larger than that of the fuel cycle circuit).

The fuel flow rate is determined by the desired power ramp, and the desired neon flow rate is determined by the neon density required at the edge of the fuel. At 600 R the initial cavity pressure necessary to maintain an edge-of-fuel neon density of 0.924 lb/ft^3 is 20 atm. As the cavity temperature increases the pressure must also increase to maintain the constant density. The required neon flow rate in the cavity is calculated from the expressions later developed later for engine dynamics studies (Eq. (10)) and the quantity of neon bypass flow is calculated on the basis of a 2650 R mixed-mean outlet temperature. The total neon flow rate required during start-up is shown in Fig. 6 for the three start-up ramps investigated. The neon flow rates were assumed to reach their steady-state operating value at the end of the start-up power ramp. Since the fission product decay heat is a function of time, as shown in Fig. 3, it will not reach the value used in the steady-state calculations until after the termination of the start-up ramp. The outlet temperatures in the fuel cycle circuit will, therefore, gradually increase to the steady-state value of 2650 R during full-power opearation. If it is desirable to smooth out the variation of flow rate with time, the neon flow rate may exceed the values shown in Fig. 6, but they may not be less than those shown without increasing fuel loss rates and affecting the stability of the vortex. The total flow of neon buffer gas required is 24.5 lb/sec, and any additional flow bypasses the cavity.

Secondary Hydrogen Circuit Conditions

The heat deposition in the secondary circuit is calculated using the equations developed in the dynamic analysis for the conduction, convection, and radiation heat loads to the transparent structure and cavity liner. The neutron and gamma ray heating in the secondary circuit is relatively small during the initial phases of start-up and was neglected. It was determined that an initial hydrogen flow rate of 4.23 lb/sec with a linear increase with time during start-up would be sufficient to eliminate the possibility of exceeding the temperature limits in the transparent structure.

It is assumed that all of the heat deposited in the secondary hydrogen circuit would be transferred to the primary hydrogen propellant in the hydrogen-hydrogen heat exchanger.

Primary Hydrogen Propellant Circuit Conditions

The model of the primary hydrogen propellant circuit consisted of the primary pump, two heat exchangers, the turbine, a BeO moderator region, a graphite moderator region, and the cavity region. The temperature rise in the heat exchangers is calculated from the heat rejected from the fuel cycle and secondary hydrogen circuits, and the temperature changes in the primary pump and turbine are calculated from the turbopump equations. The large mass of moderator material has a considerable heat capacity which must be considered in these regions. The effect of this heat capacity is to cause a lag in the moderator temperature relative to the fuel temperature rise. During a large portion of the start-up transient (about 60 percent), the primary hydrogen propellant is heating the moderator material rather than removing heat. The average temperature in the BeO and graphite regions are shown in Figs. 7 and 8, respectively. Although the propellant inlet temperature does not rise as rapidly as the fuel temperature due to the heat capacity of the moderator, the propellant outlet temperature follows the fuel temperature more colsely due to the radiation heating in the cavity. The variation of propellant outlet temperature with time for the three start-up ramps is shown in Fig. 9.

As previously discussed, the pressure in the cavity must increase with the temperature in order to maintain the required edge-of-fuel density. The cavity pressure during start-up is shown in Fig. 10. In order to avoid pressure differentials in the transparent structure, the propellant pressure (and, therefore, the pressure throughout the engine) must follow cavity pressure. This is accomplished by varying the nozzle throat area during start-up.

Once the flow rate, temperature, and pressure levels in the propellant circuit have been determined, the variation in nozzle throat area which is consistent with these conditions may be calculated. The nozzle throat flow parameter can be determined from Ref. 11 and the known values of flow, temperature, and pressure can be used to find the throat area. The required nozzle throat area for the three start-up ramps is shown in Fig. 11. The reason for the decrease in nozzle flow area in the initial phases of start-up is the lag in propellant temperature relative to propellant pressure. If the pressure increases at a relatively constant propellant temperature, the nozzle area must be reduced to maintain a linear increase in flow rate.

Critical Mass During Start-Up

Critical mass requirements using U-233 nuclear fuel were calculated for the 60 sec and 600 sec start-up ramps using a one-dimensional spherical model of the full-scale engine configuration. The criticality calculations were performed using the cross section energy group structures and nuclear codes employed in the analysis of Ref. 2.

The results of the critical mass calculations are shown in Fig. 12. For cases in which the length of the start-up ramp is short (60 sec start-up) relative to the moderator heating time (200 to 300 sec), the critical mass rises to a value of 28.2 lb when full power is reached and then approaches the asymptotic full-power critical mass of 30.9 lb at t $\cong$ 300 sec. This lag in reaching steady-state critical mass is attributed to the lag in bulk moderator temperatures reaching their asymptotic values.

Critical mass requirements during a longer start-up ramp (600 sec) increase throughout the start-up period and reach a maximum value when full-power conditions are reached. In this case, moderator temperatures reach their asymptotic values at approximately the same time that full power is reached because the start-up time is long relative to the moderator heating time. Thus, there is no lag in reaching the asymptotic, full-power critical mass.

Fuel weight flow requirements during start-up were calculated using the results of the criticality calculations in the neutron kinetics equations assuming that: (1) power level was directly proportional to the neutron level; (2) the average fuel residence time of 20 sec (i.e., λ_F = 0.05 sec^{-1}) was constant throughout start-up; and (3) contributions to neutron levels by delayed neutron precursors during start-up could be neglected. Under these assumptions, the neutron level equation can be written at any point during the start-up ramp as

$$\frac{dn}{dt} = \frac{dP}{dt} = \frac{\delta k - \beta}{\ell^*} n \tag{3}$$

Eq. (3) was solved for δk, and the amount of excess fuel loading required to provide the excess reactivity was obtained from the values of $(\delta k/k)/(\Delta M/M)$ from the criticality calculations. The fuel weight flow profiles required to maintain the assumed linear power ramps for start-up are shown in Fig. 13. The excess fuel weight flows to sustain the assumed start-up power ramps were less than 1 percent of the total weight flows shown in Fig. 13.

Results of Start-Up Studies

General Engine Response

The response of the engine to the three linear power ramps is basically similar as shown in Figs. 5 through 10. There is a rapid increase in fuel temperature during the early phase of start-up when the heat transfer by radiation is small. This rapid temperature rise must be accompanied by a rapid pressure rise to maintain a high neon buffer gas density so that the vortex flow will remain stable. The turbopump unit must be capable of providing sufficient head rise to follow the required pressure variation shown in Fig. 10.

The major difference in the response to the various start-up ramps is in the average temperature of the solid moderator regions. The heat capacity of the solid moderator caused a considerable lag in the moderator temperature relative to the fuel and propellant temperature. The amount of energy required to bring the solid moderator regions from an initial temperature of 600 R to their nominal, full-power operating temperature is on the order of 3×10^7 Btu. The heat generation rate in the solid moderator at full-power operating conditions is on the order of 2×10^5 Btu/sec, so that the average heat generation during a linear power ramp is of the order of 10^5 Btu/sec. Based on the average heat deposition rate during a linear power ramp, the solid moderator regions would require approximately 300 sec to reach nominal, full-power operating conditions. It may be seen from Figs. 7 and 8 that, for a 60-sec start-up ramp, the BeO and graphite regions reach their nominal full-power value 200 to 300 sec after start-up, and a similar length of time would be required for any ramp of less than 300 sec.

The total quantity of hydrogen expended during start-up varies directly with the length of the start-up ramp. For a 60-sec start-up time, a total of 1400 lb of hydrogen is expended during start-up. This quantity of hydrogen is equal to the amount of hydrogen expended during 33 sec of full-power operation, and is negligible when compared to the hydrogen consumed in a 20-min operating period. For a 600-sec start-up time, 14,000 lb of hydrogen would be expended; this is equivalent to 5.5 min at full power and would necessitate a 27 percent increase in the amount of hydrogen required for 20 min of engine operation at full power. From this standpoint, the shorter start-up times are preferable.

Auxiliary Power Requirements for Start-Up

A comparison of the turbopump characteristics with the pressure and flow requirements during start-up indicated that there is insufficient power available during the initial phases of start-up to provide for the pumping requirements and to overcome the inertia of the turbopump unit. Approximately 405,000 Btu are required to bring the turbopump unit up to the design wheel speed of 22,000 rpm and, considering

the pressures required (Fig. 10), the turbopump unit must be up to 60 percent of design wheel speed within the first 3 percent of the start-up time. Since the engine power level at this time is insufficient to provide the pumping power, an alternative method of providing the required flow rates and pressure levels is required.

A method considered for providing pumping power is a chemically powered turbine unit which would produce sufficient energy to bring the turbopump up to its nominal wheel speed prior to the injection of fuel in the engine. Such a system could use a portion of the stored hydrogen and cryogenically stored or liquid oxidizer. The size of the turbine would be dependent upon the time allowed to bring the turbopump unit up to nominal speed. Once the turbine is rotating at nominal wheel speed, its inertia would be sufficient to provide power for the steep pressure rise and to sustain the desired flow rate until the energy released in the engine was sufficient to provide the necessary pumping power.

Temperature Differences in Specific Components

The temperature responses of the various engine components were applied to the physical characteristics of the engine design to determine if thermal stress problems would be encountered during start-up. The principal regions which were studied were the solid moderator, the cavity liner, and the transparent structure.

The solid regions do not experience any rapid temperature variations due to their high heat storage capacity. The solid moderator and the structural components in these regions, such as the tie rods and flow dividers, would not be subjected to any rapid temperature variations or large temperature differentials.

The cavity liner is heated by convection from the propellant. A rapid increase in this heat load occurs during the early phases of start-up. In the present design of the cavity liner, the tubes which comprise the liner are U-shaped so that the coolant enters and exits the liner at the upper end of the engine (the accessory end). The lower end of the tubes is not fixed so that differential growth of the liner relative to the moderator is permitted, and no stesses would be experienced due the difference in moderator and cavity liner temperature. There will be some thermal stress in the tubes due to the fact that the inlet leg of the tube will be at a lower temperature than the outlet leg. The thermal stress resulting from this situation will be the greatest at the full-power operating condition.

The heat load to the transparent structure primarily consists of a radiation heat load from the cavity side and a convective heat load from the propellant side. At the nominal full-power operating conditions, the Stanton number in the propellant region must be reduced to minimize the heat load from the propellant. The pro-

pellant temperature is proportional to the fuel radiating temperature, and the lag in propellant temperature relative to fuel radiating temperature is small in all cases (1 to 2 sec). The radiant heat load to the transparent wall is proportional to the fourth power of the radiating temperature; the convection heat load from the propellant is proportional to the product of the fourth power of the radiating temperature and the Stanton number. The Stanton number may be expressed as

$$St = \frac{0.023}{(Re)^{0.2}(Pr)^{2/3}} \tag{4}$$

For a constant Prandtl number and constant geometry, the Stanton number can be expressed as:

$$St = K\left(\frac{\mu}{W}\right)^{0.2} \tag{5}$$

where

μ = viscosity, lb/ft sec

W = flow rate, lb/sec

K_D = constant dependent upon geometry, ft$^{0.2}$

The minimum value of the Stanton number will occur at full-power conditions and the maximum value will occur at the beginning of the start-up. The maximum value calculated is 1.34 times the minimum value. The maximum Stanton number occurs during the early phases of start-up when the heat fluxes are low and the thermal stresses in the transparent structure should be small throughout the start-up regardless of the duration of the ramp.

Since there appears to be no large temperature differentials generated during the shortest start-up time investigated and since auxiliary power is required for all start-up ramps, additional investigations of start-up ramps of 6 to 10 sec duration should be made.

ENGINE DYNAMICS STUDY

A mathematical model of the nuclear light bulb engine was developed for the purpose of investigating the stability of the engine, determining the control requirements at full-power operating conditions, and predicting the transient response of the reactor to selected perturbations. The model is a UNIVAC 1108 digital-computer simulation of the thermal, fluid dynamics and neutron kinetics equations. Due to the complexity of the system, the thermal and fluid dynamics model and the neutron kinetics model were developed separately by treating the factors which would be feedbacks from one system to the other as input parameters. In this manner, the response of each of the systems to specific perturbations could be investigated without encountering the coupling effects of multiple feedbacks. After each system of equations had been checked in this manner, the systems were combined. The complete model is based on the basic engine design described in Ref. 1 with some modifications which resulted from revisions in moderator configuration, heat deposition rates and changes in the moderator cooling sequence.

The details of the engine dynamics model are divided into discussions of the thermal and fluid dynamics model and the neutron kinetics model. The results of the initial engine dynamics studies are then presented, and preliminary concepts for engine control are discussed.

Thermal and Fluid Dynamics Model

The thermal and fluid dynamics model is used to calculate the transient response of reactor temperature and pressure levels to variations in reactor power. The power variations are calculated from the neutron kinetics model; the predicted temperature and pressure levels are then used to generate the various reactivity feedback coefficients in the neutron kinetics model. The thermal and fluid dynamics model is a finite difference approximation of the transient heat transfer and fluid flow equations which result from an analysis of the engine configuration previously discussed (see section entitled NUCLEAR LIGHT BULB ENGINE DESIGN). The model consists of three major parts: (1) the temperature equations; (2) the fuel-containment parameters; and (3) the flow and pressure equations.

Temperature Equations

The calculation of temperature levels throughout the engine was divided into three parts corresponding to the three coolant circuits in the engine (see Fig. 2). These three circuits are interconnected by the heat exchangers. The initial investigations of temperature response to power variations were conducted for each circuit separately by assuming that all of the heat generated in the fuel cycle circuit and the secondary hydrogen circuit would be transferred through the heat exchangers.

The basic technique employed to investigate the time response of coolant temperatures is a finite-difference approximation of the percent change in heat rejected to the coolant with time. As an example, if a 10 percent positive step change in power level is assumed to occur in a particular component at time $t = t_o$, the final converged value of the coolant temperature rise in that component should be 110 percent of the nominal full-power temperature rise in that component. This final value will not be attained until the fluid which entered the component at $t = t_o$ reaches the outlet of the component. There is, therefore, a coolant residence time associated with each component which is determined by the coolant mass flow rate and the geometry of the coolant passages. The variation of the coolant temperature rise with time in a particular component may be approximated by the equation

$$\Delta T = (\Delta T)_0 \left(1 + \sum_{i=1}^{\frac{\tau_R}{\Delta t}} \frac{\delta P}{P_0} \frac{\Delta t}{\tau_R} \right) \tag{6}$$

where

ΔT = temperature difference at any time t, deg R

$(\Delta T)_o$ = steady-state temperature difference $(t = 0)$, deg R

Δt = time increment, sec

τ_R = residence time in component, sec

$\delta P/P_o$ = percentage change in power (current value of power perturbation divided by steady-state power)

Equation (6) yields an estimate of the current value of temperature rise by taking the summation of the percentage changes in power level which have occurred during the preceding $\tau_R/\Delta t$ time increments. The number of terms in the summation is equal to the number of time increments in the component residence time.

Equation (6) may be further generalized by substituting

$$\Delta T = T_{OUT} - T_{IN} \tag{7}$$

$$(\Delta T)_0 = Q_0 / W C_p \tag{8}$$

where

T_{out} = outlet temperature from component, deg R

T_{in} = inlet temperature to component, deg R

Q_0 = steady state heat generation rate in component, Btu/sec

W = coolant mass flow rate, lb/sec

C_p = specific heat of coolant, Btu/lb-deg R

Equation (6) becomes:

$$T_{OUT} = T_{IN} + \frac{Q_0}{W C_p} \left(1 + \sum_{i=1}^{\frac{\tau_R}{\Delta t}} \frac{\delta P}{P_0} \frac{\Delta t}{\tau_R} \right) \tag{9}$$

Since the components in any circuit are cooled in series, Eq. (9) may be applied to each component in sequence and the outlet temperature of one component is substituted for the inlet temperature of the next component in the following time step.

Referring to the example previously mentioned, if a 10 percent positive step change in power is assumed, the value of $\delta P / P_0$ in Eq. (9) would be constant, 0.10. If it is further assumed that τ_R in the particular component being investigated is equal to $4 \Delta t$, then, $\Delta t / \tau_R$ will be equal to 0.25, and the summation would be taken over four time increments. The value of the summation would be 0.025 after the first time step since there is no power variation before t_0 and the three preceeding values of $\delta P / P_0$ would be zero. After four time steps the value of the summation would reach 0.10 and, since the number of terms in the summation remains constant, it would remain at 0.10 as long as the power perturbation is present.

This technique was employed for the prediction of temperatures throughout the engine with appropriate terms for $\delta P/P_o$ depending upon the heat capacity of the component and whether or not the heat deposition is directly proportional to power changes. The actual values used in the summations for each component are noted in the discussions of the various coolant circuits below. The summation-type expression of Eq. (9) may be used for any desired power variation and, in the combined program, a current value of $\delta P/P_o$ is calculated for each time step from the neutron kinetics portion of the program.

It should be noted that there must be an integral number of terms in each summation so that the value used for the term $\tau_R/\Delta t$ is the closest integral number; the value of $\Delta t/\tau_R$ used in the summation will be the reciprocal of this integer. Actually, τ_R is not necessarily an integral number of time increments and it can vary with the mass flow rate in the component. The variations which may be caused by these factors were investigated and it was determined that if the time increments are small relative to the coolant residence times, no appreciable error is introduced by making τ_R an integral number of time increments. It was also determined that the change in coolant residence time with coolant flow rate could be neglected for small changes in flow rate. The effect of a small change in residence time on the value of the summation is negligible relative to the change in the term Q_o/WC_p in Eq. (9) caused by a change in flow rate. Therefore, it was assumed that the coolant residence times at the nominal full-power operating conditions would be considered as constant during the transient analysis for small changes in flow rate (10 percent or less) and that a constant time increment would be used in any particular analysis to eliminate the requirement for recalculating the value of $\tau_R/\Delta t$ during the analysis.

Subsequent analysis of the turbopump equations indicated that the momentum of the turbopump was large and would tend to maintain constant coolant flow rates regardless of the type of perturbation introduced.

Fuel Cycle Circuit

The fuel cycle circuit includes the fuel injection circuit and the neon buffer gas circuit. The total mass flow of fuel in the circuit is a relatively small part of the total neon and fuel flow (approximately 8 percent) and its contribution to the temperature conditions in the circuit was approximated by an equivalent neon flow rate which was added to the actual neon flow between the cavity inlet and the fuel separator. The neon flow is divided into two parts, the neon buffer flow which passes through the cavity and drives the vortex, and the bypass neon flow which is mixed with the neon buffer flow as it leaves the cavity. The general characteristics of the neon flow and the fuel region are discussed in Ref. 1. The assumptions used in determining the required neon buffer flow rates are (1) an axial velocity of the

neon buffer flow at the edge of the fuel of 1.95 ft/sec in the vicinity of the end walls, (2) a constant dynamic pressure across the neon buffer layer, (3) a linear temperature gradient between the neon buffer flow inlet and the edge of the fuel, and (4) the neon buffer flow follows the perfect gas law. Based on these assumptions and a constant fuel radius, the required neon buffer flow may be determined by integrating the product of neon density and velocity over the thickness of the buffer layer. The resulting expression for neon buffer flow rate is

$$W_B = \frac{1.36 \sqrt{p_c}}{\left(\frac{1}{T_N} - \frac{1}{T^*}\right)^2} \left\{ 0.4\left[\left(\frac{1}{T_N}\right)^{1.5} - \left(\frac{1}{T^*}\right)^{1.5}\right] - 0.666\left[\frac{1}{T^*} - 6.5\left(\frac{1}{T_N} - \frac{1}{T^*}\right)\right] \times \right.$$
$$\left. \left[\left(\frac{1}{T_N}\right)^{2.5} - \left(\frac{1}{T^*}\right)^{2.5}\right] \right\} \tag{10}$$

where

W_B = neon buffer flow per cavity, lb/sec

p_c = cavity pressure, atm

T_N = inlet temperature of neon buffer flow, deg R

T^* = fuel radiating temperature, deg R

The total heat transferred to the neon buffer flow by conduction and convection is

$$Q_B = 0.483 \, W_B \, C_p \, (T^* - T_N) \tag{11}$$

where

Q_B = total heat transferred for cavity, Btu/sec

C_p = specific heat of neon, Btu/lb-deg R

The conduction and convection heating, the heat due to fission product decay and the heat contained in the entrained fuel determine the temperature of the neon-fuel mixture leaving the cavity. In order to condense the fuel so that it can be separated from the neon, the temperature of the mixture must be reduced to approximately 2650 R. This is accomplished by the addition of more neon which has bypassed the cavity. The quantity of bypass neon flow required is based on a bypass neon temperature of 200 R and a mixed-mean temperature of 2650 R in the combined bypass and buffer flow.

It is assumed that all changes in heat deposition in the cavity occur instantaneously and no appreciable heat storage capacity exists in this circuit. The only time lags used in the fuel cycle circuit are the time delays which exist as a result of the piping between the cavities and the hydrogen-neon heat exchangers. After rejecting heat to the primary hydrogen propellant, the neon passes through a pump and then is returned to the cavity region.

Secondary Hydrogen Coolant Circuit

The secondary coolant circuit analyzed in the dynamic model is simplified from that shown in Fig. 2 by considering the pressure vessel, nozzles, and end walls as a single component and combining the cavity liner, flow divider, and tie rods into a single component.

The majority of the heat deposited in the secondary circuit (about 85 percent) is from conduction, convection, and radiation to the cavity liner and transparent structure. These heat loads are, therefore, functions of fuel radiating temperature or propellant temperature rather than a direct function of operating power level. The only component in the secondary circuit which has a heat deposition rate and a coolant temperature rise which is directly proportional to power level is the pressure vessel. Consequently, the transient temperature equation of the form of Eq. (9) was applied to the pressure vessel, and a modified form of Eq. (9) was applied to the cavity liner and transparent structure. The modified equation is

$$T_{OUT} = T_{IN} + \frac{1}{W c_p} \left(Q_0 + \sum_{i=1}^{\frac{\tau_R}{\Delta t}} \frac{\delta Q}{Q_0} \frac{\Delta t}{\tau_R} \right) \tag{12}$$

where

$\frac{\delta Q}{Q_0}$ = percentage change in heat deposited (current value of variation in heat deposition divided by the steady state heat deposition)

Q_0 = steady state heat deposition, Btu/sec

Expressions for the heat deposited in the transparent structure and the cavity liner were based on the analysis of Ref. 6. The radiation heat load to the transparent structure is a function of fuel radiating temperature and the absorption coefficient of the transparent structure. If the fuel radiating temperature is between 10,000 R and 15,000 R, the heat deposition in the transparent structure is proportional to the fourth power of the fuel radiating temperature ($Q = K_1 T*^4$). If the fuel

radiating temperature is between 15,000 R and 20,000 R, the heat deposition is proportional to the ninth power of the fuel radiating temperature ($Q = K_2 \, T*^9$). In order to consider this effect, two equations for the total heating in the transparent structure were used:

$$Q_{TW} = 0.423 \, (T* - 2000) + 1.029 \times 10^{-12} \, T*^4 + 8.98 \times 10^{-13} \, T*^4 + 10,200 \, \frac{P}{P_0} \qquad (13a)$$

$$T* \leq 15,000 \, R$$

$$Q_{TW} = 0.423 \, (T* - 2000) + 1.029 \times 10^{-12} \, T*^4 + 1.18 \times 10^{-33} \, T*^9 + 10,200 \, \frac{P}{P_0} \qquad (13b)$$

$$T* > 15,000 \, R$$

where in each equation the first term represents heat conducted from the fuel, the second term represents heat convected from the propellant, the third term represents radiation from the fuel, and the fourth term represents the internal heat generation.

A similar expression for the heat deposited in the cavity liner is

$$Q_{LT} = 1.435 \times 10^{-12} \, T*^4 + 16,152 \, \frac{P}{P_0} \qquad (14)$$

where the first term is the convection heating and the second term is the internal heat generation. Current values of Q based on values of T* and P are used to calculate the percentage variation in heat deposited, $\delta Q/Q_0$. These values of $\delta Q/Q_0$ are used in the transient equation (Eq. (12)) to introduce the lag due to coolant residence time. Additional time lags between the heat exchangers and the cavity region were included in the calculation of the circuit response.

Since the components in the secondary circuit have a relatively small mass, it was assumed that there would be no heat storage capacity effects in this circuit.

Primary Hydrogen Propellant Circuit

All of the components of the primary hydrogen propellant circuit, as shown in Fig. 2, were included in the dynamic model. The solid moderator component was divided into six regions: (1) upper-end graphite, (2) upper-end BeO, (3) axial BeO, (4) lower-end BeO, (5) lower-end graphite, and (6) axial graphite.

The heat deposited in the fuel cycle and secondary hydrogen circuits is transferred to the primary hydrogen propellant in the two heat exchangers. The heat transferred in the heat exchanger may be expressed in the form

$$Q_{TRANS} = K_H \, C_H \, \overline{\Delta T} \qquad (15)$$

where

Q_{trans} = heat transferred in the heat exchanger, Btu/sec

K_H = constant dependent upon heat exchanger configuration (i.e, number of tubes and tube diameter), $ft^{0.2}$

C_H = constant dependent upon fluid properties (Prandtl number, thermal conductivity, viscosity and flow rate), Btu/sec-$(ft)^{0.2}$-deg R

$\overline{\Delta T}$ = average temperature difference between fluids, deg R

Since the heat transferred, determined from the above equation, is added to one fluid and extracted from the other, the outlet temperature in the primary hydrogen propellant circuit (T1025, for example, see Fig. 2) may be calculated from the inlet temperature of the primary hydrogen propellant (T1020) and the inlet temperature of the secondary hydrogen circuit (T2040). The procedure used in the program was to calculate the inlet temperatures from the fuel cycle circuit (T3030) and the secondary hydrogen circuit (T2040) at the end of the first time step and to use these values to calculate the primary hydrogen propellant temperatures (T1015 and T1025, respectively) during the subsequent time step. A similar procedure was used to predict the heat exchanger outlet temperatures in the fuel cycle and secondary hydrogen circuit so that variations in heat exchanger performance would be included in the transient responses.

The solid moderator regions of the primary hydrogen propellant circuit contain a large mass of material, and the effects of heat storage capacity must be included in the transient equations. The average temperature in the moderator material may be calculated by combining the average coolant temperature, the coolant-to-wall temperature difference, and the internal temperature difference. The coolant-to-wall temperature difference is calculated by the analysis of Ref. 12 and the internal temperature difference for an internally cooled solid is calculated from Ref. 13.

The simulation of components with appreciable heat storage capacity and internal heat generation requires a modified form of Eq. (9) in which the change in internal temperature is considered. Assuming that the physical properties of the moderator are constant over the range of temperatures experienced in any transient, the effect of the heat storage capacity can be accounted for by the addition of a term which is proportional to the percentage change in the average temperature of the component. The revised equation used is of the form

$$T_{OUT} = T_{IN} + \frac{Q_0}{WC_p} \left\{ 1 + \sum_{i=1}^{\frac{\tau_R}{\Delta t}} \left[\frac{\delta P}{P_0} - \frac{\delta T_m}{(T_m)_j} \right] \frac{\Delta t}{\tau_R} \right\} \qquad (16)$$

where

δT_m = change in average moderator temperature, deg R

$(T_m)_j$ = average moderator temperature from previous time increment, deg R

Thus, if $\delta P/P_0$ is positive, $\delta T_m/(T_m)_j$ will also be positive, and the effect of the power change on coolant temperature rise will be reduced by the quantity of energy necessary to raise the average moderator temperature. If a new equilibrium temperature is reached, as in a sustained step change in power, $\delta T_m/(T_m)_j$ will eventually become equal to zero. The coolant temperature rise will reach the same value as would be calculated from Eq. (9), but the total time lag will be longer. The effect of moderator mass and specific heat in each region are included in the equations used to calculate $\delta T_m/(T_m)_j$.

Fuel Containment Parameters

Containment of a heavy gas (such as nuclear fuel) in a light-gas vortex flow field depends upon many parameters including the buffer-gas injection geometry and tangential velocity, the position of heavy-gas injectors, the dynamic pressure of the buffer and heavy gases at injection, the heavy-gas-to-buffer gas weight flow ratio, and the buffer-gas bypass flow. However, for a fixed-geometry vortex chamber with constant-area gas injectors and a fixed buffer-gas bypass flow fraction, the principal factors effecting heavy gas containment are the buffer gas density at the edge of the fuel cloud and the ratio of fuel-to-buffer-gas weight flow.

In the nuclear light bulb engine, the buffer gas density is effected by the edge-of-fuel temperature (approximately 80 percent of the equivalent black-body radiating temperature) and the chamber pressure in accordance with the ideal gas

law. Experimental results from isothermal two-component gas vortex tests have indicated that heavy-gas containment is related to the ratio of simulated fuel weight flow to buffer gas weight flow according to

$$\bar{\rho}_F / \rho_B = \left(\frac{W_F}{W_B} \right)^{1.2} \tag{17}$$

The empirical relationship expressed by Eq. (17) was obtained by fairing curves through the experimental data reported in Refs. 4, 14, 15, and 16. More recent investigations indicate that the weight-flow-ratio exponent may be as low as 0.9 (Ref. 4). However, for the small perturbations used in this study, the effect of this variation in the exponent is relatively insignificant. On the basis of buffer gas density and weight flow containment parameters, the steady state stored mass of nuclear fuel can be expressed by

$$M_F = K_M \frac{p_C}{T^*} \left(\frac{W_F}{W_B} \right)^{1.2} \tag{18}$$

where K_M is a constant of proportionality. An expression for W_B is shown in Eq. (10). Expressions for chamber pressure, p_c, equivalent black-body radiating temperature, T^*, and fuel weight flow rate, W_F, are discussed later. The methods by which heavy-gas containment parameters are introduced into the expression for variations of stored nuclear fuel with time are also discussed in a later section.

Flow Rates and Pressure Losses

The pumping power required in the engine is provided by a turbopump unit consisting of a single turbine located in the primary hydrogen propellant circuit and separate pump units for the primary hydrogen propellant, the secondary hydrogen circuit, the neon circuit, and the fuel injection circuit. Detailed studies of a turbopump specifically designed for the nuclear light bulb engine have not been made. It was assumed in the dynamics model that the characteristics of the turbopump would be similar to the turbopump units which were designed for the open-cycle engine described in Ref. 17 using a single unit rather than four units. The major design variables used in the dynamic model were a moment of inertia for the turbopump disc of 130 ft-lb-sec^2 and a nominal full-power wheel speed of 22,000 rpm. It was assumed in the dynamics model that the flow rates in the turbopump would be directly

proportional to wheel speed, and that the pressure rise in the pumps would be proportional to the square of the wheel speed. The variations in turbopump wheel speed with the turbine and pump requirements are, from Ref. 18,

$$\frac{I}{2} \frac{d\nu^2}{dt} = Q_T - \sum_{i=1}^{4} (Q_P)_i \qquad (19)$$

where

I = moment of inertia of turbopump disc, ft-lb-sec^2

ν = wheel speed, radians/sec

Q_T = turbine output power ft-lb/sec

$\sum (Q_P)_i$ = summation of pump power requirements, ft-lb/sec

At nominal full-power operating conditions

$$Q_T = \sum_{i=1}^{4} (Q_P)_i \qquad (20)$$

and there is no change in wheel speed. The majority of the pumping power requirement is in the primary hydrogen propellant pump; the summation of all pumping power requirements was estimated to be 1.1 times the primary hydrogen propellant pump requirement.

The variation in wheel speed with time was determined from Eq. (19) using current values of turbine power and pumping power from the appropriate circuit temperature equations. New values of flow rate and pressure rise were then calculated from the relationships

$$W = W_0 \frac{\nu_0 + \delta\nu_1 + \delta\nu_2}{\nu_0} \qquad (21)$$

$$\Delta P = (\Delta P)_0 \frac{(\nu_0 + \delta\nu_1 + \delta\nu_2)^2}{\nu_0^2} \tag{22}$$

where

ν_0 = steady-state wheel speed, rpm

$\delta\nu_1$ = input perturbation to wheel speed (where applicable), rpm

$\delta\nu_2$ = feedback perturbation to wheel speed (from Eq. (19)), rpm

Since the wheel speed is high, the momentum of the turbopump tends to damp out variations in flow or pump pressure rise.

The pressure levels in the primary hydrogen propellant circuit and the secondary hydrogen circuit are given in Tables II and III, respectively. The pressure losses in all of the components are a combination of frictional losses and expansion and contraction losses. Assuming that all passages are smooth, the pressure losses may be expressed as

$$\Delta P = K_1 W^2 + K_2 W^{1.8} \tag{23}$$

where

ΔP = component pressure loss

W = coolant flow rate in component

K_1 & K_2 = constants based on flow passage geometry and coolant properties

The total pressure losses due to friction, expansion and contraction losses are 10 atm in the primary hydrogen propellant circuit and 12 atm in the secondary hydrogen circuit.

Neutron Kinetics Model

The principal unusual factor in the kinetic behavior of a nuclear light bulb engine is that the nuclear fuel is injected continuously into the active core volume. Experimental results for constant-temperature gas vortex tests indicate that the average residence time of nuclear fuel in a full-scale nuclear light bulb engine would probably be on the order of 20 sec. If this is the case, then delayed neutron precursors which emit delayed neutrons at time periods greater than 20 sec after the fission event would contribute essentially no neutrons to the active volume of the reactor core. This problem is quite similar to that for circulating-fuel reactors; the important difference is that compressible gases are employed in a nuclear light bulb engine, whereas in the circulating-fuel reactors, the fuel solution is an incompressible liquid. Due to compressibility, it is possible to have fluctuations in total fuel loadings which result from fluid dynamic fluctuations in the heavy-gas residence time. Thus, both the fraction of delayed neutrons which are lost from the active core and the total mass of nuclear fuel within the active core will vary with time. These are primary considerations in the overall control of the engine.

Neutron Kinetics Equations

The expression describing the dependence of nuclear light bulb power level on the product of neutron level, fission cross section, and mass of nuclear fuel is given by

$$P = M_F \, \sigma_f \, n \tag{24}$$

where M_F is the nuclear fuel mass, σ_f is the average fission cross section, and n is the neutron level. The average fission cross section varies with average moderator temperature as

$$\sigma_f = \sigma_{f_0} - 0.183 \, \frac{\Delta T_m}{T_{m_0}} \tag{25}$$

The variation of σ_f with moderator temperatures was taken from Ref. (2). The equations describing the space-independent kinetics of the neutron level are:

$$\frac{dn}{dt} = \frac{\delta k - \beta}{l^*} \, n + \sum_{i=1}^{6} \lambda_i C_i \tag{26}$$

$$\frac{dC_i}{dt} = \frac{\beta_i}{\ell^*} n - (\lambda_i + \lambda_F) C_i \tag{27}$$

Neutron level in Eq. (26) is affected by a time varying reactivity coefficient, δk, and by the concentrations of delayed neutron precursors, C_i. The time behavior of the six groups of delayed neutron precursors is described by Eq. (27), in which it is assumed that the delayed neutron precursors have the same residence time as the nuclear fuel. Thus, variations in the nuclear fuel residence time, $1/\lambda_F$, result in variations in the fraction of delayed neutrons emitted in the active core of the nuclear light bulb engine. Discussions of the feedbacks which contribute to the variations of δk and λ_F are presented below. The delayed neutron fractions, β_i, and precursor decay constants, λ_i, are from Ref. 19 and are shown in Table XII.

Nuclear Fuel Loading Equations

The variation of nuclear fuel mass stored in the active core of the nuclear light bulb engine is described by

$$\frac{dM_F}{dt} = W_F - \lambda_F M_F \tag{28}$$

where W_F is the fuel injection rate and λ_F is the fuel decay constant (the inverse of the average fuel residence time).

In a preceeding discussion of fuel containment parameters, it was shown that the amount of nuclear fuel retained in the vortex flow field was a function of the ratio of average fuel density to buffer gas density at the edge of the fuel cloud, and the fuel-to-buffer gas weight flow ratio. Since the average fuel residence time is 20 sec, any change in a containment parameter (under conditions of constant fuel injection) will initiate a change in stored fuel which will approach a new equilibrium level approximately 20 sec after the change. Therefore, changes in containment parameters were introduced into the mass equations through the fuel decay constant, λ_F, where

$$\lambda_F \ \alpha \ \frac{1}{\rho_{B_6}} \left(\frac{W_B}{W_F} \right)^{1.2} \tag{29}$$

31

Since ρ_{B6} varies as p_c/T^*, the equation describing λ_F is:

$$\lambda_F = K_\lambda \frac{T^*}{p_c} \left(\frac{W_B}{W_F} \right)^{1.2} \tag{30}$$

where K_λ is a constant of proportionality.

The surface radiating temperature is established from the identity that

$$\sigma T^{*4} S_F = 0.87 P \tag{31}$$

where σ is the Stefan-Boltzmann constant and the P coefficient of 0.87 represents the fraction of total power which is radiated from the fuel cloud surfaces. The chamber operating pressure, p_c, is obtained from the assumption that pressure within the system is regulated to follow the propellant pressure. Since propellant flow is choked, it follows that

$$\frac{W_P \sqrt{T_P}}{p_c} = K_P \tag{32}$$

where K_P is a constant. Thus,

$$p_c = \frac{W_P \sqrt{T_P}}{K_P} \tag{33}$$

The expressions to obtain W_P and T_P have been discussed previously.

The ratio of fuel-to-buffer gas weight flows must also be evaluated for Eq. (30). The buffer gas weight flow is described by Eq. (10). It is anticipated that fuel injection at full-power operating conditions will be accomplished by injecting nuclear fuel in particulate form with a carrier gas. The heavy-gas injection velocities required in isothermal, two-component gas vortex tests were of the order of 100 ft/sec

(Ref. 14). If this injection velocity is used for the full scale engine and if it is assumed that the fuel-to-carrier gas weight flow ratio is 5-to-1, then $V_F = 100$ ft/sec and $\rho_M = 285$ lb/ft^3 in the expression

$$\Delta p = \frac{1}{2} \rho_M V_F^2 \tag{34}$$

Δp in Eq. (34) is equal to approximately 20 atm. It follows from Eq. (34) that fuel weight flow, W_F, is given by

$$W_F = K_F \sqrt{\Delta p / \Delta p_0} \tag{35}$$

If, as before, it is assumed that chamber pressure is governed by the hydrogen propellant pressure under conditions of choked flow through the thrust nozzles, then

$$W_F = K_F \left(\frac{520 - p_c}{20} \right)^{0.5} \tag{36}$$

where p_c is given by Eq. (33) above. K_F is a calibration factor that can be arbitrarily perturbed to alter the fuel injection rate which is then either retarded or enhanced by the resulting variations in p_c in the manner described by Eq. (36).

Reactivity Feedbacks

The reactivity coefficient, δk, in Eq. (26) is made up of three terms.

$$\delta k(t) = \delta k_0 + \delta k_1 + \delta k_2 \tag{37}$$

δk_0 represents the amount of excess reactivity required to compensate for the loss of delayed neutrons as a result of removal of delayed neutron precursors from the active core volume. The expression for δk_0 is derived in Appendix A and is given by

$$\delta k_0 = \sum_{i=1}^{6} \frac{\beta_i \lambda_{F_0}}{\lambda_i + \lambda_{F_0}} \tag{38}$$

δk_1 is a time varying perturbation term used as an input driving function for the neutron level equations (physically, like a movement of a control rod in a conventional reactor).

δk_2 is a combination of reactivity feedbacks associated with changes in nuclear fuel loading, average moderator temperature, propellant density, moderator coolant density, and fuel region radius. The linear coefficients relating changes in these parameters to reactivity were taken from Table IV of Ref. 2. The expression combining all the contributing factors in δk_2 is given as

$$\delta k_2 = 0.384 \left(\frac{\Delta M_F}{M_F} \right) + 0.045 \left(\frac{\Delta T_m}{T_{m_0}} \right) + 0.0544 \left(\frac{\Delta \rho_H}{\rho_{H_0}} \right)_{PROP}$$
$$+ \left(\frac{\Delta \rho_H}{\rho_{H_0}} \right)_{MOD} - 0.0413 \left(\frac{\Delta R_F}{R_{F_0}} \right) \tag{39}$$

The calculation of changes in hydrogen densities were done on the basis of ideal gas laws using the average hydrogen temperatures in the propellant and moderator regions. The moderator region temperatures were based on the average of the coolant inlet and outlet temperatures for each region and nuclear fuel masses were calculated using Eq. (28). The fuel region radius was varied only by input perturbations.

Engine Dynamics Simulation Program

The equations describing the dynamic behavior of the nuclear light bulb engine were programmed for the UNIVAC 1108 digital computer. In the process of developing the simulation program, models of each subsystem (i.e., neutron kinetics, primary coolant circuit, secondary coolant circuit, and fuel cycle system) were programmed and debugged separately. Coupling and feedbacks between systems were treated as input parameters, and in this manner, responses of individual systems to specific parameter variations were checked analytically before all of the subsystem programs were combined into the final engine simulation.

The principal assumptions which were employed in the engine simulation have been described in the preceding sections and are summarized in Table XIII. The simulation program flow diagram is shown in Fig. 14. Basically, the program is designed to process input, calculate steady-state conditions, calculate coefficients, and then calculate neutron level, power level, temperatures, flow conditions, and feedback parameters (in that order) for each time step.

Results of Engine Dynamics Studies

The responses of the uncontrolled engine to various perturbations in reactivity, fuel injection rate, fuel cloud radius, chamber pressure, and turbopump wheel speed were calculated. Typically, the responses were in the form of oscillations in power which were usually damped, but in some instances were sustained at some constant asymptotic amplitude. The natural frequency of the oscillations was about 1 cps, thus allowing reasonably long control system response times to further dampen the oscillatory responses. Two factors tend to drive the oscillatory responses: (1) a positive reactivity coefficient associated with moderator temperature, and (2) the tendency to inject fuel at a rate above the steady-state level whenever chamber pressure goes below 500 atm (see Eq. (36) for expression describing fuel injection rate).

Responses to a step change in imposed reactivity causing the reactor to go prompt critical are shown in detail for several parameters throughout the engine in Figs. 15a and b. A damped oscillatory response is characteristic of all the parameters shown. The asymptotic values return very nearly to their original steady-state values with the exception of the nuclear fuel mass, which is reduced to 29.867 lb. This reduction in nuclear fuel mass causes a reduction in $\Delta M/M_0 = -0.00443$ which, when multiplied by the nuclear fuel reactivity coefficient of 0.384, results in a contribution to δk_2 of -0.001701, nearly the total required compensation for the input perturbation of $\delta k_1 = +0.001707$.

Responses of parameters throughout the engine to a positive step change in the fuel injection flow rate calibration factor by 10 percent are shown in Figs. 16a and b. Once again, the damped oscillatory response is characteristic of all the parameters, but the damping is considerably slower than in the response shown previously to the step reactivity insertion. It can be seen that power, radiating temperature, and transparent-wall temperature respond by approaching higher values than in the steady state. These higher values result in higher chamber pressure $((p_c)_{asy} = 503.4)$ which serves to retard the fuel injection rate in accordance with Eq. (36), returning it nearly to its original value of $W_{F_0} = 1.5$ lb/sec.

A sustained 10 percent step increase in the fuel injection flow rate calibration factor is a relatively severe sustained perturbation. More probable fuel injection disturbances might be the sudden injection of agglomerated fuel (solid uranium metal) over a period of milliseconds, or an intentional ramp increase or decrease in fuel flow rate to a different steady-state level. Power level responses to the sudden injection of solid uranium metal for 5 and 50 msec are shown in Fig. 17a and b, respectively, while power level responses to ramp changes in the fuel injection flow rate calibration factors to different steady-state levels are shown in Fig. 18a and b. It can be seen in Fig. 18 that power level changes can be achieved relatively smoothly by varying fuel injection.

Sustained oscillatory response appears to result when chamber pressure is perturbed such that oscillations occur about 500 atm, resulting in oscillations in fuel injection rate about the steady-state value which drive the power response. Thus, a decrease in chamber pressure (for example, a pressure change caused by a step increase in nozzle-throat area) results in greater fuel injection, causing a compensating increase in power until chamber pressure rises to retard fuel flow rate drive the power level down again. Similarly, a decrease in turbopump wheel speed causes a decrease in pressure and drives sustained oscillations. These sustained oscillations are not damped because the assumed inertia of the turbopump prevents the wheel-speed feedback term, $\delta \nu_2$, from rapidly compensating for the imposed wheel-speed change. Conversely, when chamber pressure is increased, fuel injection is retarded and the system decreases in power until a compensating pressure drop calls for more fuel injection. In these cases, however, the reactor, in seeking its original equilibrium pressure levels, continues to feel the original pressure change and the fuel injection rate is permanently retarded, causing a damping of the oscillations. Typical responses to chamber pressure and turbopump wheel speed perturbations are shown in Figs. 19 and 20.

An increase in fuel radius decreases surface radiating temperature for a given power level due to an increase in radiating surface area. The buffer-gas flow also decreases due to a decrease in flow area. The decrease in T* also increases buffer gas density at the edge of the fuel. These effects both tend to increase the stored fuel according to Eq. (18), giving rise to sustained oscillatory response to an increase in fuel radius. A decrease in fuel radius has an exactly opposite effect and results in damped oscillations in power approaching a level below that of the steady state. Typical calculated response to step and ramp changes in fuel region radius are shown in Figs. 21 and 22.

It should be emphasized here that the responses calculated thus far are those of an uncontrolled engine model. Furthermore, no model of a fluid dynamic restoring force on fuel radius has been derived, nor has any limiter or variable injection supply pressure been imposed on fuel injection rate (the current simulation employs a constant fuel injection supply pressure of 520 atm). Finally, there is also no turbine control system in the simulation. All of these factors, when incorporated in an engine dynamics model, will tend to further dampen the power level responses to perturbations.

Gain and phase diagrams for responses of the engine to small sinusoidal oscillations in reactivity and fuel injection rate over a range of frequencies from 0.2π to 200π radians/sec are shown in Figs. 23 and 24, respectively. The principal features of the responses are that gain falls off at a rate of 20 db/decade and 40 db/decade with increasing frequency for reactivity and fuel flow rate oscillations, respectively, and that in no case does the phase angle equal -180 degrees.

Preliminary Concepts for Engine Control

The results of engine simulation calculations thus far indicate that fuel injection control can achieve further damping of power level responses of the uncontrolled engine. In particular, a limiter on fuel injection rate will limit the level of excess fuel injection caused by pressure reduction in the fuel chamber. In addition to a limiter, it may also be desirable to control the injection supply pressure (assumed to be a constant 520 atm in this study) and thereby provide a means of following or responding to system pressure changes more rapidly. There is more than enough power to operate all of the engine pumps (approximately 87 percent of the available power is used to drive the turbopumps at steady-state full power operation) at full power so that a wide range of control on various flow rates is available.

RECOMMENDATIONS FOR FUTURE RESEARCH

Additional refinements of both the engine start-up and dynamics model are necessary in order to determine the response of the engine to various types of controls and to permit the analysis of design tolerance effects. The initial results of the engine dynamics have also indicated that additional analysis is required to improve the model in some specific areas. In particular, a model describing the behavior of fuel cloud radius and the forces tending to maintain it at some equilibrium location should be devised. However, a balance must be struck between model refinement and evaluation of constants associated with the systems, such as reactivity coefficients. Therefore, it is also recommended that the reactivity coefficients be recalculated for small variations about the steady-state full-power operation point with temperatures and densities of materials based on the results of the current simulation calculations.

Results of both the engine dynamics studies and the start-up studies have shown a need for detailed turbopump specifications. The magnitude of the turbopump inertia and the design wheel speed affect both dynamic response of the engine and the auxiliary power requirements during start-up. The investigation of the turbopump characteristics should also consider whether direct-coupled pumps for all the flow circuits are desirable. This problem could be approached from the standpoint of the effects of a specific turbopump design on the engine kinetics or by an analysis of the engine kinetics to determine the most desirable characteristics of a turbopump unit.

In addition, various means of controlling fuel injection and turbopump output should be devised and analyzed to determine the best modes of control for the engine. Additional research is required to determine the feasibility and design of a fuel handling system. The particular facets of a fuel handling system requiring further investigation are a determination of the achievable fuel-to-carrier-gas weight flow ratios, the behavior of nuclear fuel in a vortex flow field during the transitions through the solid-to-liquid and liquid-to-vapor phase changes, and the feasibility of condensing the hot spent fuel with cold bypass flow while simultaneously preventing the fuel from plating on the thru-flow duct walls.

REFERENCES

1. McLafferty, G. H. and H. E. Bauer: Studies of Specific Nuclear Light Bulb and Open-Cycle Vortex-Stabilized Gaseous Nuclear Rocket Engines. United Aircraft Research Laboratories Report F-910093-37, prepared under Contract NASw-847, September 1967. Also issued as NASA CR-1030.

2. Latham, T. S.: Nuclear Studies of the Nuclear Light Bulb Rocket Engine. United Aircraft Research Laboratories Report G-910375-3, prepared under Contract NASw-847, September 1968. Also issued as NASA CR-1315.

3. Roman, W. C., J. F. Klein, and P. G. Vogt: Experimental Investigations to Simulate Thermal Environment, Transparent Walls, and Propellant Heating in a Nuclear Light Bulb Engine. United Aircraft Research Laboratories Report H-910091-19, prepared under Contract NASw-847, September 1969.

4. Mensing, A. E. and J. F. Jaminet: Experimental Investigation of Heavy Gas Containment in R-F Heated and Unheated Two-Component Vortexes. United Aircraft Research Laboratories Report H-910091-20, prepared under Contract NASw-847, September 1969.

5. Krascella, N. L.: Theoretical Investigation of the Radiant Emission Spectrum from the Fuel Region of a Nuclear Light Bulb Engine. United Aircraft Research Laboratories Report H-910092-12, prepared under Contract NASw-847, September 1969.

6. McLafferty, G. H.: Absorbtion of Thermal Radiation in the Transparent Wall of a Nuclear Light Bulb Rocket Engine. Journal of Spacecraft and Rockets, Vol. 4, No. 6, 1967.

7. Ragsdale, R. G.: Are Gas-Core Nuclear Rockets Attainable? Paper No. 68-570, AIAA 4th Propulsion Joint Specialist Conference, Cleveland, Ohio, June 1968.

8. Untermeyer, S. and J. T. Weills: Heat Generation in Irradiated Uranium. Argonne National Laboratories Report ANL 4790, February 1952.

9. DeWitt, R.: Uranium Hexafluoride -- A Survey of the Physico-Chemical Properties. Goodyear Atomic Corporation, August 12, 1960.

10. Nesmeyanov, A. N.: Vapor Pressures of the Chemical Elements. Elsinor Publishing Company, Amsterdam, 1963.

REFERENCES (Continued)

11. Roback, R.: Theoretical Performance of Rocket Engines Using Gaseous Hydrogen in the Ideal State at Stagnation Temperatures up to 200,000 R. United Aircraft Research Laboratories Report E-910093-30, prepared under Contract NASw-847, October 1966. Also issued as NASA CR-696.

12. McLafferty, G. H.: Analytical Study of Moderator Wall Cooling of Gaseous Nuclear Rocket Engines. United Aircraft Research Laboratories Report C-910093-9, prepared under Contract NASw-847, September 1964. Also issued as NASA CR-214.

13. Sparrow, E. M.: Temperature Distribution and Heat Transfer Results for an Internally-Cooled, Heat-Generating Solid. Journal of Heat Transfer, November 1960, pp. 389 to 393.

14. Kendall, J. S., W. C. Roman, and P. G. Vogt: Initial Radio-Frequency Gas Heating Experiments to Simulate the Thermal Environment in a Nuclear Light Bulb Reactor. United Aircraft Research Laboratories Report G-910091-17, prepared under Contract NASw-847, September 1968. Also issued as NASA CR-1311.

15. Kendall, J. S., A. E. Mensing, and B. V. Johnson: Containment Experiments in Vortex Tubes with Radial Outflow and Large Superimposed Axial Flows. United Aircraft Research Laboratories Report F-910091-12, prepared under Contract NASw-847, May 1967. Also issued as NASA CR-993.

16. Kendall, J. S.: Experimental Investigation of Containment in Constant-Temperature Radial-Inflow Vortexes. United Aircraft Research Laboratories Report F-910091-15, prepared under Contract NASw-847, September 1967. Also issued as NASA CR-1029.

17. McLafferty, G. H., H. E. Bauer, and D. E. Sheldon: Preliminary Conceptual Design Study of a Specific Vortex-Stabilized Gaseous Nuclear Rocket Engine. United Aircraft Research Laboratories Report E-910093-29, prepared under Contract NASw-847, September 1966. Also issued as NASA CR-698.

18. Smith, H. P., Jr. and A. H. Stenning: Open Loop Stability and Response of Nuclear Rocket Engines. Nuclear Science and Engineering, Vol. 11, 1961, pp. 76-94.

19. Keepin, R. G. and T. F. Wimett: Reactor Kinetics Functions: A New Evaluation. Nucleonics, Vol. 16, No. 10, 1958, p. 86.

LIST OF SYMBOLS

A, B, C, D   Constant coefficients (see text)

c_p Specific heat, Btu/lb-(deg R)

C_H Heat exchanger coefficient (see text, Eq. (15))

C_i Concentration of delayed neutron precursors, precursors/cm^3

I   Moment of inertia of turbopump, ft-lb-sec^2

K_g Proportionality constant,   g = 1, 2, D, H, M, P, λ, (see text)

K_F Fuel injection flow rate calibration factor, lb/sec

k   Effective multiplication factor

ℓ^* Prompt neutron lifetime, sec

M   Mass, lb

M_c Critical mass, lb

M_F Nuclear fuel loading, gms or lbs

m   Slope of approximate temperature equations (see text)

n   Neutron density, neutrons/cm^3

P   Engine power level, mw

p_c Total chamber pressure, atm

Pr   Prandtl number

Q   Heat deposition rate, Btu/sec

Q_B Heat deposition rate in buffer gas, Btu/sec

Q_P Pump power requirement, Btu/sec

Q_T Turbine power output, Btu/sec

LIST OF SYMBOLS (Continued)

Q_{LT} Heat deposition rate in liner tubes, Btu/sec

Q_{TW} Heat deposition rate in transparent structure, Btu/sec

Re   Reynolds number

R_F Fuel region radius, ft

St   Stanton number

S_F Fuel region surface area, ft^2

T   Temperature, deg R

T_F Fuel temperature, deg R

T_m Average moderator temperature, deg R

T_n Inlet temperature of neon buffer gas, deg R

T_p Propellant exit temperature, deg R

T_w Transparent wall temperature, deg R

T^* Equivalent black body radiating temperature, deg R

t   Total elapsed time since initiation of perturbation, sec

t_o Starting time of perturbation, sec

V_F Fuel injection velocity, ft/sec

W   Coolant mass flow rate, lb/sec

W_B Buffer gas flow rate, lb/sec

W_F Fuel injection rate, lb/sec

W_p Propellant mass flow rate, lb/sec

ΔM Change in fuel mass, gm or lbs

Δp Pressure differential, atm

ΔR_F Change in fuel region radius, cm or in.

LIST OF SYMBOLS (Continued)

ΔT Temperature difference, deg R

$\overline{\Delta T}$ Average fluid temperature difference in heat exchangers, deg R

ΔT_m Change in average moderator temperature, deg R

Δt Time increment, sec

$\Delta \rho_H$ Change in hydrogen propellant density, lb/ft3

β Total of delayed neutron fractions

β_i Delayed neutron fraction

δk_o Reactivity required to compensate for loss of delayed neutrons

δk_1 Imposed reactivity change

δk_2 Feedback reactivity change

δP Power perturbation, mw

δQ Heat generation rate perturbation, Btu/sec

δT_m Perturbation in average moderator temperature, deg R

δW_F Perturbation in fuel mass flow rate, lb/sec

$\delta \nu_1$ Input perturbation of turbine wheel speed, rpm

$\delta \nu_2$ Feedback perturbation of turbine wheel speed, rpm

λ_F Fuel decay constant, sec^{-1} (reciprocal of fuel residence time)

λ_i Precursor decay constants, sec^{-1}

μ Fluid viscosity, lb/ft-sec

ν Turbopump wheel speed, rpm

ρ_M Fuel and carrier gas mixture density, lb/ft^3

LIST OF SYMBOLS (Continued)

ρ_B Buffer gas ensity, lb/ft^3

$\bar{\rho}_F$ Average fuel density, lb/ft^3

ρ_H Hydrogen propellant density, lb/ft^3

ρ_{B6} Buffer gas density at edge of fuel region, lb/ft^3

σ Stefan-Boltzmann constant, $0.48 \times 10^{-12} Btu/sec\text{-}ft^2\text{-}(deg\ R)^4$

σ_f Thermal neutron fission cross section, barns

τ_R Coolant residence time in region, sec

τ_i Mean lifetime of ith delayed neutron group, sec

Subscripts

o   Denotes reference condition

asy   Denotes asymptotic value

APPENDIX A

DERIVATION OF STEADY-STATE REACTIVITY REQUIRED TO COMPENSATE FOR LOSS OF DELAYED NEUTRONS

As a result of a finite fuel and delayed neutron precursor residence time in the nuclear light bulb engine, an excess amount of reactivity is required to compensate for the loss of delayed neutrons emitted outside the active reactor core. Criticality is defined as the state in which the neutron level and delayed neutron precursor concentrations remain constant with time.

The equations of state for one prompt neutron group and six delayed neutron groups can then be given by:

$$\frac{dn}{dt} = \frac{\delta k - \beta}{\ell^*} n + \sum_{i=1}^{6} \lambda_i C_i \qquad (A-1)$$

and

$$\frac{dC_i}{dt} = \frac{\beta_i n}{\ell^*} - (\lambda_i + \lambda_F) C_i \qquad (A-2)$$

where

n = neutron population, function of time, n/cm^3

δk = reactivity, dimensionless

C_i = delayed neutron precursor concentration, function of time, $precursor/cm^3$

λ_F = fuel decay constant, function of time, sec^{-1}

ℓ^* = prompt neutron lifetime, sec

β_i = i^{th} delayed neutron group fraction, dimensionless

λ_i = decay constant for the ith delayed neutron precursor, sec^{-1}

β = total delayed neutron fraction, dimensionless

In the steady state Eqs. (A-1) and (A-2) become

$$0 = \frac{\delta k_0 - \beta}{\ell^*} n_0 + \sum_{i=1}^{6} \lambda_i (C_i)_0 \qquad (A-3)$$

and

$$0 = \frac{\beta_i n_0}{\ell^*} - \left(\lambda_i + (\lambda_F)_0\right)(C_i)_0 \qquad (A-4)$$

Rearranging and solving for $(C_i)_0$, Eq. (A-4) becomes

$$(C_i)_0 = \frac{\beta_i n_0}{\ell^*} \left(\frac{1}{\lambda_i + (\lambda_F)_0}\right) \qquad (A-5)$$

Substituting Eq. (A-5) into Eq. (A-3), we obtain

$$0 = \frac{\delta k_0 - \beta}{\ell^*} n_0 + \sum_{i=1}^{6} \frac{n_0}{\ell^*} \left(\frac{\beta_i \lambda_i}{\lambda_i + (\lambda_F)_0}\right) \qquad (A-6)$$

Since

$$\beta = \sum_{i=1}^{6} \beta_i$$

we can solve for δk_0

$$\delta k_0 = \sum_{i=1}^{6} \beta_i - \frac{\beta_i \lambda_i}{\lambda_i + (\lambda_F)_0} = \sum_{i=1}^{6} \frac{\beta_i (\lambda_F)_0}{\lambda_i + (\lambda_F)_0} \qquad (A-7)$$

Now if the "dollar" is defined as the amount of excess reactivity needed to become critical on prompt neutrons alone, then, for a prompt critical reactor with an infinite fuel and precursor residence time, successive neutron generations are related by

$$\frac{N_j}{N_{j-1}} = \frac{\overbrace{(1-\beta)}^{\text{Prompt N's}} + \overbrace{\beta}^{\text{Delayed N's}} + \overbrace{\delta k_1}^{\text{Added Reactivity}}}{(1-\beta) + \beta} \qquad (A-8)$$

It can be seen that if $\delta k_1 = \beta$, the reactor is critical on prompt neutrons alone.

However, for a prompt-critical reactor with a finite fuel and precursor residence time, successive neutron generations are given by:

$$\frac{N_j}{N_{j-1}} = \frac{\overbrace{(1+\delta k_0 - \beta)}^{\text{Prompt N's}} + \overbrace{(\beta - \delta k_0)}^{\text{Delayed N's}} + \overbrace{\delta k_1}^{\text{Added Reactivity}}}{(1-\delta k_0 - \beta) + (\beta - \delta k_0)} \qquad (A-9)$$

Thus, the reactor is critical on prompt neutrons alone if

$$1 + \delta k_0 - \beta + \delta k_1 = 1 \qquad (A-10)$$

The "dollar" of reactivity is therefore, from Eq. (A-10)

$$\delta k_1 = \beta - \delta k_0 = {}^\$ 1.00 \qquad (A-11)$$

For the nuclear light bulb reactor, with U-233 fuel and a fuel decay constant of $\lambda_F = 0.05 \text{ sec}^{-1}$, \$1.00 = 0.001707.

TABLE I

STEADY-STATE MODERATOR AND STRUCTURE HEAT DEPOSITION RATES

Fuel - U-233

Region	Mechanism of Heating	Heat Deposition Rate Btu/sec**
Pressure Vessel	Neutron and Gamma	0.1093×10^{5}*
Nozzles	Neutron and Gamma	0.0008×10^{5}
Flow Divider	Neutron and Gamma and Conduction	0.0676×10^{5}
Tie Rods	Neutron and Gamma and Conduction	0.0510×10^{5}
Cavity End Walls	Thermal Radiation and Conduction	0.0606×10^{5}
Cavity Liner	Thermal Radiation and Conduction	0.7661×10^{5}
Transparent Structure	Thermal Radiation and Conduction	1.1290×10^{5}
Fuel Recycle System	Removal of Heat from Fuel	0.605×10^{5}
Moderator End Plugs	Neutron and Gamma	0.6640×10^{5}
Beryllium Oxide	Neutron and Gamma	0.8457×10^{5}
Graphite	Neutron and Gamma	0.4607×10^{5}
Direct Hydrogen Heating	Neutron and Gamma	0.5564×10^{5}
	Total	5.32×10^{5}
	Percent of Total Power	12.15 percent

* Total heating in pressure vessel is 0.165×10^{5}. It is assumed that only 2/3 of the total will be removed by the closed secondary hydrogen coolant circuit and the remaining 1/3 will be removed by the transpiration cooling circuit.

* 10^{5} Btu/sec = 105.5 megw

TABLE II

STEADY-STATE TEMPERATURE, ENTHALPY, AND PRESSURE LEVELS IN
PRIMARY HYDROGEN PROPELLANT CIRCUIT OF NUCLEAR LIGHT BULB ENGINE

Hydrogen Propellant Flow = 42.3 lb/sec
Note: Station Numbers Refer to Locations Shown in Fig. 2

Station	Location	Temperature Deg R	Enthalpy Btu/lb	Pressure Atm
1000	Pump inlet	36	120	1.0
1010	Fuel Cycle Heat Exchanger Inlet	90	550	713
1020	Secondary Heat Exchanger Inlet	640	1,483	712
1025	Secondary Heat Exchanger Outlet	2095	7,158	710
1040	Turbine outlet	1889	6,600	507
1060*	Upper End Plug Outlet	2039	7,135	506.9
1070*	Axial Beryllium Oxide Outlet	2608	9,134	500.64
1090*	Lower End Plug Outlet	2907	10,172	500.4
1110	Graphite Outlet	3217	11,262	500
1115	Propellant, Including Direct H_2 Heating	3592	12,577	500

* Lumped in solid moderator region in Fig. 2

TABLE III

STEADY-STATE TEMPERATURE, ENTHALPY, AND PRESSURE LEVELS IN CLOSED
SECONDARY HYDROGEN CIRCUIT OF NUCLEAR LIGHT BULB ENGINE

Hydrogen Coolant Circuit Flow = 42.3 lb/sec
Note: Station Numbers Refer to Locations Shown in Fig. 2

Station	Location	Temperature Deg R	Enthalpy Btu/lb	Pressure Atm
2010	Pressure Vessel Liner Inlet	741	2250	510
2016	Nozzle Inlet	843	2508	508
2017	Lower End Wall Liner Inlet	843	2510	507.5
2020	Tie Rod Flow Divider and Cavity Liner Inlet	858	2582	507.5
2026	Upper End Wall Liner Inlet	1439	4673	502.4
2030	Transparent Wall Inlet	1454	4745	502.4
2040	Transparent Wall Outlet	2195	7414	500
2000	Heat Exchanger Outlet	739	2250	498

TABLE IV

STEADY-STATE TEMPERATURE AND ENTHALPY LEVELS IN FUEL CYCLE
CIRCUIT OF NUCLEAR LIGHT BULB ENGINE

Total Neon Flow Per Cavity = 21.1 lb/sec
Total Fuel Flow Per Cavity = 0.15 lb/sec

Station	Location	Temperature Deg R	Enthalpy Btu/lb
3000	H-Ne Heat Exchanger Outlet	184	47
3010	Pump Outlet*	189	48
3020	Cavity Outlet	2663	675
3030	H-Ne Heat Exchanger Inlet	2663	675

* The required neon flow rate into each cavity is 3.51 lb/sec; the remaining
17.59 lb/sec of neon bypasses the cavity and is mixed with the flow which exits
from the cavity in order to condense the fuel before the neon-fuel mixture
enters the separator.

TABLE V

SOLID MODERATOR FLOW DIVIDER
FOR NUCLEAR LIGHT BULB ENGINE

Beryllium Wall Thickness, in.	0.048
Clearance Between Walls, in.	0.10
Pyrolytic Graphite Insulation Thickness, in.	
Beryllium Oxide Side	0.335
Graphite Side	0.440
Total Flow in Divider Region, lb/sec	1.44
Total Flow Area, in.^{2}	32.2
Total Heat Deposition Rate, Btu/sec	6759
Coolant Inlet Temperature, deg R	858
Coolant Outlet Temperature, deg R	1439
Film Temperature Difference, deg R	12
Temperature Difference in Beryllium Wall, deg R	4
Maximum Beryllium Temperature, deg R	1455
Reynolds Number	9600

TABLE VI

SPECIFICATIONS FOR BERYLLIUM TIE RODS
FOR NUCLEAR LIGHT BULB ENGINE

Inside Diameter, in.	1.0
Outside Diameter, in.	1.358
Pyrolytic Graphite Insulation Thickness	0.26
Overall Diameter, in.	1.878
Number of Rods	24
Total Flow Per Rod, lb/sec	0.0842
Total Heat Deposition Per Rod, Btu/sec	212
Coolant Inlet Temperature, deg R	858
Coolant Outlet Temperature, deg R	1439
Film Temperature Difference Inside Rods, deg R	65
Temperature Difference in Beryllium Wall, deg R	1558
Reynolds Number in Rod	4800

TABLE VII

CAVITY LINER CONFIGURATION AND STEADY-STATE OPERATING
CONDITIONS FOR NUCLEAR LIGHT BULB ENGINE

Inside Radius of Liner at Propellant Inlet, ft	0.911
Inside Radius of Liner at Propellant Outlet, ft	1.320
Average Radius of Liner, ft	1.1355
Length of Liner Tubes, ft	13.5
Average Liner Tube Inside Diameter, in.	0.125
Average Liner Tube Outside Diameter, in.	0.139
Number of Tubes Per Cavity	302
Thickness of Reflective Coating on Outside Walls, in.	0.002
Total Secondary Hydrogen Coolant Flow Per Cavity, lb/sec	5.36
Total Heat Deposition in Liner Per Cavity, Btu/sec	10,944
Coolant Inlet Temperature, deg R	858
Coolant Outlet Temperature, deg R	1439
Film Temperature Difference Inside Tubes, deg R	46
Temperature Difference in Beryllium Wall, deg R	7
Maximum Tube Surface Temperature Adjacent to Propellant, deg R	1492
Dynamic Pressure in Tubes, atm	0.228
Total Pressure Loss in Liner Tubes, atm	5.05
Reynolds Number in Tubes	1.93×10^5

TABLE VIII

TRANSPARENT STRUCTURE REGION CONFIGURATION AND STEADY-STATE
OPERATING CONDITIONS FOR NUCLEAR LIGHT BULB ENGINE

Inside Radius of Transparent Structure, ft	0.802
Length of Transparent Structure, ft	6.0
Tube Inside Diameter, in.	0.050
Tube Wall Thickness, in.	0.005
Tube Outside Diameter, in.	0.060
Number of Tubes in Each 120-Degree Segment of Each Cavity	1200
Total Hydrogen Secondary Coolant Flow Per Cavity, lb/sec	6.04
Total Heat Deposition in Transparent Structure Per Cavity, Btu/sec	16,130
Coolant Inlet Temperature, deg R	1454
Coolant Outlet Temperature, deg R	2195
Film Temperature Difference Inside Tubes, deg R	105
Temperature Difference in Wall, deg R	190
Maximum Tube Surface Temperature, deg R	2490
Dynamic Pressure in Tubes, atm	0.134
Total Pressure Loss in Tubes, atm	1.66
Reynolds Number in Tubes	33,800
Feeder and Collector Pipe Average Inside Diameter, in.	1.2
Average Dynamic Pressure in Feeder and Collector Pipes, atm	0.16
Pressure Loss in Feeder Pipe, atm	0.270
Pressure Loss in Collector Pipe, atm	0.420
Average Reynolds Number in Feeder and Collector Pipes	7.2×10^5
Total Pressure Loss in Transparent Structure, atm	2.35

TABLE IX

SOLID MODERATOR STEADY-STATE COOLING REQUIREMENTS
FOR NUCLEAR LIGHT BULB ENGINE

Item	Region					
	Upper Graphite	Upper BeO	Axial BeO	Lower BeO	Lower Graphite	Axial Graphite
Total Volume, ft^3	56.0	18.5	36.0	17.6	64.4	126.0
Density, lb/ft^3	114.8	178.2	178.2	178.2	114.8	114.8
Void Fraction	0.05	0.05	0.05	0.05	0.05	0.05
Total Weight, lb	6100	3120	6100	2980	7000	13,700
Length, ft	1.11	0.64	6.0	0.95	0.93	9.63
Coolant Passage Diameter, in.	0.974	0.107	0.138	0.110	0.198	0.492
Number of Coolant Passages Per ft^2	9.66	804	482	757	234	38
Coolant Passage Configuration	Circular Passages on Triangular Pitch					
Coolant Passage Spacing, in.	4.15	0.455	0.586	0.467	0.841	2.10
Coolant Inlet Temperature, deg R	1889	1906	2039	2608	2798	2907
Coolant Outlet Temperature, deg R	1906	2039	2608	2798	2907	3217
Temperature Difference, Coolant to Wall, deg R	100	100	100	100	100	100
Maximum Temperature in Solid Moderator, deg R	2113	2062	2965	2943	2932	3457
Dynamic Pressure, atm	0.003	0.014	0.577	0.043	0.002	0.053
Pressure Loss, atm	0.004	0.060	6.25	0.180	0.006	0.405
Reynolds Number	84,600	17,970	140,780	25,600	9800	114,000

TABLE X

HEAT EXCHANGER SPECIFICATIONS
FOR NUCLEAR LIGHT BULB ENGINE

	H-H Heat Exchanger	H-Ne Heat Exchanger
Number of Heat Exchangers	7	1
Hydrogen Flow Rate Per Unit, lb/sec	6.04	42.3
Heat Transferred Per Unit, Btu/sec	31,270	60,460
Tube Inside Diameter, in.	0.03125	0.171
Tube Wall Thickness, in.	0.005	0.0275
Tube Spacing, in.	0.0578	0.360
Number of Tubes Per Unit	11,628	530
Length of Tubes, in.	53.76	48.0
Cross Sectional Area of Tube Bundle, Per Unit in.^{2}	10.10	11.66
Pressure Loss, atm	2.0	1.0
Tube Wall Material	Stainless Steel	
Wall Material Density, lb/ft^3	500	
Tube Weight Per Unit, lb	1060	1500
Number of Units	7	1
Total Heat Exchanger Weight (1.1 x total tube weight), lb	8162	1650

TABLE XI

SEQUENCE OF EVENTS DURING START-UP

1.   Bring turbopump up to design speed (22,000 rpm) using external power source.

2.   Start hydrogen and neon flow to establish the following initial conditions:

      Hydrogen propellant flow rate, 4.23 lb/sec
      Secondary coolant flow rate,   4.23 lb/sec
      Neon buffer gas flow rate,   21   lb/sec
      Internal pressure level in reactor, 20 atm

3.   Start fuel injection and increase linearly with time to design flow rate
      of 1.55 lb/sec.

4.   Hydrogen propellant flow and secondary circuit flow are increased
      linearly with time from the initial value to the design flow rate
      (42.3 lb/sec).

5.   Neon flow rate in the fuel cycle is increased according to the schedule
      shown in Fig. 6. The total flow through the cavity remains constant
      after reaching a value of 24.51 lb/sec and all additional neon flow
      bypasses the cavity.

6.   Nozzle throat area is varied according to the schedule shown in Fig. 11.

TABLE XII

DELAYED NEUTRON YIELDS FOR U-233

Total Delayed Neutron Fraction, $\beta = 0.0025$

Mean Life, τ_i sec	Decay Constant, λ_i sec^{-1}	Yield Fraction, β_i
0.321	3.12	0.000061
0.788	1.27	0.000194
3.300	0.303	0.000845
7.650	0.131	0.000604
29.900	0.0335	0.000730
79.500	0.0126	0.000024

TABLE XIII

ASSUMPTIONS EMPLOYED IN ENGINE DYNAMICS SIMULATION

1. Reactivity feedback coefficients and operating characteristics at nominal full power were taken from Refs. 1 and 2, and have the following values:

Operating Power	= 4,600 megw
Chamber Pressure	= 500 atm
Fuel Radiating Temperature	= 15,000 deg R
Propellant Exit Temperature	= 12,000 deg R
Average Fuel Residence Time	= 20 sec
Critical Mass	= 30 lb
Prompt Neutron Lifetime	= 0.000516 sec
Fuel Radius	= 0.681 ft
Average Thermal Fission Cross Section	= 193 barns
Steady-State Fuel Injection Rate	= 1.5 lb/sec

Reactivity Feedback Coefficients:

$$\text{Fuel, } (\delta k/k)/(\Delta M_F/M_F) = +0.384$$
$$\text{Moderator Temperature, } (\delta k/k)/(\Delta T_M/T_M) = +0.045$$
$$\text{Propellant Density, } (\delta k/k)/(\Delta \rho_H/\rho_{H_O})_{prop} = +0.0544$$
$$\text{Moderator Coolant Density, } (\delta k/k)/(\Delta \rho_H/\rho_{H_O})_{mod} = +0.0315$$
$$\text{Fuel Region Radius, } (\delta k/k)/(\Delta R_F/R_F) = -0.0413$$

2. Heat storage capacity is negligible in all components except the solid moderator region. The assumed values of mc_p in the solid moderator regions were 5124 Btu/deg R for the BeO and 6440 Btu/deg R for the graphite.

3. Choked flow conditions exist in the exit nozzle throat and in the turbine nozzles.

4. The turbopump characteristics used in the program are:

    Steady-state wheel speed = 22,000 rpm
    Moment of inertia of turbopump unit = 130 ft-lb-sec^2

5. The total flow rate in all circuits will vary directly with turbine wheel speed and the pump head rise will vary with the square of the wheel speed.

6. Fission product heating in the fuel cycle circuit varies with time according to the expression $Q_{FP} = 1890 \sqrt{t}$, where t is the total elapsed time of operation.
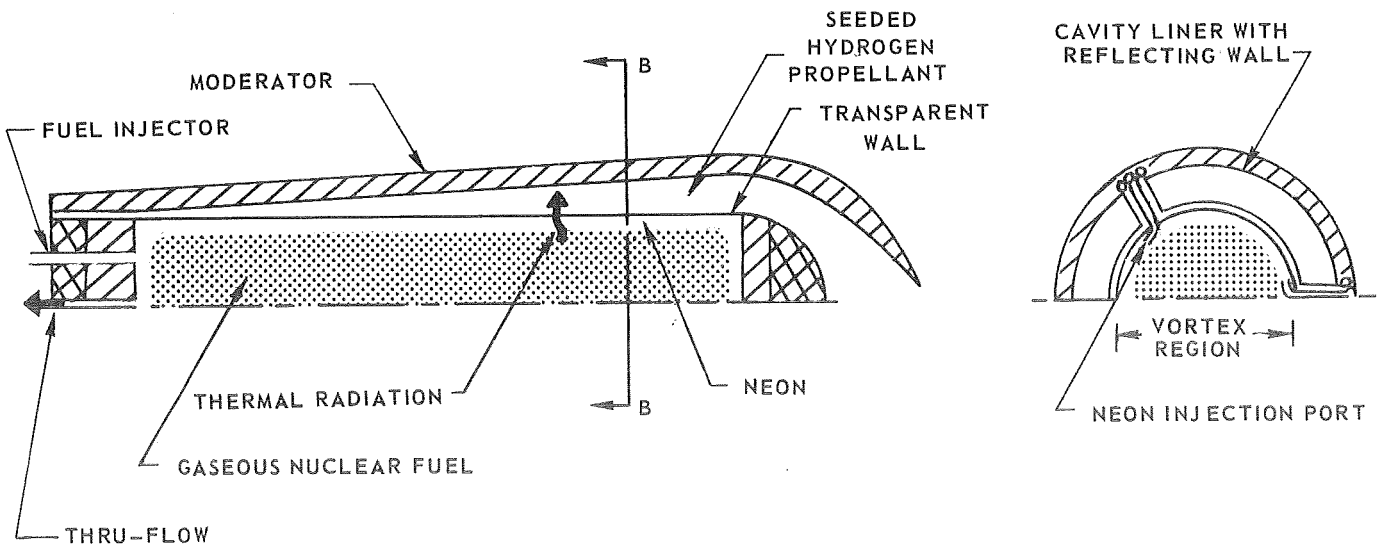
TABLE XIII (Continued)

7.   Constant physical properties of the coolants are used in each region.

8.   Chamber pressure varies as the product of propellant weight flow and the square root of propellant temperature, $p_c \propto W_p \sqrt{T_p}$, a result of choked flow conditions in the exit nozzle.

9.   Constant transport lags assumed for all regions and piping systems on the basis of reference coolant flow velocities.

10.   Fuel injection rate assumed to vary as the square root of the injection system pressure drop, $W_F \propto \sqrt{p_I - p_c}$ where p_I regulated to be 520 atm.

FIG. 1

SKETCHES ILLUSTRATING PRINCIPLE OF OPERATION OF NUCLEAR LIGHT BULB ENGINE

a) OVERALL CONFIGURATION

MODERATOR FLOW DIVIDER

UPPER END
MODERATOR

A

NOZZLES

SECTION A-A

PRESSURE SHELL

LOWER END
MODERATOR

REGION FOR PUMPS,
HEAT EXCHANGERS,
PLUMBING, SEPARATORS, ETC.

A

UNIT CAVITY

BeO MODERATOR

GRAPHITE MODERATOR
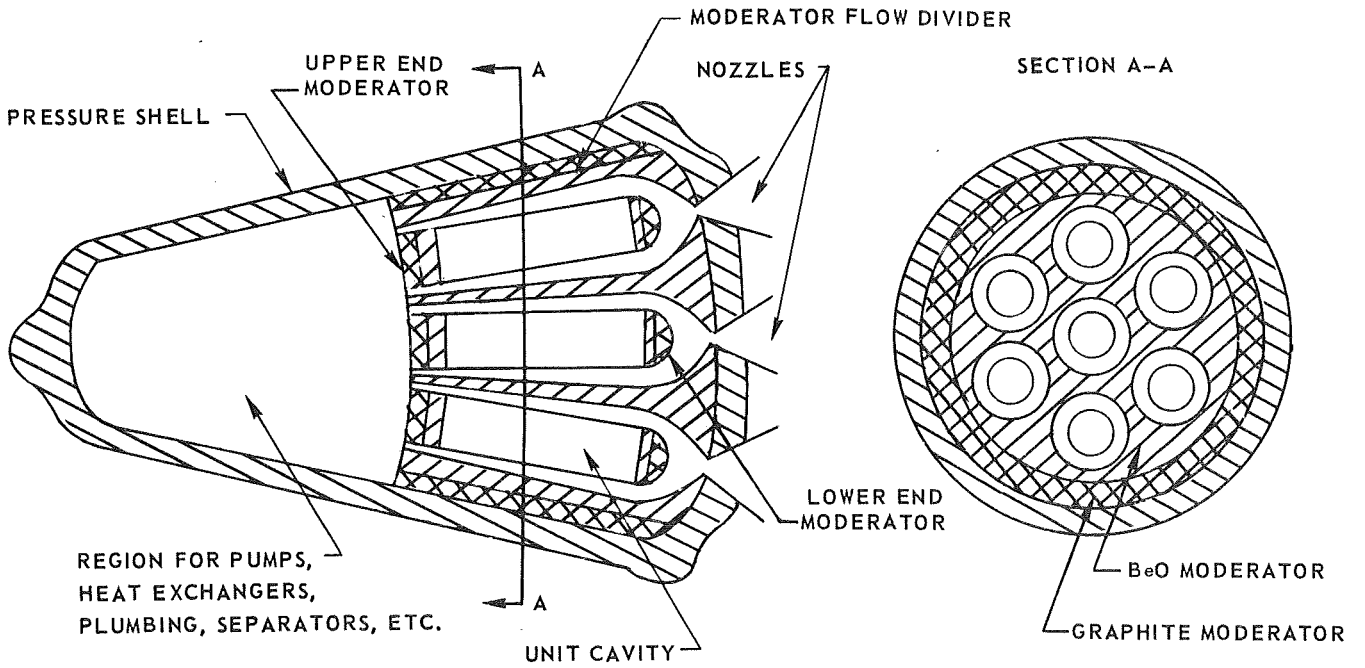
b) CONFIGURATION OF UNIT CAVITY

SECTION B-B

SEEDED
HYDROGEN
PROPELLANT

CAVITY LINER WITH
REFLECTING WALL

B

MODERATOR

TRANSPARENT
WALL

FUEL INJECTOR

B

NEON

VORTEX
REGION

THERMAL RADIATION

GASEOUS NUCLEAR FUEL

NEON INJECTION PORT

THRU-FLOW

NUCLEAR LIGHT BULB FLOW DIAGRAM
STATIONS DENOTED BY FOUR-DIGIT NUMBERS
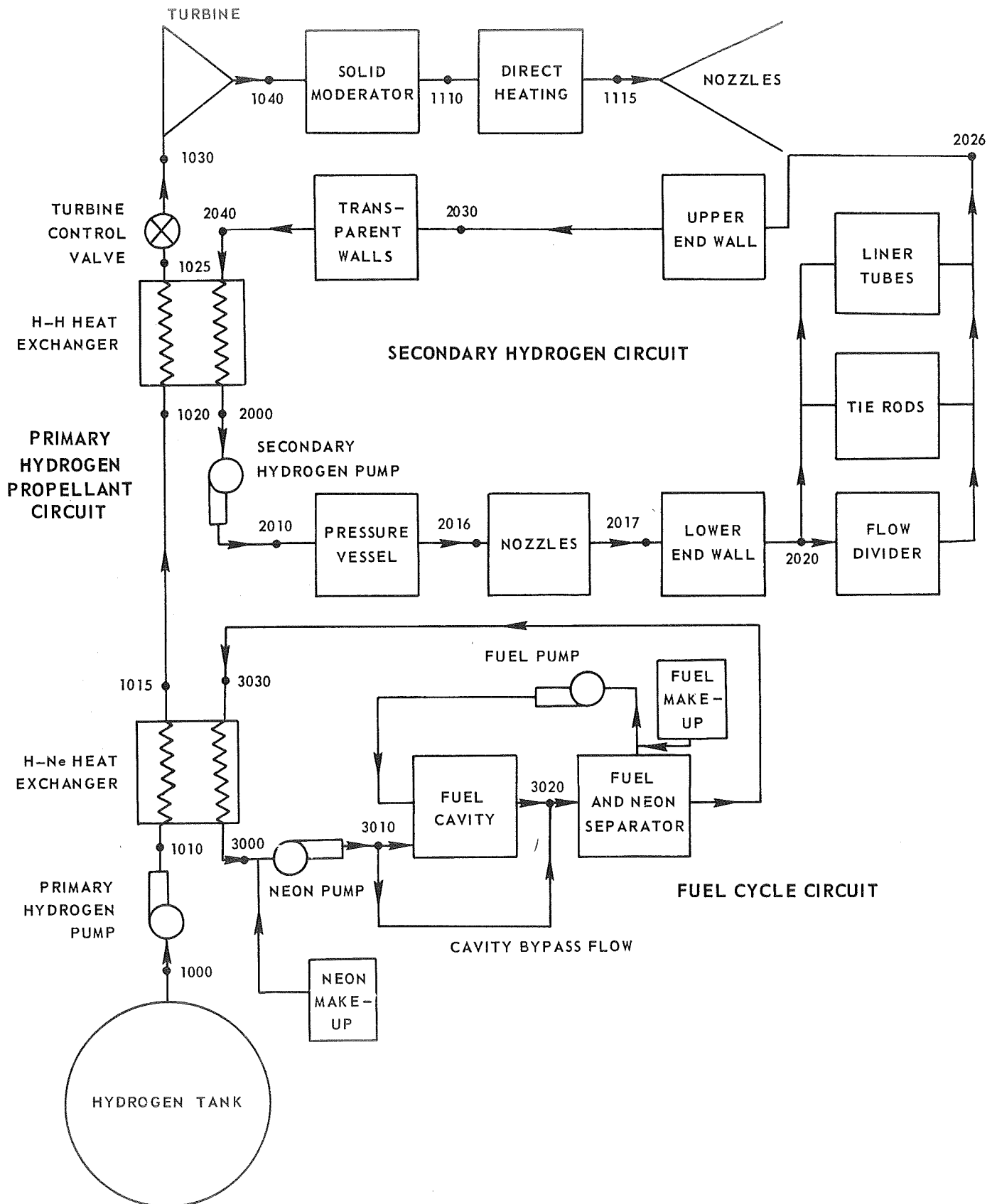
VARIATION OF FISSION PRODUCT DECAY HEATING WITH TOTAL OPERATING TIME

DECAY HEAT DATA OBTAINED FROM REF. 3

FISSION PRODUCT DECAY HEAT, MW

FISSION PRODUCT DECAY HEAT, BTU/SEC

TIME AT FULL POWER, MIN
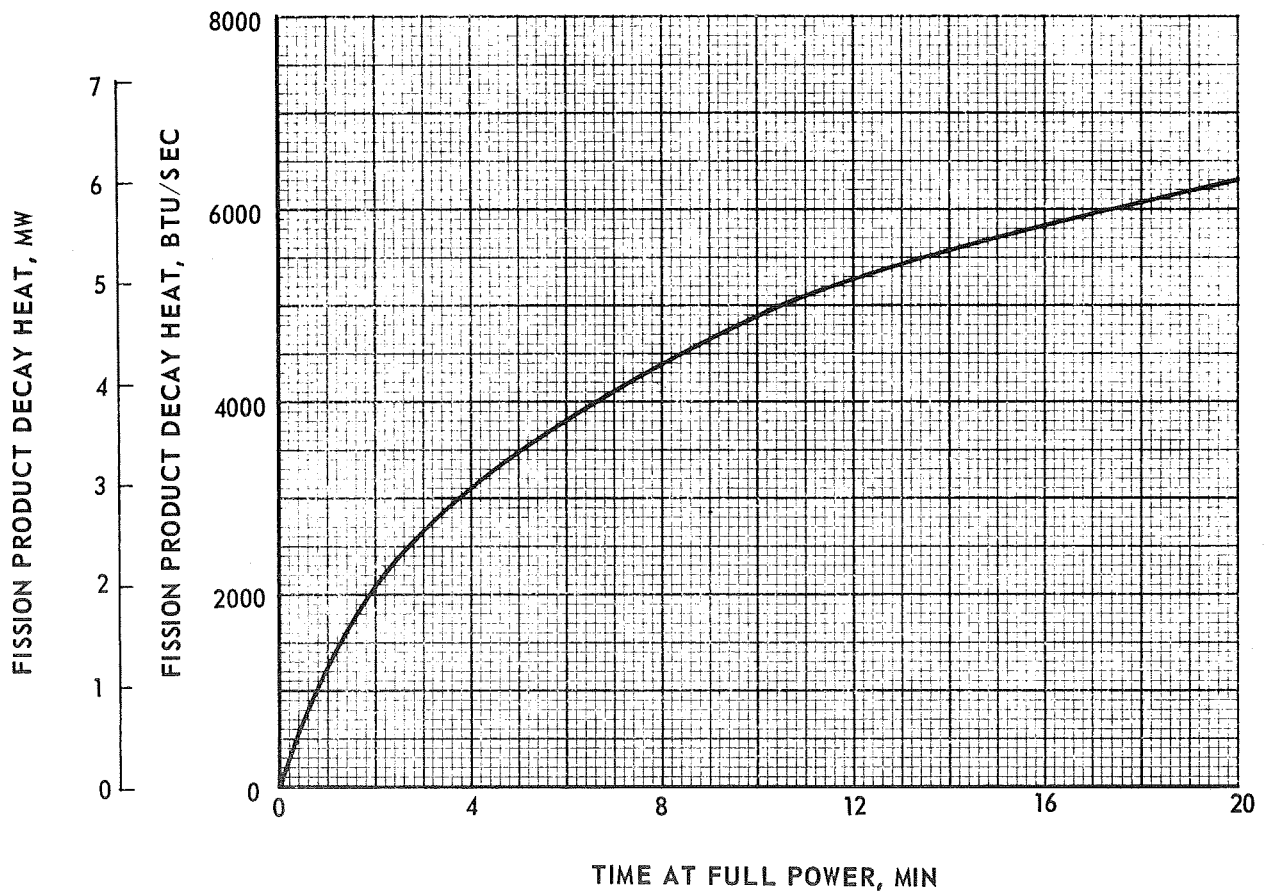
VAPOR PRESSURE OF UF$_6$

DATA TAKEN FROM REF. 9
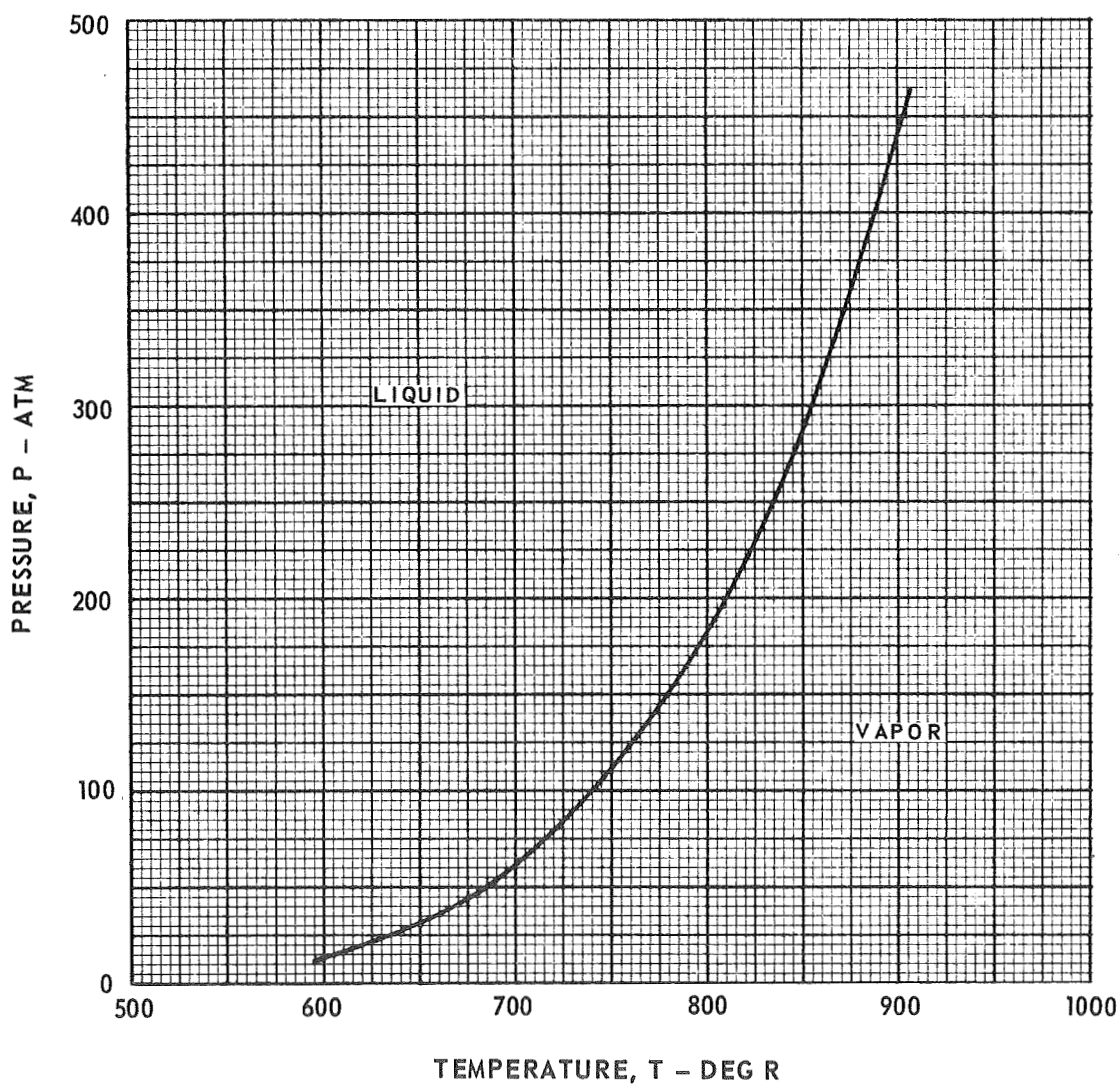
FIG. 5

AVERAGE FUEL TEMPERATURE DURING START-UP POWER RAMPS

$T^* = T_F/3.0$

LINEAR POWER VARIATION ASSUMED DURING START-UP

60 SEC START-UP	dP/dt = 76.67 MW/SEC
300 SEC START-UP	dP/dt = 15.33 MW/SEC
600 SEC START-UP	dP/dt = 7.667 MW/SEC

FULL POWER VALUE

60 SEC START-UP
300 SEC START-UP
600 SEC START-UP

TIME, t – SEC.

AVERAGE FUEL TEMPERATURE, T_F – DEG R

FIG. 6
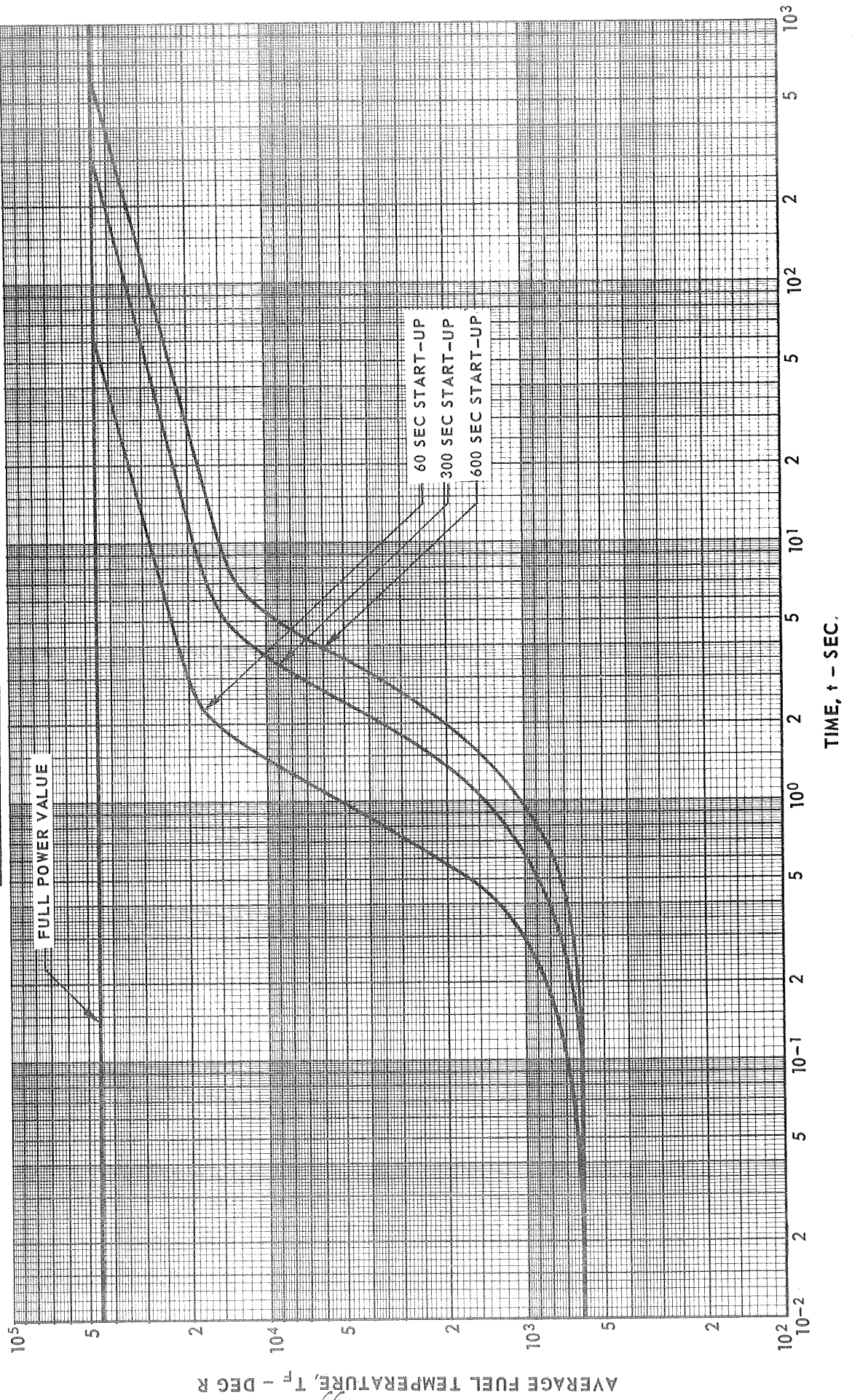
TOTAL NEON FLOW RATE DURING START-UP POWER RAMPS

MAXIMUM CAVITY FLOW REQUIREMENT = 24.57 LB/SEC

FLOW REQUIRED TO MAINTAIN CONSTANT ρ_{B_6} = 0.924 LB/FT^3
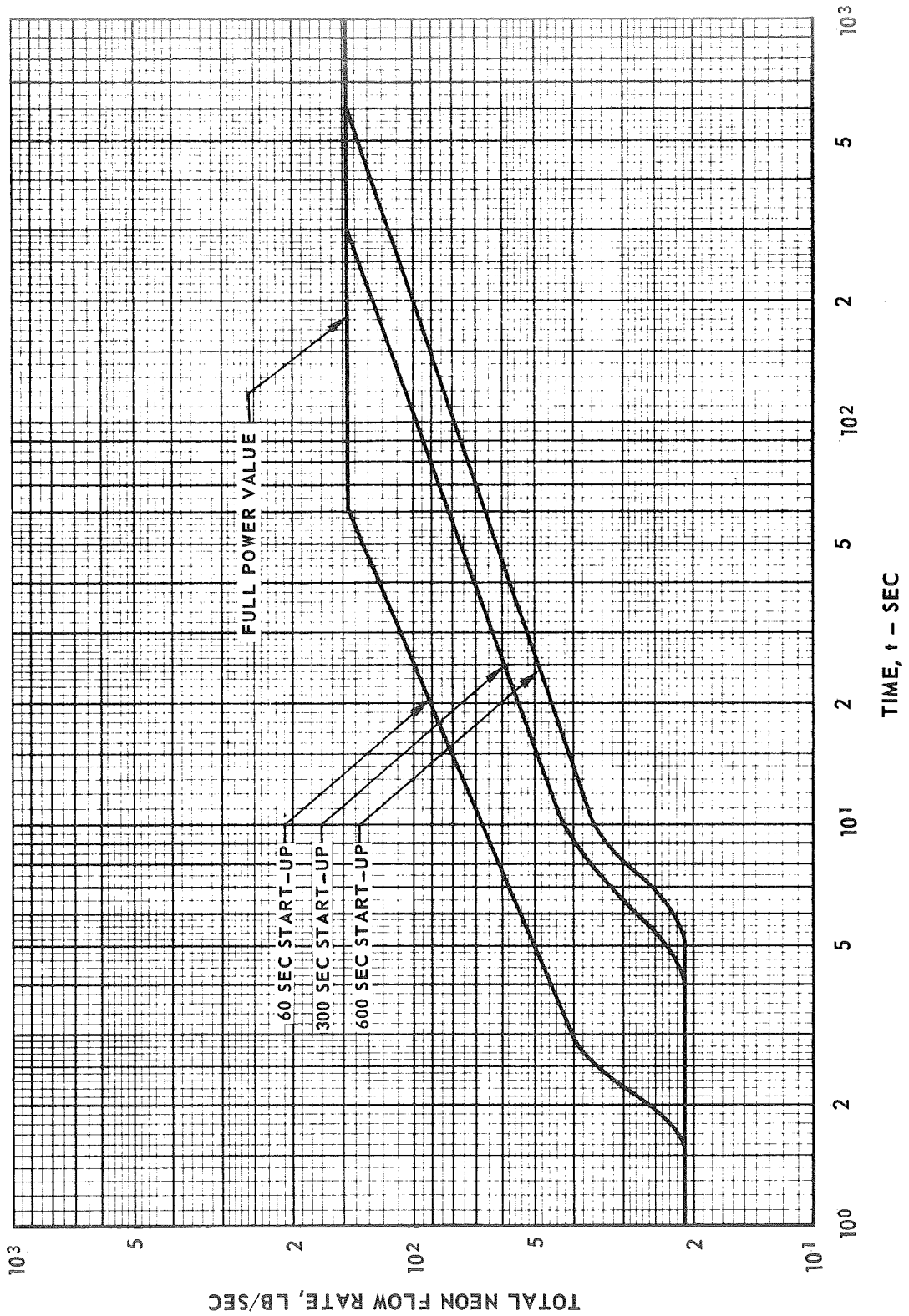
AVERAGE BeO TEMPERATURE DURING START—UP POWER RAMPS

TOTAL BeO MASS = 12,200 LB

ASSUMED VALUE OF MC_P = 5124 BTU/DEG R

FIG. 8
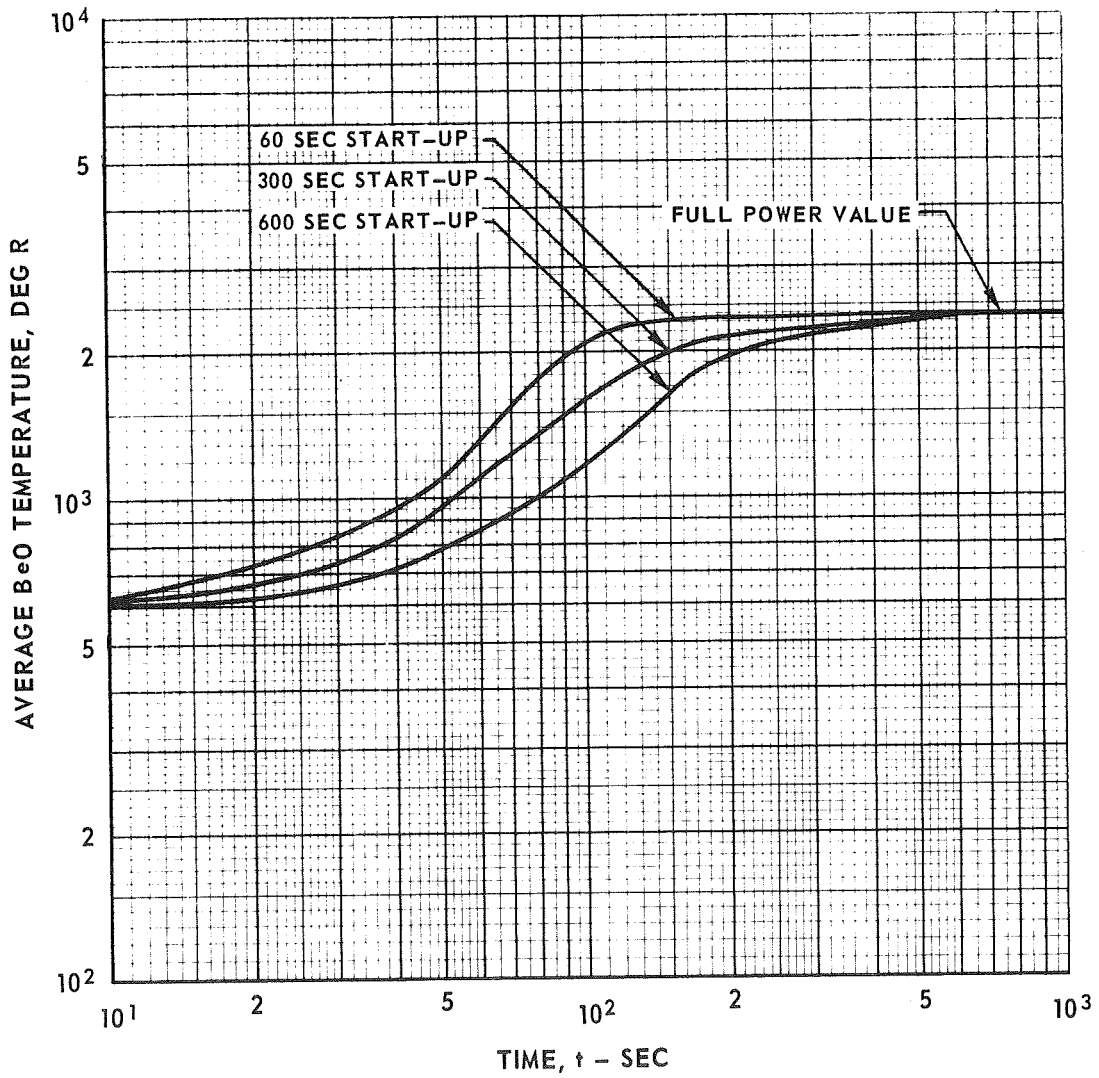
AVERAGE GRAPHITE TEMPERATURE DURING START−UP POWER RAMPS

TOTAL GRAPHITE MASS = 26,800 LB

ASSUMED VALUE OF MC_p = 6440 BTU/DEG R

FIG. 9
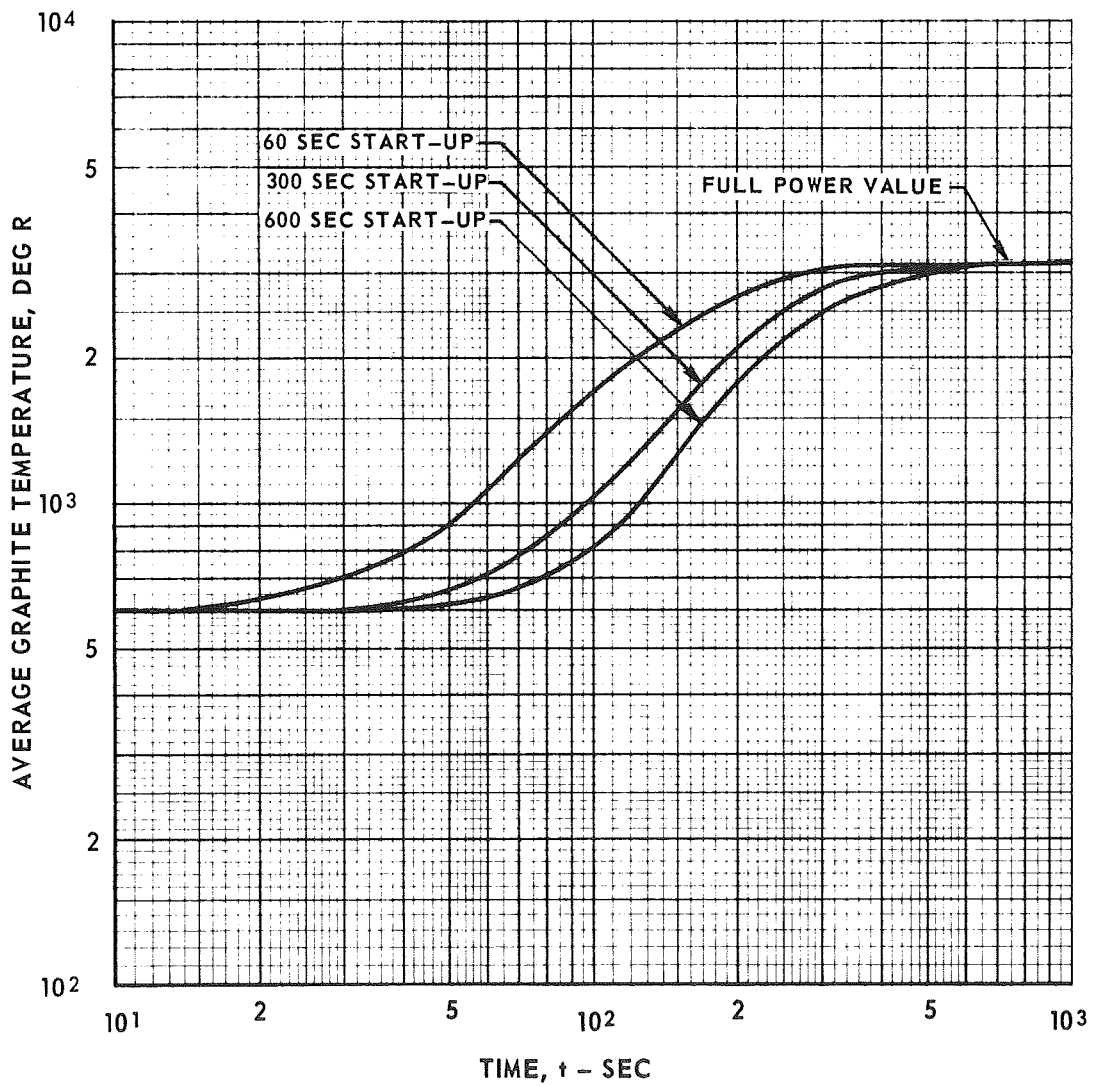
PROPELLANT TEMPERATURE DURING START–UP POWER RAMPS

FIG.10
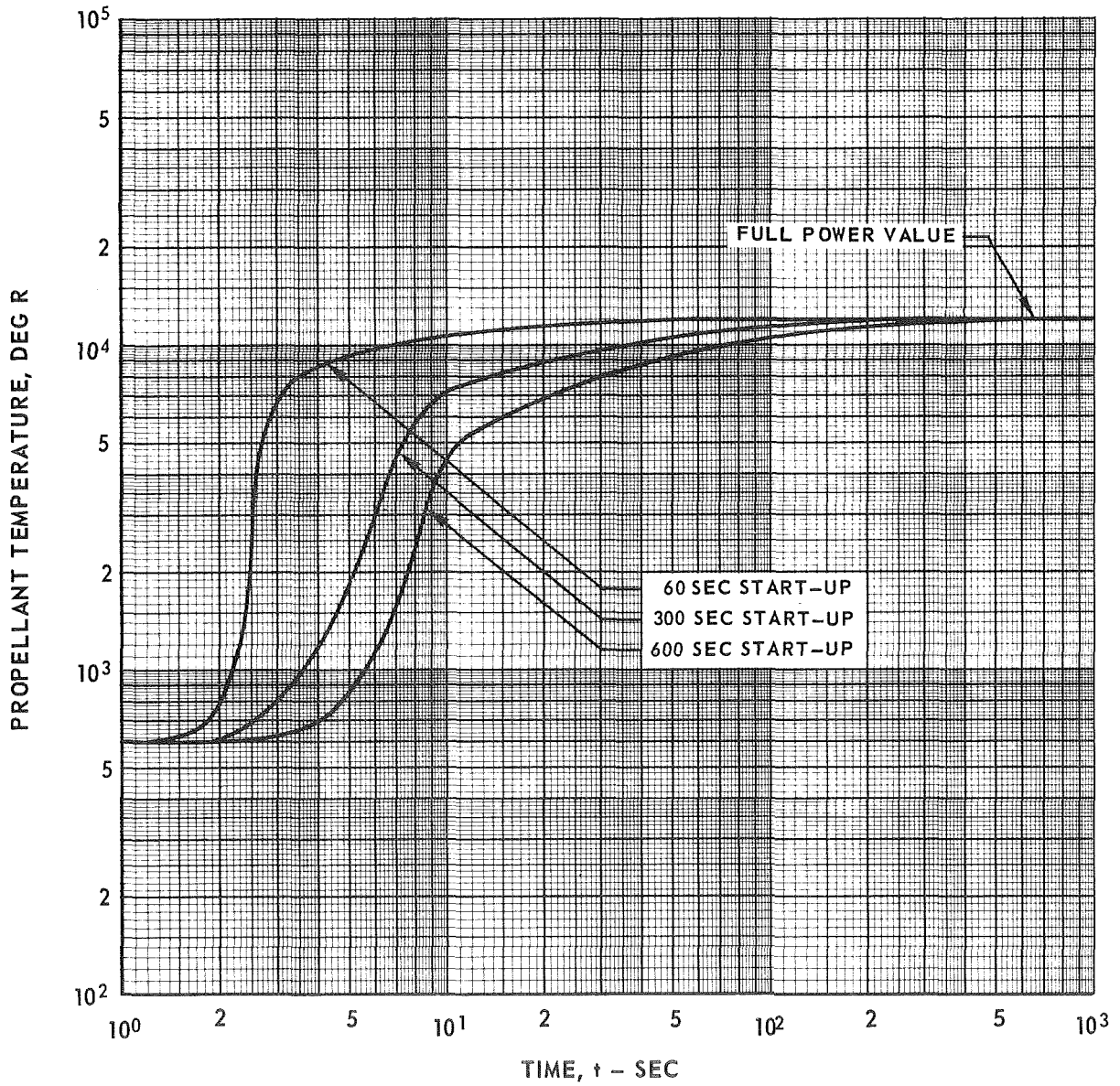
CAVITY PRESSURE DURING START-UP POWER RAMPS

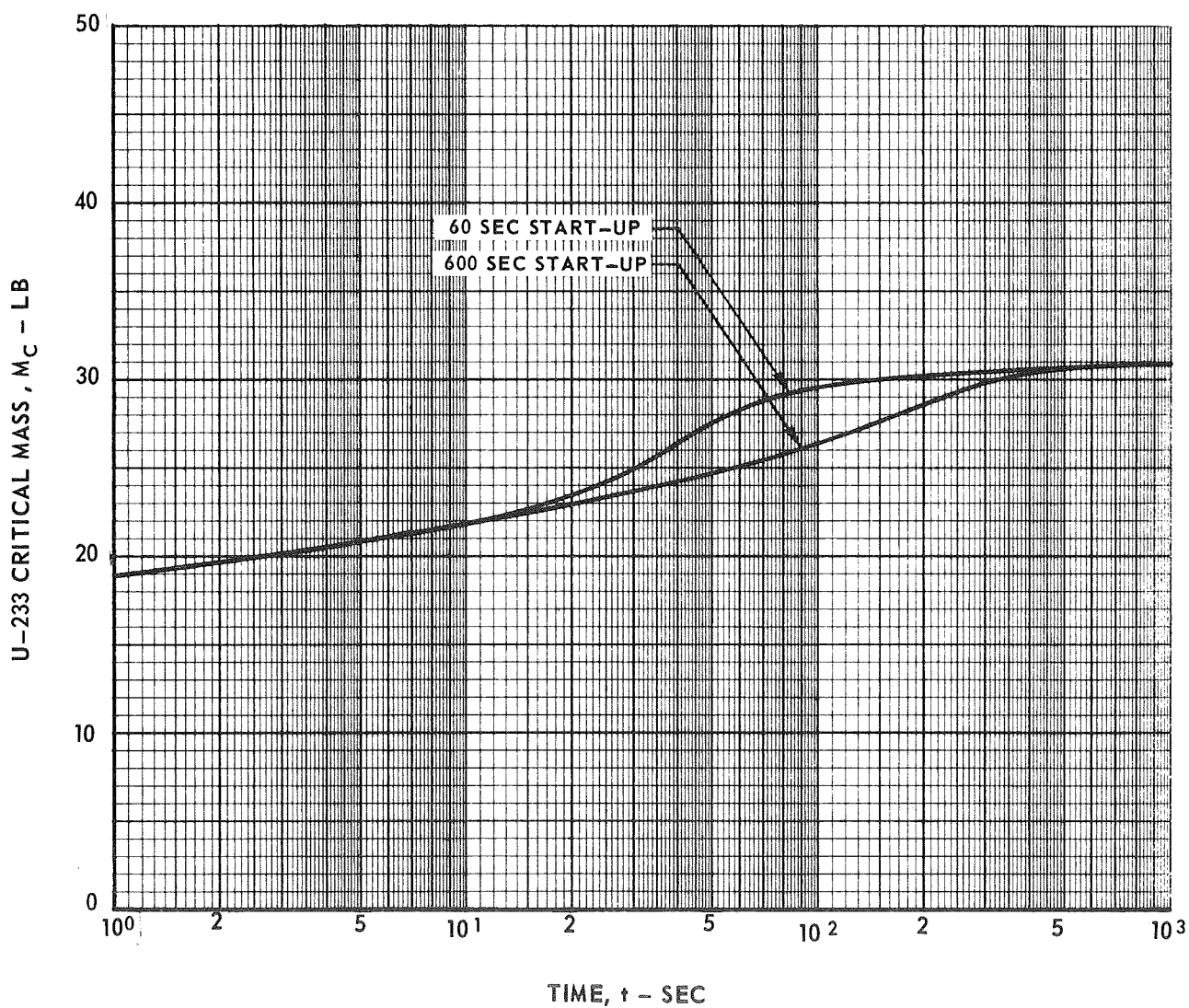PRESSURES BASED ON NEON TEMPERATURE AND DENSITY AT EDGE OF FUEL

FIG. 11
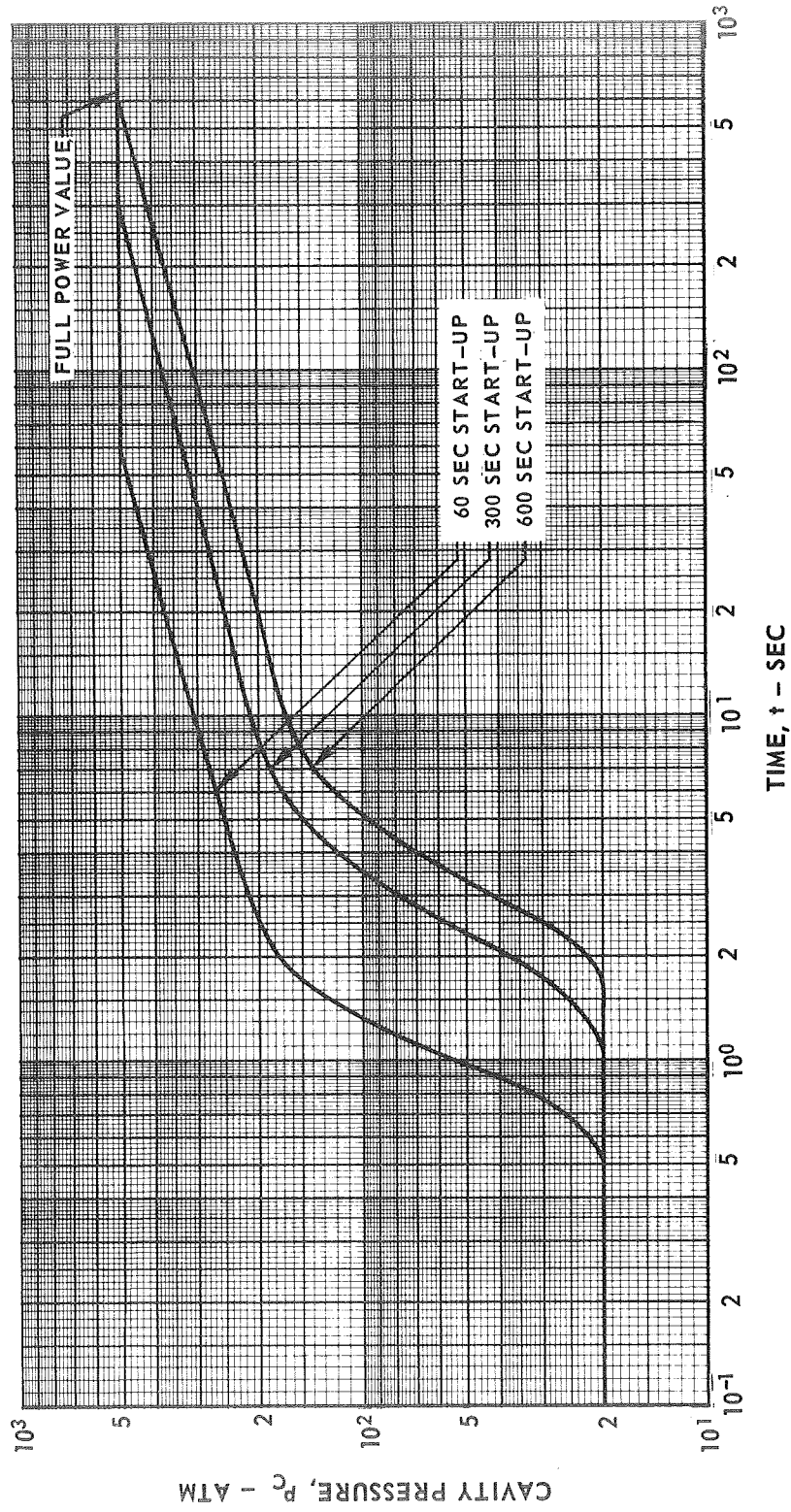
REQUIRED NOZZLE THROAT AREA DURING START-UP POWER RAMPS
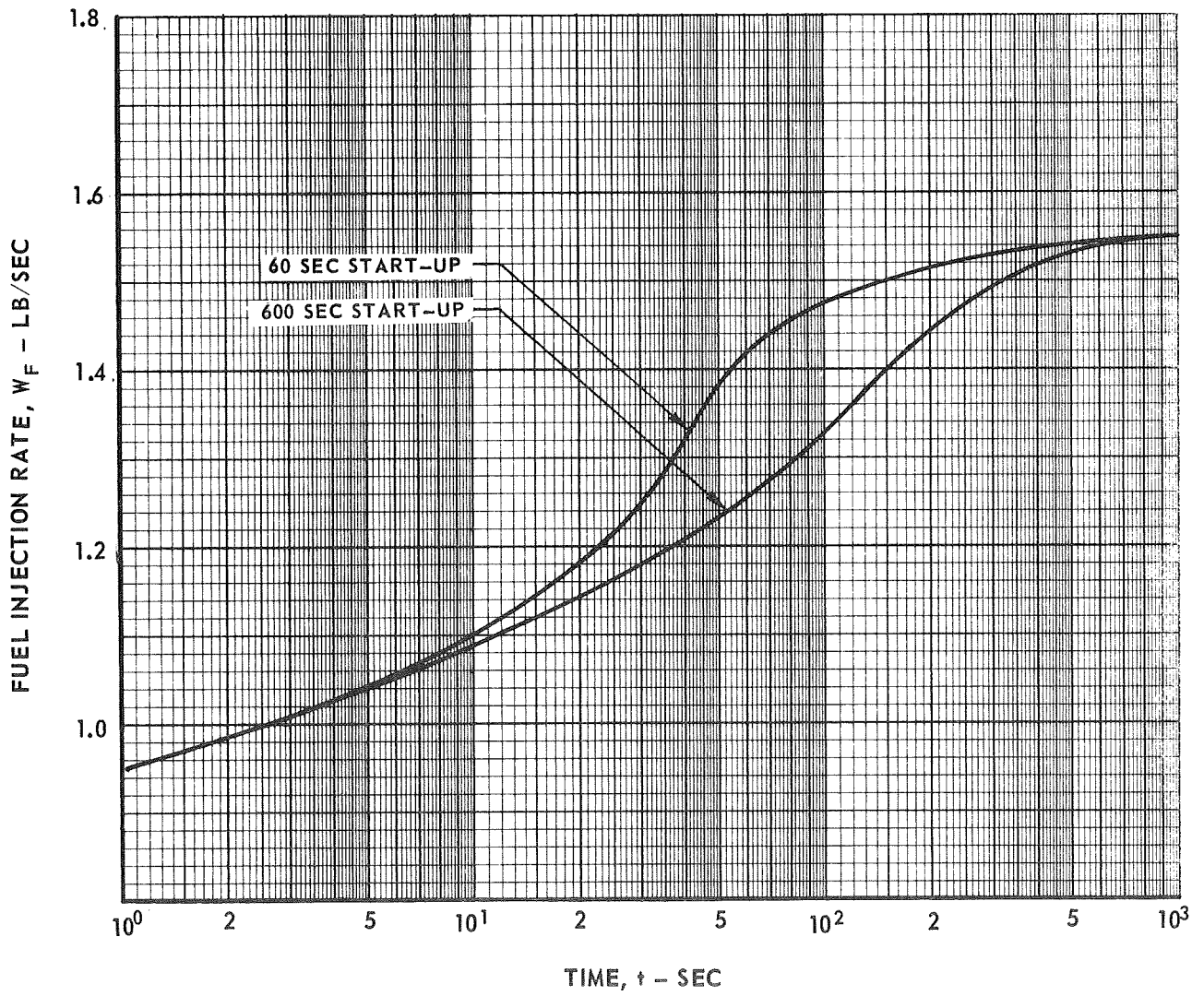
NOZZLE AREAS BASED ON THROAT FLOW PARAMETERS OF REF. 11
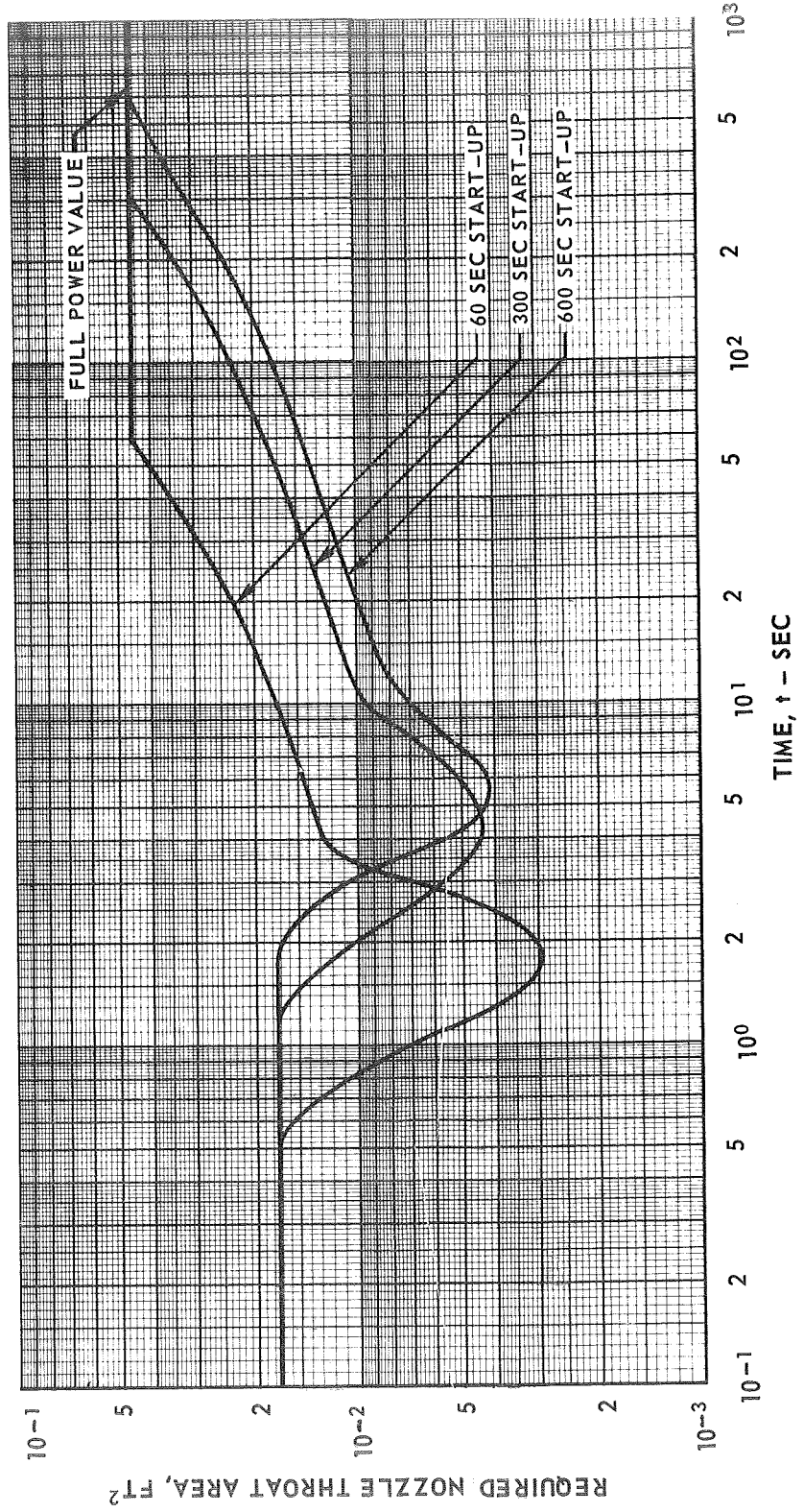
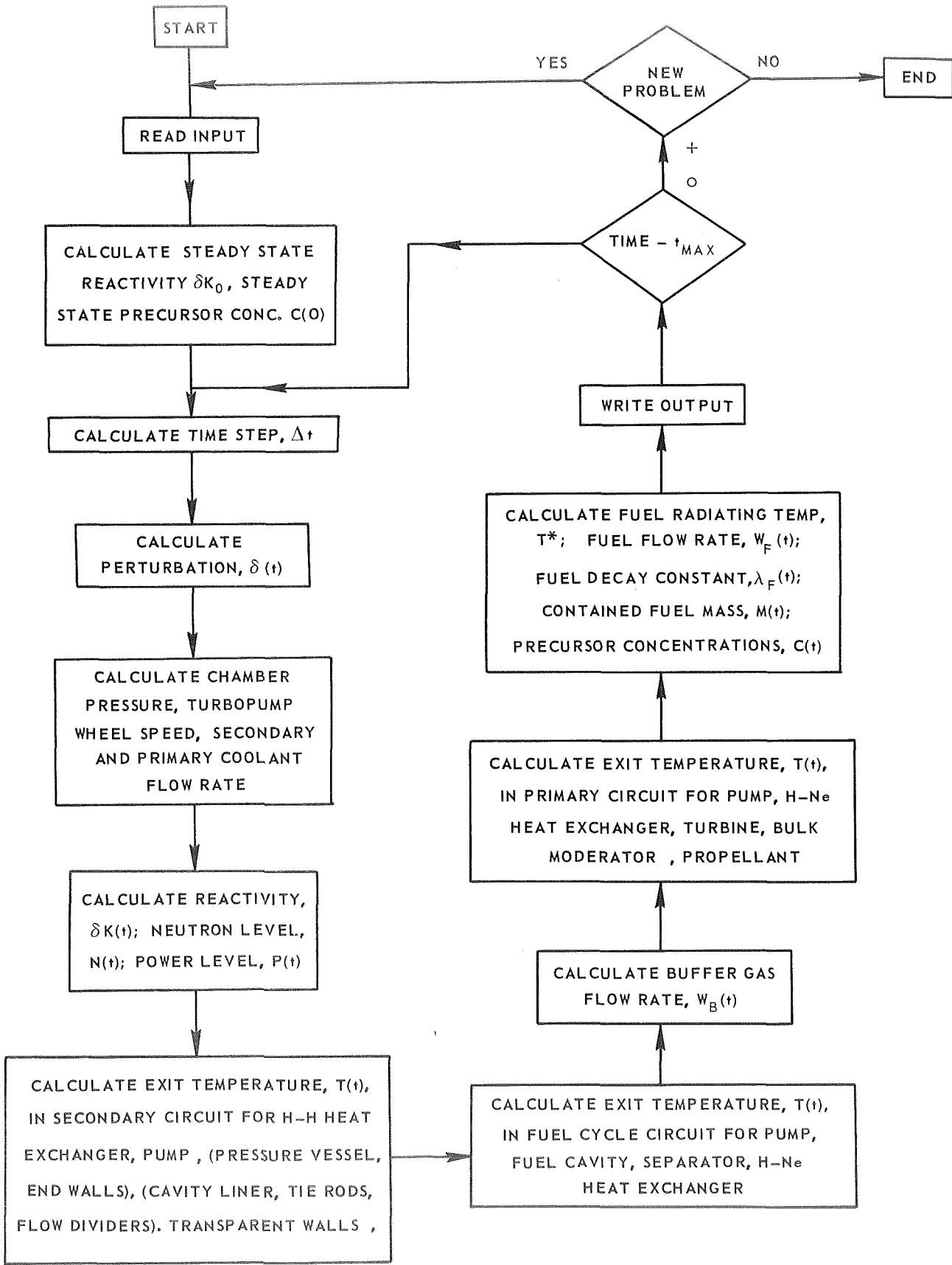## VARIATION OF U-233 CRITICAL MASS DURING START-UP POWER RAMPS

FIG. 13

VARIATION OF FUEL INJECTION RATE DURING START-UP POWER RAMPS

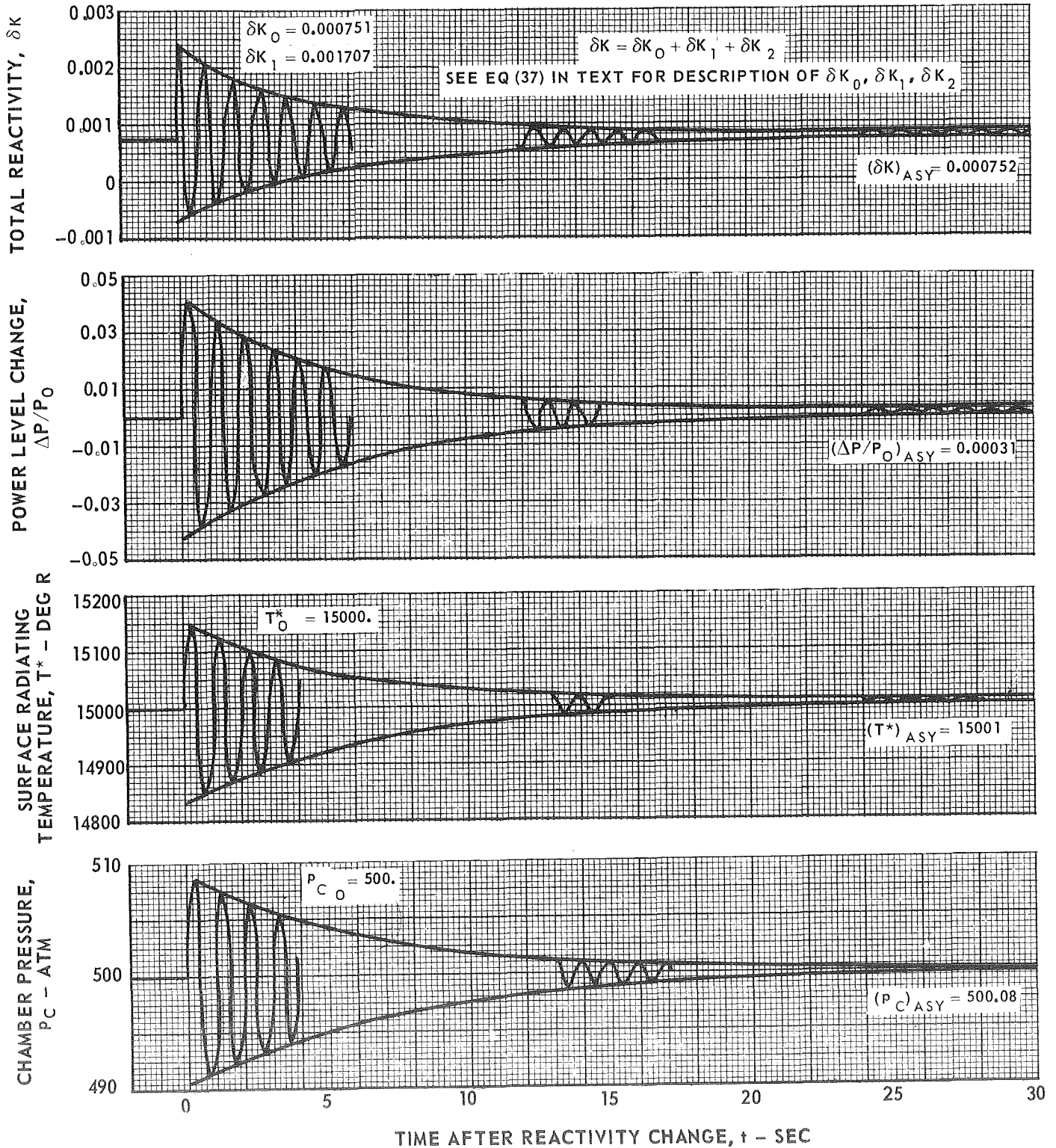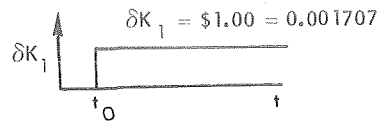WEIGHT FLOW BASED ON EXCESS NUCLEAR FUEL REQUIRED TO SUSTAIN LINEAR POWER RAMPS

FIG. 14

NUCLEAR LIGHT BULB SIMULATION PROGRAM FLOW DIAGRAM

```
                    START

                                          YES        NEW          NO
                                        ───────     PROBLEM     ───────        END
          READ INPUT
                                                       +

                                                       o

    CALCULATE STEADY STATE
      REACTIVITY δK₀, STEADY              TIME – t_MAX
    STATE PRECURSOR CONC. C(O)

                                               WRITE OUTPUT
    CALCULATE TIME STEP, Δt

                                       CALCULATE FUEL RADIATING TEMP,
         CALCULATE                        T*;   FUEL FLOW RATE, W_F(t);
    PERTURBATION, δ(t)                    FUEL DECAY CONSTANT,λ_F(t);
                                          CONTAINED FUEL MASS, M(t);
                                        PRECURSOR CONCENTRATIONS, C(t)
      CALCULATE CHAMBER
    PRESSURE, TURBOPUMP
    WHEEL SPEED, SECONDARY
    AND PRIMARY COOLANT            CALCULATE EXIT TEMPERATURE, T(t),
         FLOW RATE                 IN PRIMARY CIRCUIT FOR PUMP, H–Ne
                                   HEAT EXCHANGER, TURBINE, BULK
                                        MODERATOR , PROPELLANT
    CALCULATE REACTIVITY,
      δK(t); NEUTRON LEVEL,
    N(t); POWER LEVEL, P(t)
                                        CALCULATE BUFFER GAS
                                           FLOW RATE, W_B(t)

  CALCULATE EXIT TEMPERATURE, T(t),
  IN SECONDARY CIRCUIT FOR H–H HEAT   CALCULATE EXIT TEMPERATURE, T(t),
  EXCHANGER, PUMP , (PRESSURE VESSEL,  IN FUEL CYCLE CIRCUIT FOR PUMP,
  END WALLS), (CAVITY LINER, TIE RODS,   FUEL CAVITY, SEPARATOR, H–Ne
  FLOW DIVIDERS). TRANSPARENT WALLS ,        HEAT EXCHANGER
```
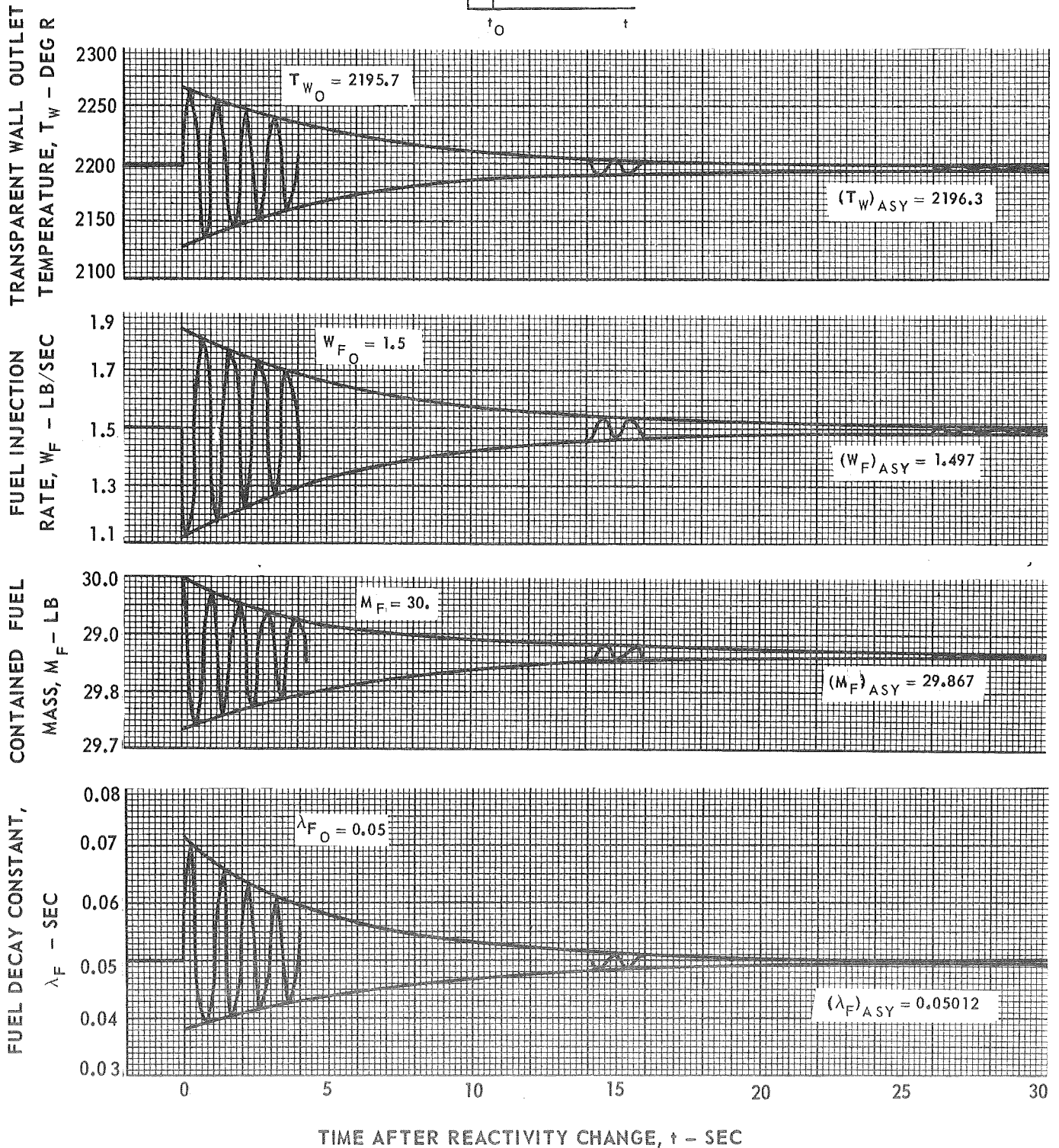
RESPONSE OF NUCLEAR LIGHT BULB ENGINE TO POSITIVE STEP CHANGE IN IMPOSED REACTIVITY

CONSTANT FUEL RADIUS

$\delta K_1 = \$1.00 = 0.001707$

$\delta K_0 = 0.000751$
$\delta K_1 = 0.001707$

$\delta K = \delta K_0 + \delta K_1 + \delta K_2$

SEE EQ (37) IN TEXT FOR DESCRIPTION OF $\delta K_0, \delta K_1, \delta K_2$

$(\delta K)_{ASY} = 0.000752$

$(\Delta P/P_0)_{ASY} = 0.00031$

$T_0^* = 15000.$

$(T^*)_{ASY} = 15001$

$P_{C_0} = 500.$

$(P_C)_{ASY} = 500.08$

TIME AFTER REACTIVITY CHANGE, t – SEC

(CONTINUED)

76

RESPONSE OF NUCLEAR LIGHT BULB ENGINE TO POSITIVE STEP CHANGE IN IMPOSED REACTIVITY

(CONTINUED)

CONSTANT FUEL RADIUS
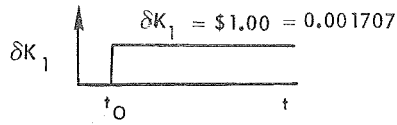
$$\delta K_1 = \$1.00 = 0.001707$$

TIME AFTER REACTIVITY CHANGE, t – SEC

RESPONSE OF NUCLEAR LIGHT BULB ENGINE TO POSITIVE STEP CHANGE IN FUEL INJECTION FLOW RATE CALIBRATION FACTOR

CONSTANT FUEL RADIUS

$W_F = K_F((520 - P_C)/20)^{1/2}$

AT $t < 0.0$, $K_F = W_{F_O} = 1.5$ LB/SEC

AT $t > 0.0$, $K_F = 1.1\ W_{F_O} = 1.65$ LB/SEC

$T_O^* = 15000.$

$T_{W_O} = 2195.7$

TIME AFTER FUEL INJECTION RATE CHANGE, t – SEC   (CONTINUED)

78
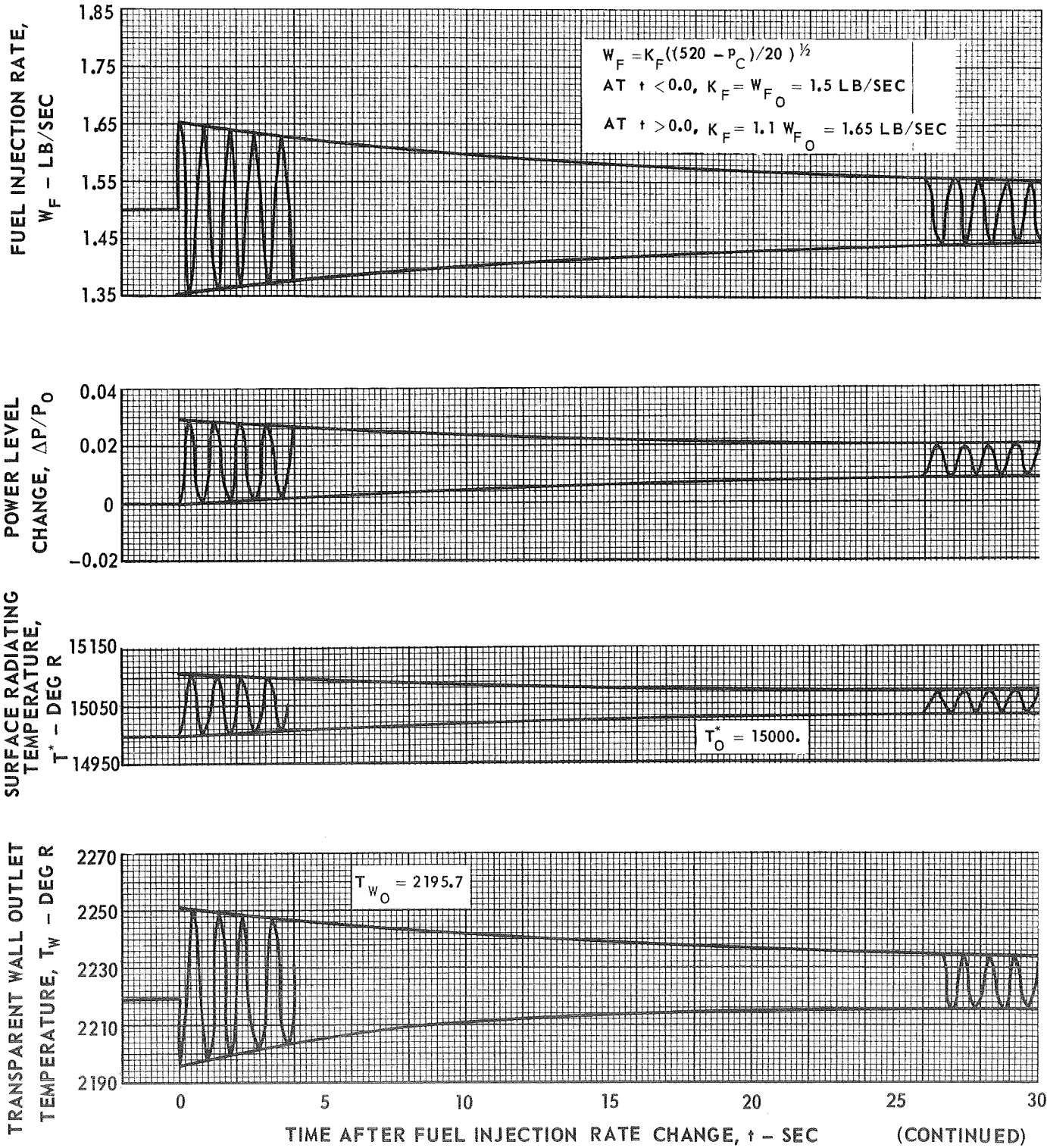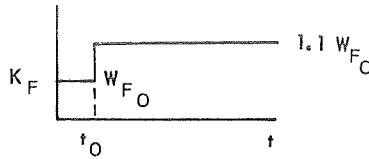
RESPONSE OF NUCLEAR LIGHT BULB ENGINE TO POSITIVE STEP CHANGE IN FUEL INJECTION FLOW RATE CALIBRATION FACTOR

(CONTINUED)

CONSTANT FUEL RADIUS

FIG. 17
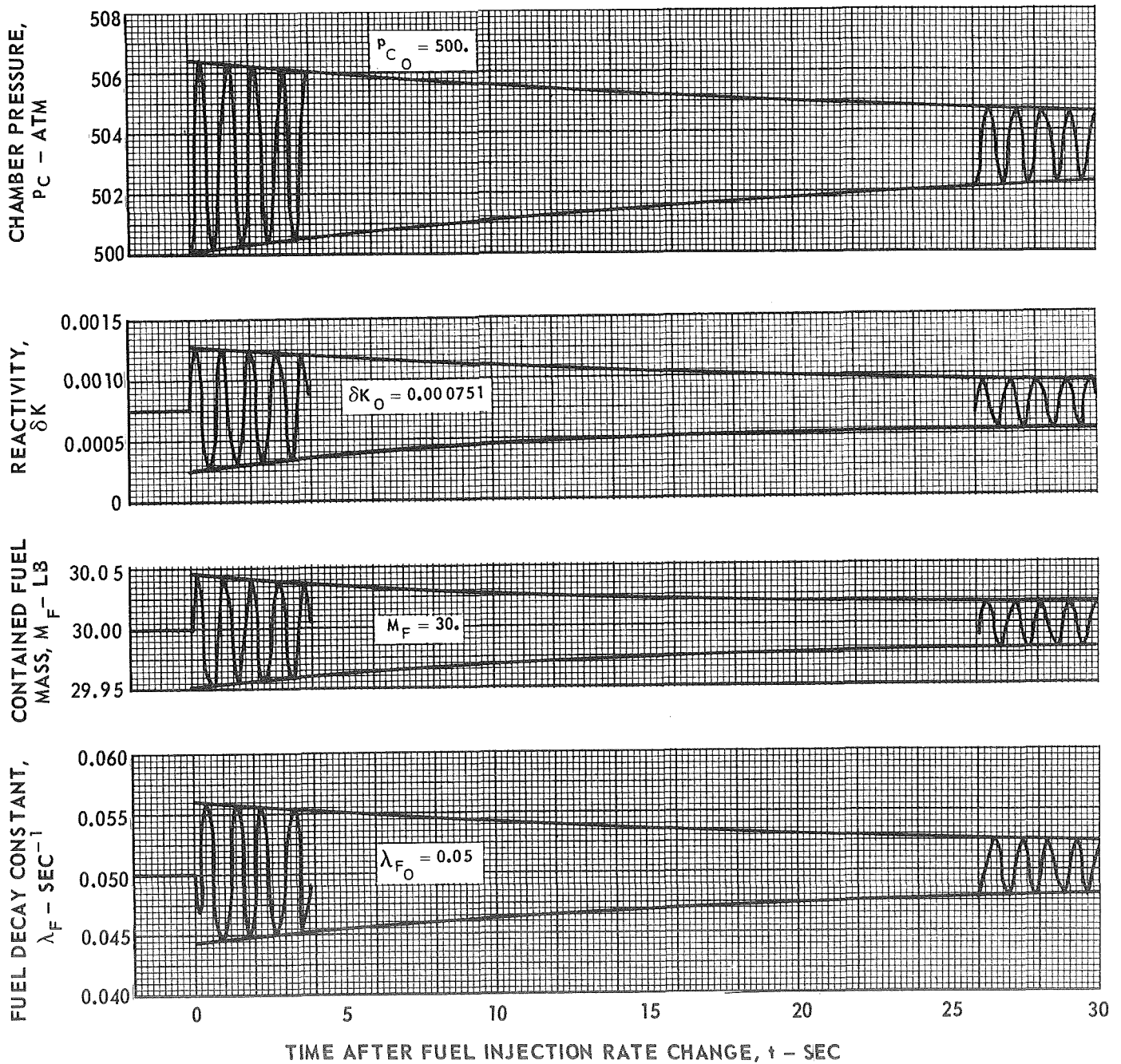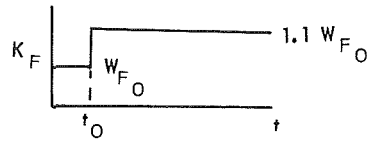
POWER LEVEL RESPONSE OF NUCLEAR LIGHT BULB ENGINE TO TERMINATING STEP CHANGE IN FUEL INJECTION FLOW RATE CALIBRATION FACTOR
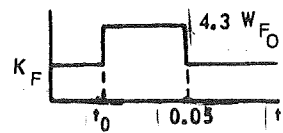
CONSTANT FUEL RADIUS

$$W_F = K_F((520 - P_C)/20)^{1/2}$$

a) $K_F = 4.3$ $W_{F_O} = 6.45$ LB/SEC

(SOLID U–233 INJECTION); $t = 0.0$ TO 0.005 SEC

$K_F = W_{F_O} = 1.5$ LB/SEC FOR $t > 0.005$
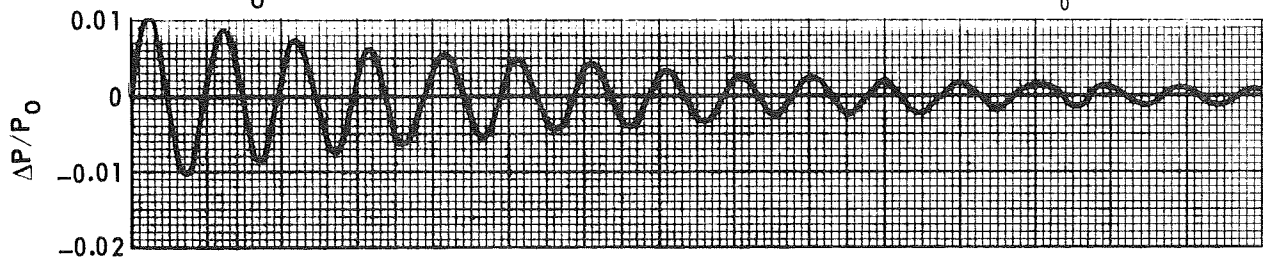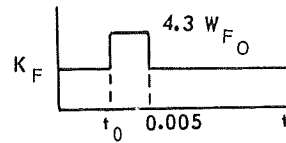
b) $K_F = 4.3$ $W_{F_O} = 6.45$ LB/SEC

(SOLID U–233 INJECTION); $t = 0.0$ TO 0.05 SEC
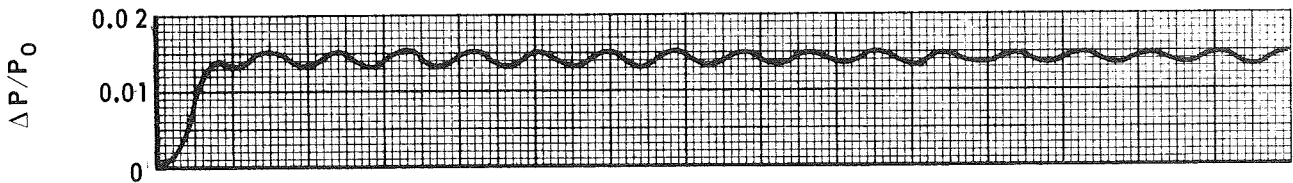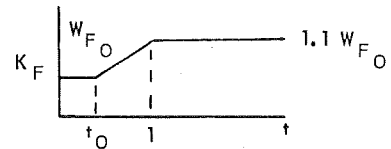
$K_F = W_{F_O} = 1.5$ LB/SEC FOR $t > 0.05$
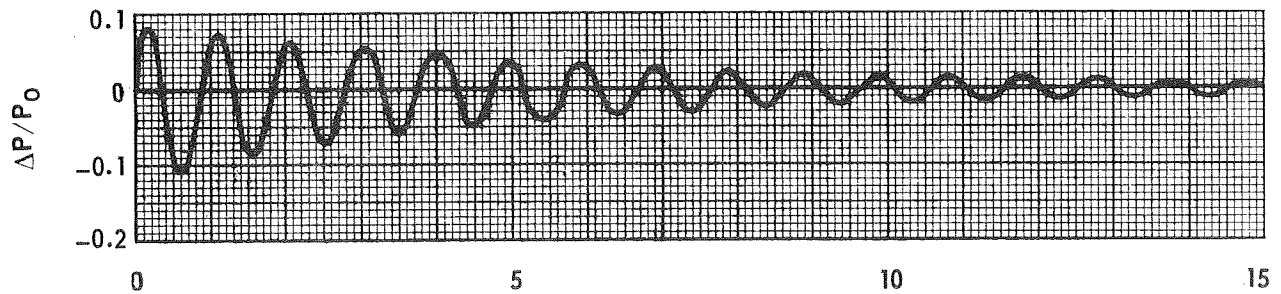
TIME AFTER START OF PERTURBATION, t – SEC

POWER LEVEL RESPONSE OF NUCLEAR LIGHT BULB ENGINE
TO TERMINATING RAMP CHANGE IN FUEL INJECTION FLOW RATE
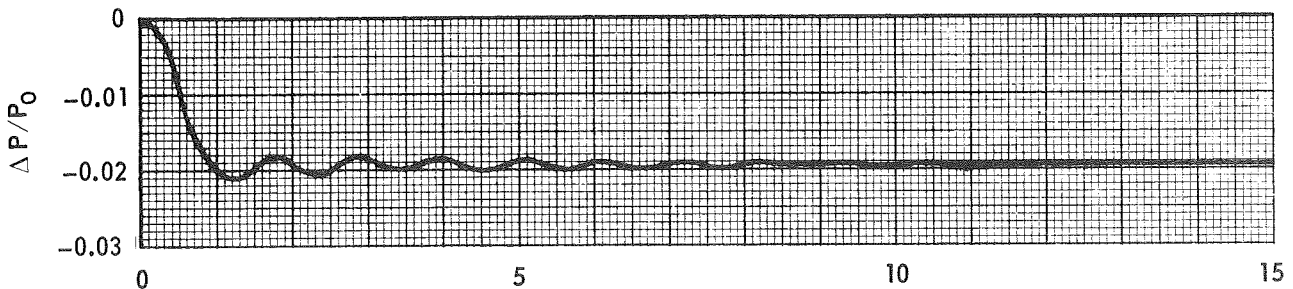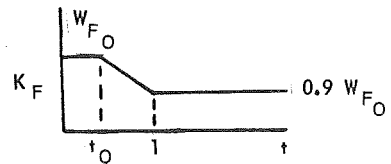### CALIBRATION FACTOR

CONSTANT FUEL RADIUS

$$W_F = K_F ((520 - P_C) / 20)^{1/2}$$

a) $K_F = 1.1 \ W_{F_O}$ /SEC FOR t = 0 TO 1.0 SEC;

$K_F = 1.1 \ W_{F_O}$ FOR t > 1.0

b) $K_F = 0.9 \ W_{F_O}$ /SEC FOR t = 0 TO 1.0 SEC;

$K_F = 0.9 \ W_{F_O}$ FOR t > 1.0

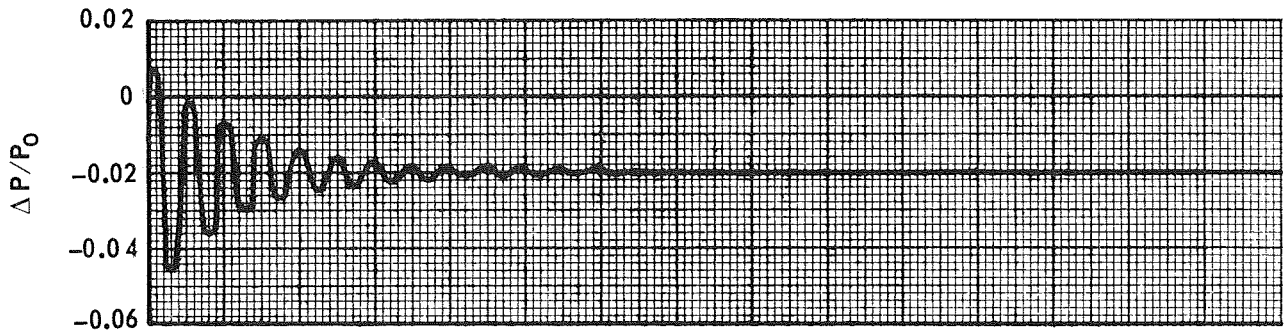TIME AFTER START OF PERTURBATION, t — SEC

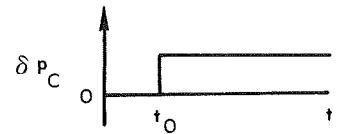# POWER LEVEL RESPONSE OF NUCLEAR LIGHT BULB ENGINE
TO STEP CHANGES IN CHAMBER PRESSURE
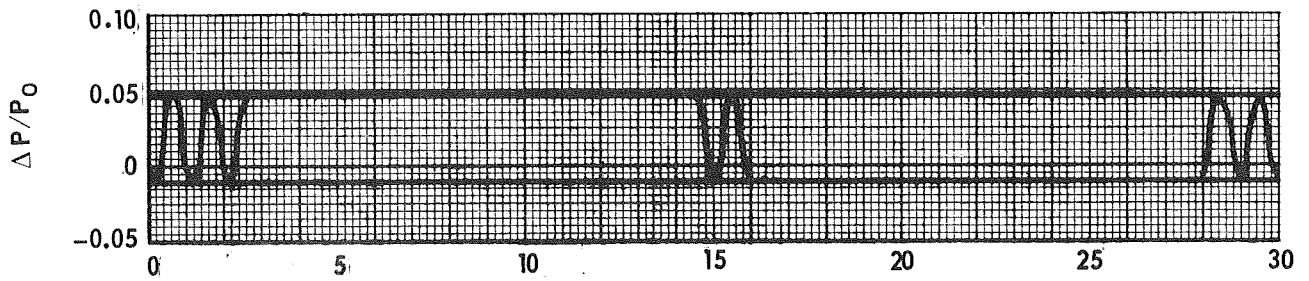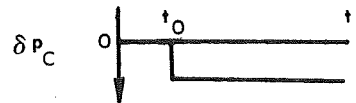
CONSTANT FUEL RADIUS

$$P_C = \left(P_{C_O} + \delta P_C \right) \left(\frac{W_P}{W_{P_O}} \sqrt{\frac{T_P}{T_{P_O}}} \right)$$

SEE EQ (33) IN TEXT FOR DESCRIPTION OF W_P, W_{P_O}, T_P, T_{P_O}

a) $\delta P_C = 0.01 \, P_{C_O}$

b) $\delta P_C = -0.01 \, P_{C_O}$

TIME AFTER START OF PERTURBATION, t — SEC

POWER LEVEL RESPONSE OF NUCLEAR LIGHT BULB ENGINE
TO TERMINATING RAMP CHANGES IN TURBO-PUMP WHEEL SPEED

CONSTANT FUEL RADIUS

$$\nu = \nu_0 + \delta\nu_1 + \delta\nu_2$$

$$\nu_0 = 22000 \quad RPM$$

$$\delta\nu_1 = \text{IMPOSED WHEEL SPEED CHANGE}$$

SEE EQ (21) IN TEXT FOR DESCRIPTION OF $\delta\nu_2$

a) $\delta\nu_1 = 0.02\nu_0$ /SEC FOR t = 0.0 TO 1.0 SEC;
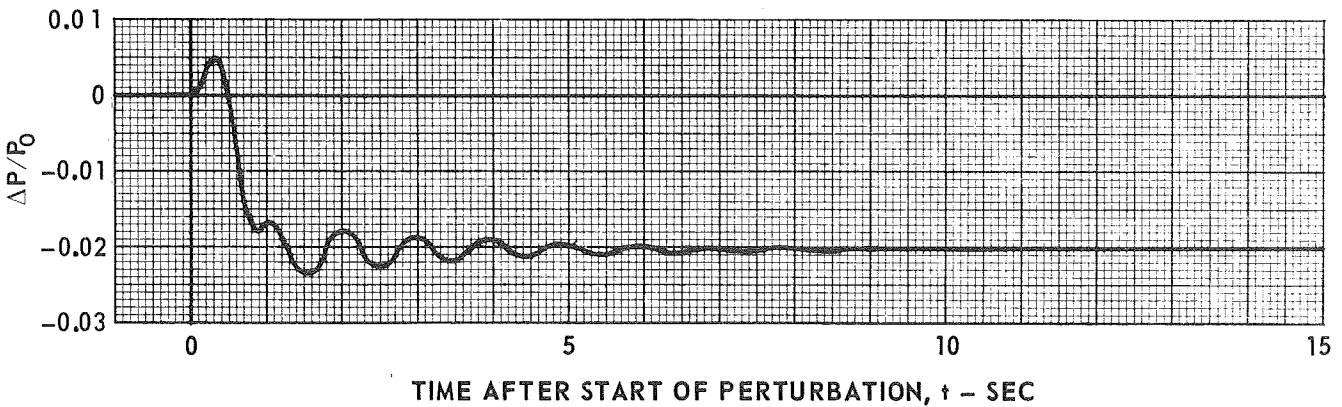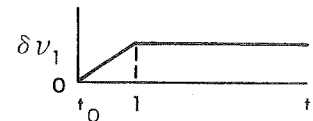
$\delta\nu_1 = 0.02\nu_0$ FOR t > 1.0

TIME AFTER START OF PERTURBATION, t – SEC

b) $\delta\nu_1 = -0.02\nu_0$ /SEC FOR t = 0.0 TO 1.0 SEC;

$\delta\nu_1 = -0.02\nu_0$ FOR t > 1.0

TIME AFTER START OF PERTURBATION, t – SEC

FIG. 21
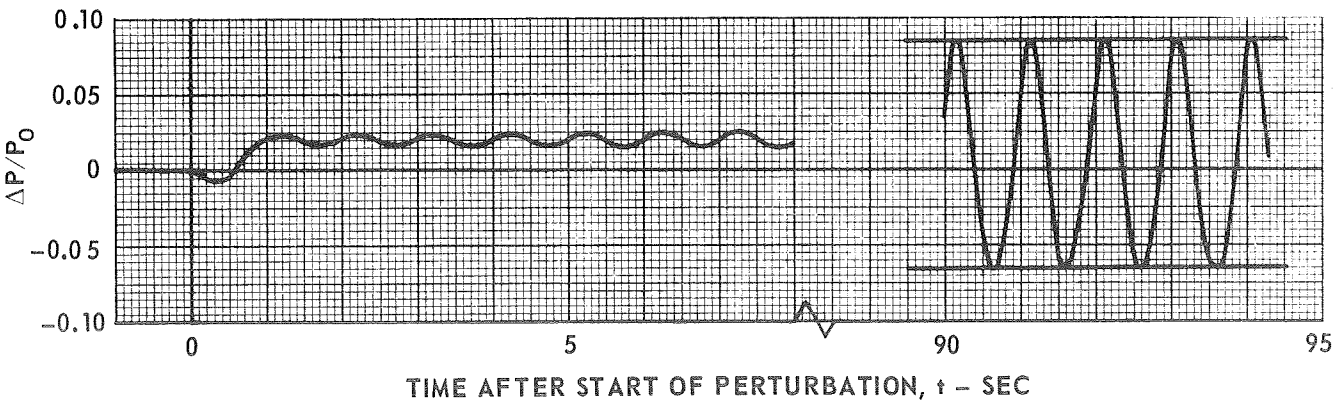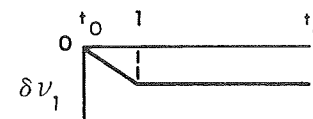
POWER LEVEL RESPONSE OF NUCLEAR LIGHT BULB ENGINE
TO STEP CHANGES IN FUEL CLOUD RADIUS

$$R_F = R_{F_O} + \delta R_F$$

a) $\delta R_F = 0.05\ R_{F_O}$

δR_F

t_O t

t_O t

δR_F

b) $\delta R_F = -0.05\ R_{F_O}$

TIME AFTER START OF PERTURBATION, t – SEC

FIG. 22

POWER LEVEL RESPONSE OF NUCLEAR LIGHT BULB ENGINE
TO TERMINATING RAMP CHANGES IN FUEL CLOUD RADIUS

$$R_F = R_{F_0} + \delta R_F$$

a) $\delta R_F = 0.05\ R_{F_0}/\text{SEC}\ t = 0\ \text{TO}\ 1.0\ \text{SEC};$

$\delta R_F = 0.05\ R_{F_0}\ \text{FOR}\ t > 1.0$

b) $\delta R_F = -0.05\ R_{F_0}/\text{SEC FOR}\ t = 0\ \text{TO}\ 1.0\ \text{SEC};$

$\delta R_F = -0.05\ R_{F_0}\ \text{FOR}\ t > 1.0$
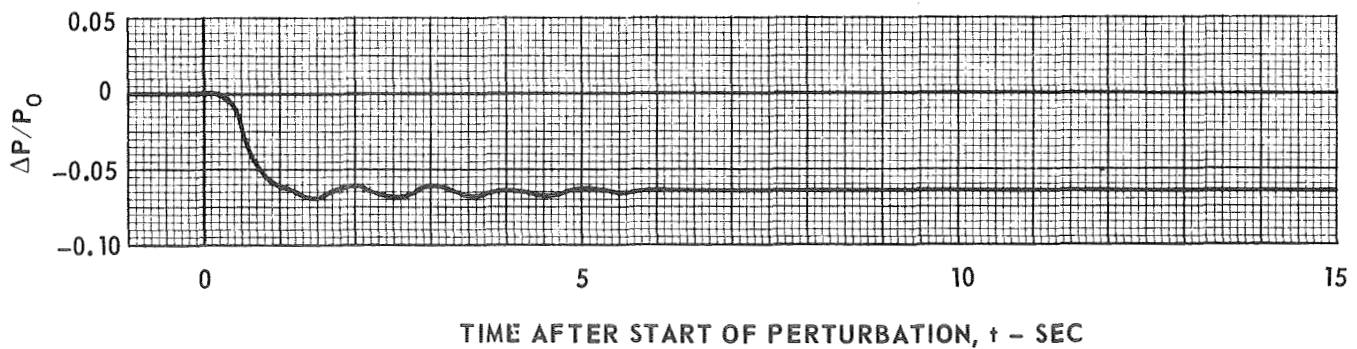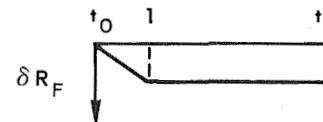
FIG. 23

GAIN AND PHASE DIAGRAMS WITH RESPECT TO FEEDBACK REACTIVITY FOR RESPONSE OF POWER
LEVEL TO SMALL SINUSOIDAL OSCILLATIONS IN REACTIVITY
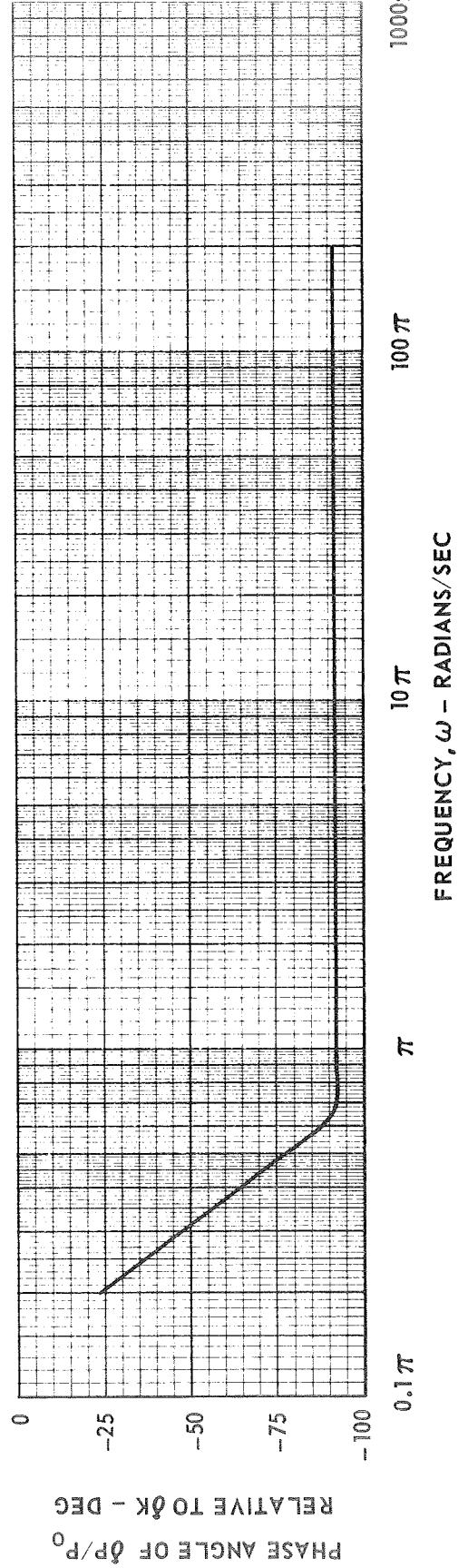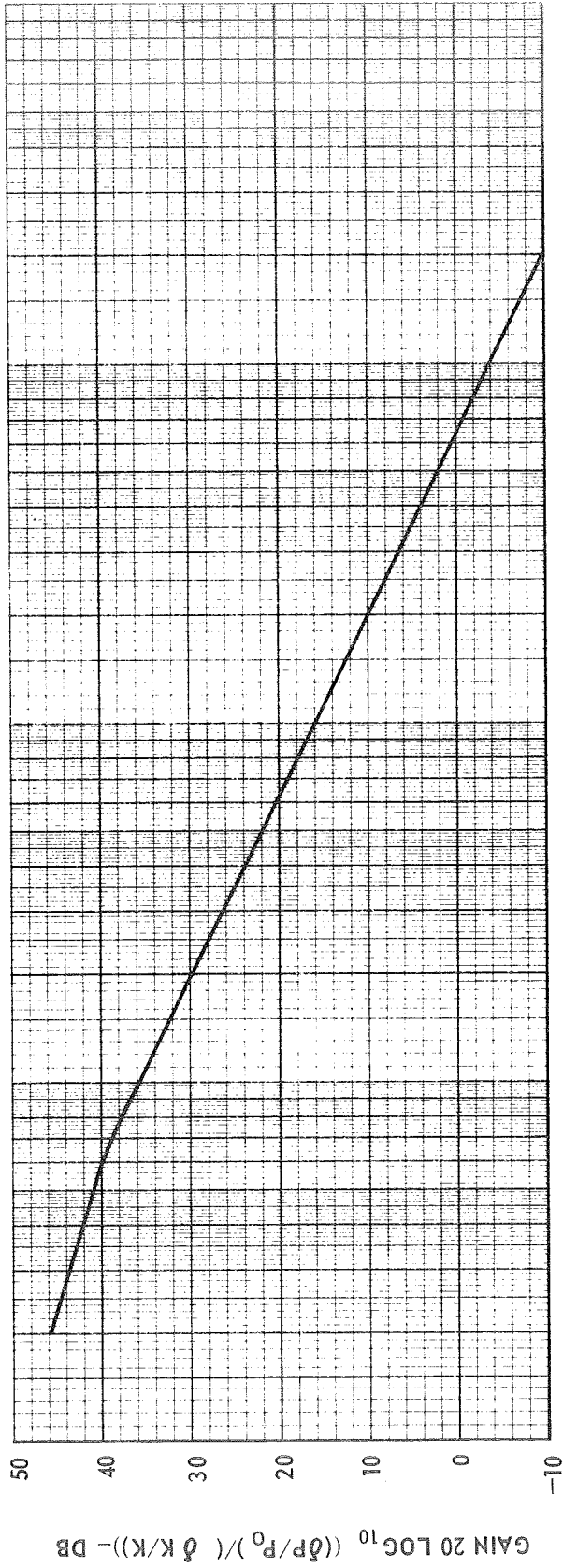
FIG. 24

GAIN AND PHASE DIAGRAMS WITH RESPECT TO FEEDBACK FUEL FLOW RATE FOR RESPONSE OF POWER LEVEL TO SMALL SINUSOIDAL OSCILLATIONS IN FUEL FLOW RATE
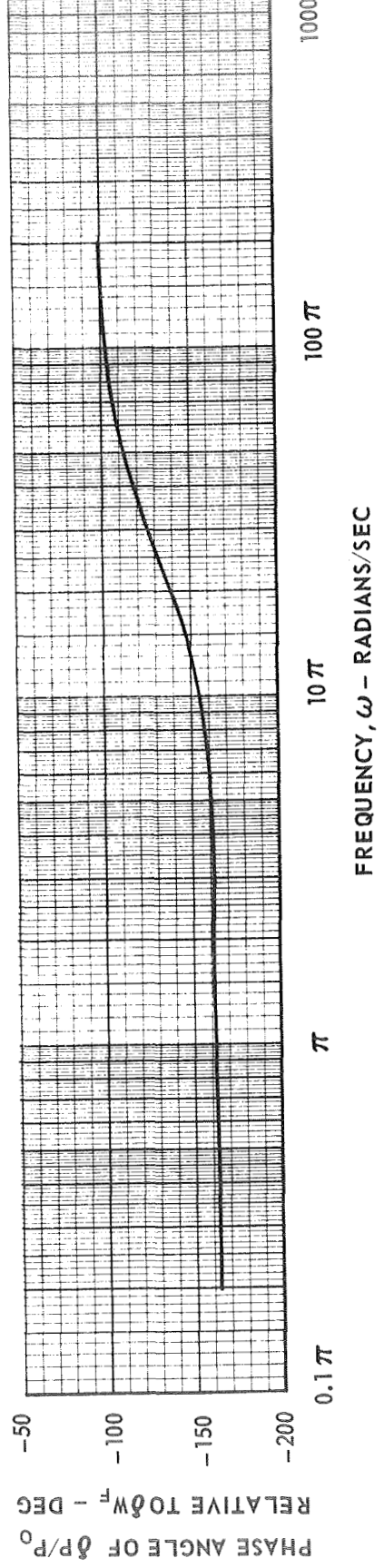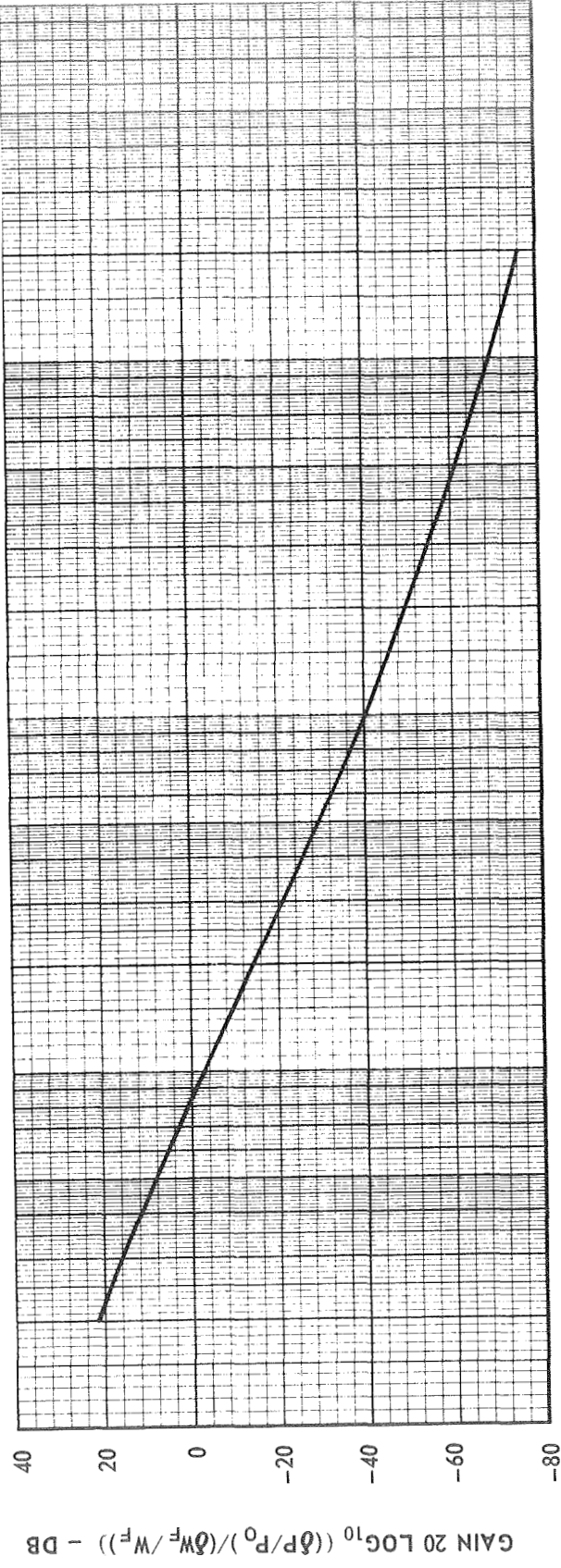
DISTRIBUTION LIST

Government	Copy No.

Mr. Milton Klein
Space Nuclear Propulsion Office
U. S. Atomic Energy Commission
Washington, D. C.   20545

1

Mr. F. C. Schwenk
Space Nuclear Propulsion Office
U. S. Atomic Energy Commission
Washington, D. C.   20545

2

Captain C. E. Franklin
Space Nuclear Propulsion Office
U. S. Atomic Energy Commission
Washington, D. C.   20545

3

Mr. R. F. Dickson
Director of Technical Division
Space Nuclear Propulsion Office
c/o Nevada Operations Office
U. S. Atomic Energy Commission
Las Vegas, Nevada

4

Mr. Frank E. Rom
Nuclear Systems Division
Mail Stop 106-1
NASA Lewis Research Center
21000 Brookpark Road
Cleveland, Ohio   44135

5

Mr. Robert G. Ragsdale
Nuclear Systems Division
Mail Stop 106-1
NASA Lewis Research Center
21000 Brookpark Road
Cleveland, Ohio   44135

6

Dr. Richard W. Patch
Nuclear Systems Division
Mail Stop 106-1
NASA Lewis Research Center
21000 Brookpark Road
Cleveland, Ohio   44135

7

Copy No.

Dr. J. C. Evvard   8
Associate Director
Mail Stop 3-5
NASA Lewis Research Center
21000 Brookpark Road
Cleveland, Ohio   44135

National Aeronautics and Space Administration   9
Office of Scientific and Technical Information
Washington, D. C.   20546
Attention: AFSS-LL

Dr. A. J. Eggers, Jr.   10
Office of Advanced Research and Technology
NASA Headquarters
1520 H Street, NW
Washington, D. C.   20546

Mr. A. E. Gessow   11
NASA Headquarters
Office of Advanced Research and Technology
Washington, D. C.   20546

Dr. Robert F. Trapp   12
Chief, Advanced Concepts & Flight Projects
(RBA)
Biotechnology & Human Research Division
National Aeronautics and Space Administration
Washington, D. C.   20546

NASA Headquarters   13
Washington, D. C.   20546
Attention: OART

National Aeronautics and Space Administration   14
Washington, D. C.   20546
Attention: Office of Technical Information
            and Educational Programs, Code ETL

Mr. R. W. Ziem (RPS)   15
National Aeronautics and Space Administration
Washington, D. C.   20546

Mr. D. R. Bartz   16
Manager, Research and Advanced Concepts Section
Propulsion Division
Jet Propulsion Laboratory
Pasadena, California   91103

Mr. Jerry P. Davis
Building 122-3
Jet Propulsion Laboratory
4800 Oak Grove Drive
Pasadena, California   91103

17

Mr. H. Denslow
Jet Propulsion Laboratory
4800 Oak Grove Drive
Pasadena, California   91103

18

Dr. Clifford J. Heindl
Building 180-805
Jet Propulsion Laboratory
4800 Oak Grove Drive
Pasadena, California   91103

19

Dr. Robert V. Meghreblian
Jet Propulsion Laboratory
4800 Oak Grove Avenue
Pasadena, California   91103

20

Mr. L. E. Newlan
Chief, Reports Groups
Jet Propulsion Laboratory
4800 Oak Grove Drive
Pasadena, California   91103

21

Mr. H. Hornby
NASA Ames Research Center
Mission Analysis Division
Moffett Field, California   94035

22

Mr. C. A. Syvertson
Associate Director for Astronautics
NASA Ames Research Center
Moffett Field, California   94035

23

Copy No.

Mr. Ronald J. Harris   24
Chief, Planetary & Nuclear Systems Group
Advanced Systems Office R-AS
Marshall Space Flight Center
Huntsville, Alabama   35812

National Aeronautics and Space Administration   25
George C. Marshall Space Flight Center
Huntsville, Alabama   35812
Attention: Library

NASA Goddard Space Flight Center   26
Glenn Dale Road
Greenbelt, Maryland
Attention: Librarian

National Aeronautics and Space Administration   27
Manned Spacecraft Center
P. O. Box 1537
Houston, Texas
Attention: Library

National Aeronautics and Space Administration   28
Langley Research Center
Langley Air Force Base
Virginia
Attention: Library

Dr. George Grover   29
N-5
Los Alamos Scientific Laboratory
P. O. Box 1663
Los Alamos, New Mexico   87544

Dr. William Kirk   30
University of California
Los Alamos Scientific Laboratory
P. O. Box 1663
Los Alamos, New Mexico   87544

Los Alamos Scientific Laboratory   31
P. O. Box 1663
Los Alamos, New Mexico   87544
Attention: N Division

Copy No.

Mr. John D. Orndoff   32
N Division
Los Alamos Scientific Laboratory
Los Alamos, New Mexico   87544

U. S. Atomic Energy Commission   33
Headquarters Library, Reports Section
Mail Station G-017
Washington, D. C.   20545

Atomic Energy Commission   34
Division of Technical Information Extension
P. O. Box 62
Oak Ridge, Tennessee

Mr. A. P. Fraas   35
Oak Ridge National Laboratory
P. O. Box Y
Oak Ridge, Tennessee   37831

Mr. E. A. Franco-Ferreira   36
Metals & Ceramics Division
Oak Ridge National Laboratory
P. O. Box X
Oak Ridge, Tennessee   37831

Dr. John J. Keyes, Jr.   37
Reactor Division
Oak Ridge National Laboratory
P. O. Box Y
Oak Ridge, Tennessee   37831

Dr. A. J. Miller   38
Oak Ridge National Laboratory
P. O. Box Y
Oak Ridge, Tennessee   37831

Mr. P. Patriarca   39
Oak Ridge National Laboratory
P. O. Box X
Oak Ridge, Tennessee   37831

Mr. John Marchaterre Argonne National Laboratory 9700 South Cass Avenue Argonne, Illinois	40
Mr. L. P. Hatch Brookhaven National Laboratory Upton, Long Island, New York 11101	41
Mr. E. L. Van Horn U. S. Atomic Energy Commission Brookhaven Area Office Upton, Long Island, New York 11101	42
Dr. Charles Beckett Heat Division National Bureau of Standards Washington, D. C.	43
Mr. Keith Boyer N Division Los Alamos Scientific Laboratory Los Alamos, New Mexico 87544	44
Mr. R. V. Mrozinski National Aeronautics and Space Council Executive Office of the President Executive Office Building, Room 11 Washington, D. C. 20502	45
Dr. Charles J. Bridgman Associate Professor of Physics Air Force Institute of Technology Wright-Patterson Air Force Base, Ohio 45433	46
The Rand Corporation 1700 Main Street Santa Monica, California 90406	47
Mr. G. Sayles (RPRRA) Air Force Rocket Propulsion Laboratory Edwards Air Force Base California 93523	48

Aerospace Corporation P. O. Box 95085 Los Angeles, California 90045 Attention: Library-Documents	49
Dr. Robert H. Fox Institute for Defense Analysis 400 Army Navy Drive Arlington, Virginia 22202	50
Mr. J. E. Jackson DDR&E (OAP) Washington, D. C.	51
DDR&E (WSEG) Washington, D. C. Attention: OSD	52
AFSC (SCTD) Andrews Air Force Base Washington, D. C.	53
Dr. Theodore B. Taylor Defense Atomic Support Agency The Pentagon Washington, D. C. 20301	54
Dr. J. F. Masi (SREP) Department of the Air Force Air Force Office of Scientific Research 1400 Wilson Boulevard Arlington, Virginia 22209	55
Commander AFSC Foreign Technology Division Wright-Patterson Air Force Base, Ohio 45433 Attention: RTD (TD-E3b)	56
Dr. Hans von Ohain Aerospace Research Laboratories (ARD-1) Wright-Patterson Air Force Base Ohio 45433	57

	Copy No.

Mr. E. C. Perkins   58
AUL (AUL3T-7143)
Maxwell Air Force Base
Alabama

Mr. Ben Pinkel   59
Rand Corporation
1700 Main Street
Santa Monica, California   90406

Dr. Martin Rosenzweig   60
Aerodynamic & Heat Transfer Department
Aerospace Corporation
P. O. Box 95085
Los Angeles, California   90045

Mr. Frederick C. Durant, III   61
Assistant Director, Astronautics
National Air Museum
Smithsonian Institute
Washington, D. C.   20560

Captain E. N. Kemler   62
Office of Research Analysis
Holloman Air Force Base
New Mexico

Superintendent   63
U. S. Naval Postgraduate School
Naval Academy
Monterey, California

Mr. George T. Lalos   64
U. S. Naval Ordnance Laboratory
White Oaks, Silver Springs
Maryland   20900

HQ-SAMSO (SMAAP/Capt. Yepp)   65
Air Force Unit Post Office
Los Angeles Air Force Station
California   90045

Copy No.

NASA Scientific and Technical Information Facility (2 copies)   66
Post Office Box 33   66.1
College Park, Maryland   20740
Attention: NASA Representative

NASA Headquarters   67
Washington, D. C.   20546
Attention: New Technology Representative, Code UT

Dr. K. Thom   68
Code RRE
NASA Headquarters
Washington, D. C.   20546

Lt. N. Kuehn   69
Defense Intelligence Agency
Attention: DIA ST-2C2
Washington, D. C.   20301

Universities

Dr. C. C. Chang   70
Head, Space Sciences & Applied Physics
Catholic University of America
Washington, D. C.   20017

Professor Abraham Hyatt   71
1700 E. Imperial Highway
El Segundo, California   90246

Professor Robert A. Gross   72
School of Engineering & Applied Science
Columbia University
New York, New York   10027

Dr. John C. Stewart   73
University of Colorado
Joint Institute for Laboratory Astrophysics
Boulder, Colorado   80302

Dr. Peter Chiarulli   74
Head, Mechanics Department
Illinois Institute of Technology
Chicago, Illinois   60616

Copy No.

Dr. Andrew Fejer Head, Mechanical & Aerospace Engineering Department Illinois Institute of Technology Chicago, Illinois 60616	75
Dr. Zalman Lavan Illinois Institute of Technology M. A. E. Department Technology Center Chicago, Illinois 60616	76
Dr. T. P. Torda Illinois Institute of Technology M. A. E. Department, Technology Center Chicago, Illinois 60616	77
Dr. Herbert Weinstein Chemical Engineering Department Illinois Institute of Technology Chicago, Illinois 60616	78
Dr. Joseph Clement Nuclear Engineering Department Georgia Institute of Technology Atlanta, Georgia 30332	79
Professor Clyde Orr, Jr. Chemical Engineering Department Georgia Institute of Technology Atlanta, Georgia 30332	80
Professor Elias P. Gyftopoulos Room 24-109 Massachusetts Institute of Technology Cambridge, Massachusetts 02139	81
Professor J. L. Kerrebrock Room 33-115 Massachusetts Institute of Technology Cambridge, Massachusetts 02139	82
Professor Edward Mason Room NW12 Massachusetts Institute of Technology Cambridge, Massachusetts 02139	83

Professor E. P. Wigner   84
Department of Physics
Princeton University
Princeton, New Jersey   08540

Professor M. J. Zucrow   85
Atkins Professor of Engineering
Mechanical Engineering Department
Purdue University
Lafayette, Indiana   49707

Dr. A. V. Grosse   86
Research Institute of Temple University
4150 Henry Avenue
Philadelphia, Pennsylvania   19144

Professor H. C. Perkins   87
Energy, Mass & Momentum Transfer Laboratory
Aerospace & Mechanical Engineering Department
University of Arizona
Tucson, Arizona   85721

Professor Rafael Perez   88
Nuclear Engineering Department
University of Florida
Gainesville, Florida   32601

Professor Terence Cool   89
Thermal Engineering Department
Cornell University
Ithaca, New York   14850

Dr. Franklin K. Moore, Head   90
Thermal Engineering Department
Cornell University
Ithaca, New York   14850

Professor Chieh Ho   91
Division of Nuclear Science
Room 287, Mudd Building
Columbia University
New York, New York   10027

Copy No.

Dr. Richard T. Schneider   100
202 Nuclear Sciences Building
Department of Nuclear Engineering
  Sciences
University of Florida
Gainesville, Florida   32601

Professor C. N. Shen   101
Rensselaer Polytechnic Institute
Troy, New York

Dr. Herman E. Unger   102
Assistant Professor
Engineering Sciences
Northwestern University
Evanston, Illinois   60201

Industry

Mr. James Carton   103
Advanced Concepts
REON Division
Aerojet-General Corporation
Sacramento, California   95801

Mr. A. B. Longyear   104
New Technology - NRO
Aerojet-General Corporation
P. O. Box 15847
Sacramento, California   95813

Mr. William J. Houghton   105
Department 7040, Building 2019A2
Aerojet-General Corporation
P. O. Box 1947
Sacramento, California   95809

Mr. W. L. Snapp   106
Aerojet-General Corporation
20545 Center Ridge Road
Cleveland, Ohio   44116

Mr. C. K. Soppet, Manager   107
Engine Test Operations
NERVA Test Operations
P. O. Box 2027
Jackass Flats, Nevada   89023

Dr. J. J. Stewart   108
Department 7040, Building 2019A2
Aerojet-General Corporation
Sacramento, California   95809

Aerojet-General Corporation   109
P. O. Box 1947
Sacramento, California   95809
Attention: Technical Information Office

Florence Walsh, Librarian   110
Aerojet-General Corporation
11711 South Woodruff Avenue
Downey, California

B. Probert   111
Aerojet-General Nucleonics
P. O. Box 78
San Ramon, California

R. R. Blackwell   112
Allison Division - GMC
P. O. Box 24013
Indianapolis, Indiana   46206

Mr. David Mallon   113
Allison Division
General Motors Corporation
2355 S. Tibbs Avenue
Indianapolis, Indiana   46206

Dr. Richard Rosa   114
AVCO Everett Research Laboratory
2385 Revere Beach Parkway
Everett, Massachusetts   02149

Mr. Jack Ravets   115
Westinghouse Astronuclear Laboratory
P. O. Box 10864
Pittsburgh, Pennsylvania   15236

Mr. Jerrold M. Yos   116
AVCO Corporation
Research & Advanced Development Division
201 Lowell Street
Wilmington, Massachusetts   01887

Bell Aerosystems   117
Box 1
Buffalo 5, New York
Attention: T. Reinhardt

Mr. R. R. Barber   118
Boeing Company
Aerospace Division
P. O. Box 3707
Seattle, Washington   98124

Mr. J. A. Brousseau   119
Chief, Propulsion Systems Technology
Mail Stop 47-18
The Boeing Company
Seattle, Washington   98124

Chrysler Corporation   120
Defense Operations Division
Box 757
Detroit 31, Michigan

Dr. Ralph S. Cooper   121
Donald W. Douglas Laboratories
2955 George Washington Way
Richland, Washington   99352

Mr. J. S. Cory   122
Donald W. Douglas Laboratories
2955 George Washington Way
Richland, Washington   99352

H-910375-4

Mr. John Peak   132
General Atomics Division
General Dynamics Corporation
P. O. Box 608
San Diego, California   92112

Mr. Louis Canter   133
General Dynamics/Astronautics
Technical Library
San Diego, California   92112

General Electric Company   134
MSVD Library Documents Group, RM 3446
3198 Chestnut Street
Philadelphia, Pennsylvania   19101

Dr. S. M. Scala   135
Manager, Theoretical Fluid Physics Section
General Electric Company
Space Sciences Laboratory
P. O. Box 8555
Philadelphia, Pennsylvania   19101

Mr. J. W. Stephenson   136
General Electric Co., NMPO
P. O. Box 15132
Cincinnati 15, Ohio

General Electric Company   137
Cincinnati 15, Ohio
Attention: Technical Information Center

Dr. Jerry Grey   138
Grey-Rad Corporation
61 Adams Street
Princeton, New Jersey   08540

Mr. M. O. Friedlander   139
Engineering Library, Plant 5
Grumman Aircraft Engineering Corporation
Bethpage, Long Island, New York

Mr. Holmes F. Crouch   140
Lockheed Missiles & Space Company
Space System Division, Dept. 62-90, Building 104
Sunnyvale, California   94408

Mr. Maxwell Hunter   141
Department 50-01, Building 102
Lockheed Missiles & Space Company
P. O. Box 504
Sunnyvale, California   94408

Mr. H. F. Plank   142
Building 153, DCS-G
Lockheed Missile & Space Company
Sunnyvale, California   94408

Miss Belle Berlad, Librarian   143
Lockheed Propulsion Company
P. O. Box 111
Redlands, California

Dr. Larry Kaufman   144
Director of Research
Manlabs, Inc.
21 Erie Street
Cambridge, Massachusetts   02139

Martin Nuclear, A Division of Martin-Marietta Corporation   145
P. O. Box 5042
Middle River 3, Maryland
Attention: Library

Mr. J. J. Norton   146
Marquardt Corporation
16555 Saticoy Street
Van Nuys, California

Naval Plant Representative Office   147
c/o UAC Pratt & Whitney Aircraft Division
East Hartford, Connecticut   06108
Attention: Mr. R. N. Schuster
            Contracts Division

North American Aviation, Inc.   148
Space and Information Systems Division
12214 Lakewood Boulevard
Downey, California
Attention: Technical Information
            Center (L. M. Foster)

Mr. W. H. Morita   149
North American Aviation, Inc.
Space & Information Systems Division
12214 Lakewood Boulevard
Downey, California

Mr. C. C. Bennett   150
Rocketdyne
P. O. Box 552
Canoga Park, California   91303

Dr. Robert Dillaway   151
Nucleonics Department
Rocketdyne
6633 Canoga Avenue
Canoga Park, California   91303

Dr. S. V. Gunn   152
Rocketdyne
6633 Canoga Avenue
Canoga Park, California   91303

Mr. Carmen Jones   153
H63 - General Electric Co.
North I-75
Cincinnati, Ohio   45215

Mr. L. A. Gore   154
Space Technology Laboratories
One Space Park
Redondo Beach, California   90277

Rocketdyne   155
6633 Canoga Park, California   91303
Attention: Library, Dept. 596-306

Mr. Henry Hunter   156
Space Technology Laboratories
One Space Park
Redondo Beach, California   90277

Copy No.

Space Technology Laboratories   157
One Space Park
Redondo Beach, California   90277
Attention: STL Technical Library Doc.
             Acquisitions

Thiokol Chemical Corporation   158
Reaction Motors Division
Denville, New Jersey
Attn: Librarian

Thompson Ramo Wooldridge   159
23555 Euclid Avenue
Cleveland, Ohio
Attention: Librarian

Mr. Walter F. Krieve   160
Building S
TRW Systems
One Space Park
Redondo Beach, California   90278

Dr. D. W. Drawbaugh   161
Astronuclear Laboratory
Westinghouse Electric Corporation
Pittsburgh, Pennsylvania   15236

Mr. F. McKenna   162
Astronuclear Laboratory
Westinghouse Electric Corporation
P. O. Box 10864
Pittsburgh, Pennsylvania   15236

Dr. John Romanko, Staff Scientist   163
Y-128, Building 197
General Dynamics
Ft. Worth Division, Box 740
Ft. Worth, Texas   76101

Dr. J. W. Hilborn   164
Reactor Physics Branch
Advanced Projects & Reactor Physics Division
Atomic Energy of Canada Limited
Chalk River, Ontario, Canada

Dr. Jacob B. Romero   165
The Boeing Company
Mail Stop 84-66
Kent, Washington

Mr. Merle Thorpe   166
TAFA Division
Humphreys Corporation
180 North Main Street
Concord, New Hampshire   03301

Dr. Henry Stumpf   167
Astronuclear Lab
Westinghouse Electric Corporation
Pittsburgh, Pennsylvania   15236

Dr. J. W. Morfitt, Manager   168
Idaho Test Station
Idaho Nuclear Corporation
P. O. Box 2147
Idaho Falls, Idaho   83401

UNITED AIRCRAFT CORPORATION